TECHNISCHE UNIVERSITÄT
KAISERSLAUTERN

A building-block model reveals new insights into the biogenesis of yeast mitochondrial ribosomes

Vom Fachbereich Biologie der Universität Kaiserslautern
zur Verleihung des akademischen Grades „Doktor der
Naturwissenschaften“ genehmigte Dissertation

Vorgelegt von **Steffen Hess**

Datum der wissenschaftlichen Aussprache:

17. September 2020

Promotionskommission:

1.Gutachter: Prof. Dr. Johannes M. Herrmann

2.Gutachter: Jun.-Prof. Dr. Felix Willmund

Vorsitzender: Prof. Dr. Matthias Hahn

Kaiserslautern, 2020 D 386

Eigenständigkeitserklärung

Hiermit erkläre ich, dass die vorliegende Arbeit ohne unzulässige Hilfe Dritter und ohne Benutzung anderer als der angegebenen Hilfsmittel von mir persönlich an der Technischen Universität Kaiserslautern in der Arbeitsgruppe Zellbiologie (Prof. Dr. Johannes M. Herrmann) angefertigt wurde. Die aus anderen Quellen übernommenen Daten und Konzepte sind unter Angabe der Quelle gekennzeichnet.

Ich habe nicht die entgeltliche Hilfe von Vermittlungs- beziehungsweise Beratungsdiensten in Anspruch genommen. Niemand hat von mir unmittelbar oder mittelbar geldwerte Leistungen für Arbeiten erhalten, die im Zusammenhang mit dem Inhalt der vorgelegten Dissertation stehen.

Die Arbeit wurde bisher weder im In- noch im Ausland in gleicher oder ähnlicher Form einer anderen Prüfungsbehörde vorgelegt.

Die Bestimmungen der Promotionsordnung des Fachbereichs Biologie der Technischen Universität Kaiserslautern sind mir bekannt. Insbesondere weiß ich, dass ich vor Vollzug der Promotion zur Führung des Doktortitels nicht berechtigt bin.

Steffen Hess

Kaiserslautern, 30.07.2020

Table of contents

Summary

Most of the mitochondrial proteins in yeast are encoded in the nuclear genome, get synthesized by cytosolic ribosomes and are imported via TOM and TIM23 into the matrix or other subcompartments of mitochondria. The mitochondrial DNA in yeast however also encodes a small set of 8 proteins from which most are hydrophobic membrane proteins and build core components of the OXPHOS complexes. They get synthesized by mitochondrial ribosomes which are descendants of bacterial ribosomes and still have some similarities to them. On the other hand, mitochondrial ribosomes experienced various structural and functional changes during evolution that specialized them for the synthesis of the mitochondrial encoded membrane proteins. The mitoribosome contains mitochondria-specific ribosomal proteins and replaced the bacterial 5S rRNA by mitochondria-specific proteins and rRNA extensions. Furthermore, the mitoribosome is tethered to the inner mitochondrial membrane to facilitate a co-translational insertion of newly synthesized proteins. Thus, also the assembly process of mitoribosomes differs from that of bacteria and is to date not well understood.

Therefore, the biogenesis of mitochondrial ribosomes in yeast should be investigated. To this end, a strain was generated in which the gene of the mitochondrial RNA-polymerase *RPO41* is under control of an inducible *GAL10*-promoter. Since the scaffold of ribosomes is built by ribosomal RNAs, the depletion of the RNA-polymerase subsequently leads to a loss of mitochondrial ribosomes. Reinduction of Rpo41 initiates the assembly of new mitoribosomes, which makes this strain an attractive model to study mitoribosome biogenesis.

Initially, the effects of Rpo41 depletion on cellular and mitochondrial physiology was investigated. Upon Rpo41 depletion, growth on respiratory glycerol medium was inhibited. Furthermore, mitochondrial ribosomal 21S and 15S rRNA was diminished and mitochondrial translation was almost completely absent. Also, mitochondrial DNA was strongly reduced due to the fact that mtDNA replication requires RNA primers that get synthesized by Rpo41.

Next, the effect of reinduction of Rpo41 on mitochondria was tested. Time course experiments showed that mitochondrial translation can partially recover from 48h Rpo41 depletion within a timeframe of 4.5h. Sucrose gradient sedimentation experiments further showed that the mitoribosomal constitution was comparable to wildtype control samples during the time course of 4.5h of reinduction, suggesting that the ribosome assembly is not fundamentally altered in Gal-Rpo41 mitochondria. In addition, the depletion time was found to be critical for recovery of mitochondrial translation and mitochondrial RNA levels. It was observed that after 36h of Rpo41 depletion, the rRNA levels and mitochondrial translation recovered to almost 100%, but only within a time course of 10h.

Finally, mitochondria from Gal-Rpo41 cells isolated after different timepoints of reinduction were used to perform complexome profiling and the assembly of mitochondrial protein complexes was investigated. First, the steady state conditions and the assembly process of mitochondrial respiratory chain complexes were monitored. The individual respiratory chain complexes and the super-complexes of complex III, complex IV and complex V were observed. Furthermore, it was seen that they recovered from Rpo41 depletion within 4.5h of reinduction. Complexome profiles of the mitoribosomal small and large subunit discovered subcomplexes of mitoribosomal proteins that were assumed to form prior to their incorporation into assembly intermediates. The complexome profiles after reinduction indeed showed the formation of these subcomplexes before formation of the fully assembled subunit. In the mitochondrial LSU

one subcomplex builds the membrane facing protuberance and a second subcomplex forms the central protuberance. In contrast to the preassembled subcomplexes, proteins that were involved in early assembly steps were exclusively found in the fully assembled subunit. Proteins that assemble at the periphery of the mitoribosome during intermediate and late assembly steps where found in soluble form suggesting a pool of unassembled proteins that supply assembly intermediates with proteins.

Taken together, the findings of this thesis suggest a so far unknow building-block model for mitoribosome assembly in which characteristic structures of the yeast mitochondrial ribosome form preassembled subcomplexes prior to their incorporation into the mitoribosome.

Zusammenfassung

Die meisten mitochondrialen Proteine in Hefe werden im Kerngenom kodiert, von cytosolischen Ribosomen synthetisiert und via TOM und TIM23 in die mitochondriale Matrix oder andere mitochondriale Subkompartimente importiert. Die mitochondriale DNA in Hefe kodiert jedoch ebenfalls für 8 Proteine, wovon die meisten hydrophobe Membranproteine sind und Kernkomponenten der OXPHOS-Komplexe bilden. Diese Proteine werden von mitochondrialen Ribosomen synthetisiert, welche entfernte Nachfahren bakterieller Ribosomen sind und daher noch einige Gemeinsamkeiten mit diesen aufweisen. Andererseits erfuhren die mitochondrialen Ribosomen während der Evolution zahlreiche strukturelle und funktionelle Veränderungen, wodurch sie für die Synthese der mitochondrial kodierten Membranproteine spezialisiert wurden. So enthalten die Mitoribosomen Mitochondrien-spezifische ribosomale Proteine und die in bakteriellen Ribosomen vorhandene 5S rRNA wurde durch Mitochondrien-spezifische Proteine und rRNA-Erweiterungen ersetzt. Außerdem sind Mitoribosomen an die innere Mitochondrienmembran gebunden um neu synthetisierte Proteine co-translational in die Innenmembran einzuführen. Daher unterscheidet sich der Assemblierungsprozess mitochondrialer Ribosomen von dem in Bakterien und ist bis heute nicht sehr gut verstanden.

In dieser Arbeit sollte die Biogenese mitochondrialer Ribosomen untersucht werden. Dazu wurde ein Hefestamm generiert, bei dem das Gen der mitochondrialen RNA-Polymerase *RPO41* mit dem induzierbaren *GAL10*-Promotor kontrolliert werden kann. Zuerst wurden die Effekte einer Rpo41-Depletion auf die zelluläre und mitochondriale Physiologie getestet. Es wurde gezeigt, dass das Zellwachstum auf respirativem Medium gehemmt ist, wenn Rpo41 depletiert ist. Außerdem war die mitochondriale ribosomale 21S und 15S rRNA stark verringert und auch mitochondriale Translation war nur minimal nachweisbar. Zusätzlich war die mitochondriale DNA stark reduziert was darauf zurückzuführen ist, dass Rpo41 für die Replikation der mtDNA benötigt wird.

Als Nächstes wurde untersucht, wie sich eine Wiederinduktion von Rpo41 auf Mitochondrien auswirkt. In einem zeitlichen Verlauf von 4,5 Stunden wurde gezeigt, dass die mitochondriale Translation teilweise wiederhergestellt werden kann, wenn Rpo41 vorher für 48 Stunden depletiert wurde. Sedimentationsexperimente mit Saccharose-Gradienten ergaben, dass die Zusammensetzung der Mitoribosomen vergleichbar war mit Kontrollproben des Wildtyp. Daraus lässt sich schließen, dass der Assemblierungsprozess der Ribosomen in Gal-Rpo41 Mitochondrien nicht fundamental verändert ist. Zusätzlich wurde beobachtet, dass die Depletionszeit entscheidend für eine Wiederherstellung der mitochondrialen Translation und der mitochondrialen rRNA ist. Nach 36 Stunden Depletion konnte die mitochondriale rRNA und Translation zu beinahe 100% wiederhergestellt werden, was allerdings einen zeitlichen Verlauf von 10 Stunden erforderte.

Schließlich wurden Mitochondrien aus Gal-Rpo41-Zellen nach verschiedenen Zeitpunkten der Wiederinduktion isoliert und Komplexom-Profile erstellt. Zuerst wurden der stationäre Zustand sowie der Assemblierungsprozess der mitochondrialen Atmungskettenkomplexe analysiert. Es konnten die einzelnen Komplexe der Atmungskette sowie die Superkomplexe von Komplex III, Komplex IV und Komplex V gezeigt werden. Des Weiteren konnte beobachtet werden, dass die Komplexe nach Rpo41-Depletion innerhalb von 4,5 Stunden wiederhergestellt wurden. Komplexom Profile der kleinen und großen Untereinheit von Mitoribosomen zeigten überraschenderweise Subkomplexe mitoribosomaler Proteine, die vermutlich zuerst gebildet werden, bevor sie während der Ribosomensynthese in Zwischenstufen der Ribosomen

eingebaut werden. Tatsächlich zeigten die Komplexom-Profile der Proben nach Wiederinduktion die Bildung genau dieser Unterkomplexe bevor die vollständig zusammengebaute Untereinheit zu detektieren war. Einer dieser Unterkomplexe der großen Untereinheit bildet die membranständige Erweiterung des Mitoribosoms und der zweite bildet die zentrale Erweiterung des Mitoribosoms. Im Gegensatz zu den Unterkomplexen wurden die Proteine, die an frühen Schritten der Ribosomensynthese beteiligt sind, nur in der vollständig zusammengesetzten Untereinheit detektiert. Proteine, die hingegen während späterer Schritte der Assemblierung in die Ribosomen eingebaut werden und auf der Oberfläche der Ribosomen zu finden sind, wurden auch in löslicher Form gefunden.

Zusammengefasst zeigen die Ergebnisse dieser Arbeit einen bisher unbekannten modularen Weg der Ribosomenbiogenese, wobei charakteristische Strukturen der mitochondrialen Ribosomen in Hefe vorgeformte Unterkomplexe bilden, bevor sie in die Mitoribosomen eingebaut werden.

1. Introduction

All organisms can be assigned to one of two different domains of life, the eukaryotes and the prokaryotes. Membrane enclosed compartments, the so-called organelles, are a hallmark of eukaryotic cells and represent therefore a major difference between eukaryotes and prokaryotes. Furthermore, multicellular organisms like plants and animals are exclusively found in the domain of eukaryotes [1].

1.1 Mitochondria

One of the essential organelles found in eukaryotic cells are mitochondria. The central role in the energy metabolism of a cell led to the commonly known byname “powerhouse of the cell”. Besides their role in energy metabolism, mitochondria are involved in several additional processes such as iron sulfur cluster biogenesis [2], calcium homeostasis [3]or apoptosis [4].

1.1.1 Mitochondrial morphology

Based on the well-established endosymbiotic theory, the origin of mitochondria is an alpha proteobacterium that got engulfed by an archaebacterium. This process thus gave rise to a double membrane system enclosing the mitochondria [5 6].

The outer membrane faces the cytosol and encloses the organelle. The inner membrane surrounds the matrix [7] and can be further subdivided into two subcompartments. First, the inner boundary membrane which faces the outer membrane and thus forms the intermembrane space of mitochondria. Second, invaginations of the inner membrane, the cristae, which largely increase the surface of the inner membrane and harbor the respiratory chain complexes [8] (Figure 1). Cristae and intermembrane space are separated from each other by the mitochondrial contact site and cristae organizing system (MICOS)[9].

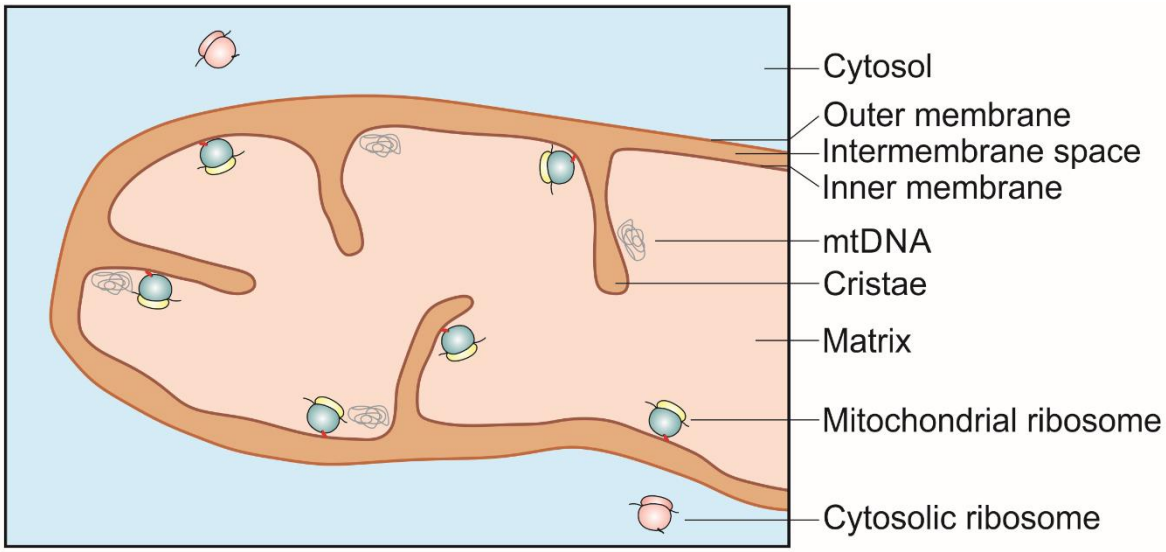

Figure 1: Schematic representation of the mitochondrial morphology

The matrix harbors the mitochondrial DNA (mtDNA). These so-called nucleoids are often associated with the inner membrane cristae and at sites where mitochondrial fission takes place [10 11]. The nucleoids are tightly packed together with various proteins. The proteins associated

with mitochondrial DNA are involved in DNA packaging (Abf2), DNA maintenance (DNA-Polymerase Mip1) and transcription (RNA-Polymerase Rpo41) as well as factors controlling mitochondrial biogenesis, metabolism and signaling pathways. Near the nucleoid, structures called RNA granules were found. These structures consist of RNA transcripts encoded by the mitochondrial DNA. Although RNA granules were only found and studied in human cell lines and other mammalian model organisms their presence in non-mammalian organisms seems likely. Especially in species where mitochondrial DNA architecture and replication are similar to those of mammalian mitochondria the existence of RNA granules would not be surprising. Several studies show that key processes of RNA processing take place at the RNA granules. These processes involve RNA maturation from polycistronic RNA to mature mRNA, polyadenylation, and posttranscriptional modification as well as RNA degradation thus leading to the hypothesis that RNA granules build the center of RNA processing in mitochondria. Furthermore, mitochondrial ribosomes are found to associate with RNA granules suggesting a role in translation initiation by supplying the mRNA to the ribosome. The function of RNA granules is at the moment not fully understood but the obvious involvement in transcription, translation and probably DNA replication shows a key role in mitochondrial gene expression and is of great interest in the field.

1.1.2 Mitochondrial DNA

The mitochondrial genome contains only a small set of genes. As a consequence of endosymbiosis many of the genes encoded by the genome of the endosymbiotic alpha-proteobacterium were lost during evolution or transferred to the nuclear genome [12]. Thus, the reduced mitochondrial genomes encode only special core components of the respiratory chain complexes, which are highly hydrophobic membrane proteins and conserved among species. Furthermore, mitochondrial tRNAs and mitochondrial rRNAs are encoded by the mtDNA enabling the organelle to build its own translation machineries. To assemble the complexes of the respiratory chain or oxidative phosphorylation system (OXPHOS) additional proteins are necessary. These proteins are encoded by genes of the nuclear genome and need to be expressed in tight coordination with the expression of mitochondrial genes to ensure a proper assembly of the respiratory chain. In total the mitochondrial proteome consists of about 1000 different proteins.

In the model organism *Saccharomyces cerevisiae* or baker's yeast the mitochondrial DNA contains 35 genes. Eight genes encode proteins from which seven are essential membrane proteins of the respiratory chain and one is a component of the small mitoribosomal subunit, the soluble protein Var1 [13] [14]. The remaining 27 genes encode for mitochondrial RNAs from which 24 are mitochondrial tRNAs, two are mitochondrial ribosomal RNAs (rRNAs) and one gene encodes the RNA component of the RNase P (*RPM1*) [15]. Besides the mitochondrial encoded *RPM1*, RNase P consists of the nuclear encoded protein Rpm2 which is synthesized in the cytosol and gets imported into the matrix. Mitochondrial RNAs are expressed as polycistronic precursors which need to be separated and processed. Mitochondrial encoded tRNAs for instance get processed both on their 5´and 3´ends by RNase P and tRNase Z to gain mature single tRNA molecules. Genetic inactivation of RNase P results in deleterious effects on mitoribosome assembly also suggesting a role in rRNA processing [11] [16].

Although the number of mitochondrial encoded proteins represents less than 1% of the whole mitochondrial proteome, it is assumed that over 200 mitochondrial proteins are needed to maintain and express this small set of OXPHOS proteins. This fact raises the question why the cell makes the huge effort to keep this small genome in mitochondria. One aspect is the

properties of the encoded proteins. The proteins of the OXPHOS are highly hydrophobic membrane proteins with several transmembrane domains and build the core centers of the individual respiratory chain complexes. Expression of these proteins on cytosolic ribosomes and importing them afterwards into mitochondria could be more challenging for the cell then keeping a second genome. The proteins would need to be protected from misfolding, aggregation and subsequent degradation as well as mislocalization to the endoplasmic reticulum or other organelles if expressed in the cytosol. These difficulties can be avoided by expressing especially the hydrophobic membrane proteins in the mitochondria. An additional advantage of expressing key components of OXPHOS by ribosomes in mitochondria is of regulatory nature. The assembly of respiratory chain complexes relies on the expression of the mitochondrial encoded OXPHOS genes. If the redox state of mitochondria, which can be a measure of health or fitness of mitochondria, is disturbed a fast response can be helpful. The downregulation of mitochondrial encoded OXPHOS genes can be such a fast response resulting in less mitochondrial respiration giving the cell the chance to find and solve the problem. Indeed, all organisms that are able to respire contain mitochondria with their own genome and these genomes contain a very similar set of genes of the OXPHOS system and the translation apparatus of mitochondria.

1.2 Ribosomes

Ribosomes are the macromolecular machines that are needed in all living cells to synthesize proteins. The genetic information encoded by messenger RNAs (mRNAs) get translated by ribosomes into protein sequences, which then can fold into their native conformation and fulfill multiple functions in a cell. The structures of ribosomes have first been discovered in the 1950s by electron microscopy [17]. In this time and due to their size ribosomes have been described in Svedberg units. This sedimentation coefficient depends on the mass and shape of a particle and its interaction with the medium in which it sediments.

Ribosomes consist of a large and small subunit, both composed of ribosomal RNA (rRNA) and ribosomal proteins. The rRNA forms the internal scaffolding and reactive center of the ribosome while the ribosomal proteins assemble around the RNA and help to keep the right folding, orientation, and stability. A common feature of ribosomal proteins is a high content of positive charged amino acids lysine and arginine which contribute to the interaction between negative rRNA and protein.

During the process of protein synthesis, the large subunit (LSU) performs the peptidyl-transferase activity where a new delivered amino acid gets covalently bound to the already existing protein chain. The function of the small subunit (SSU) is mainly recognition and binding of the mRNA.

1.2.1 Mechanism of protein synthesis

The mammalian cytosolic ribosome is an 80S particle. The LSU consists of three rRNAs with a size of 28S, 5.8S and 5S. In addition, 49 proteins contribute to build a functional LSU which has a final size of 60S. The SSU contains only one rRNA with the size of 18S and 33 ribosomal proteins ending up in a 40S particle.

The mechanism of protein synthesis on ribosomes is universal. All ribosomes contain three binding sites for amino-acyl transfer RNA (tRNA) which are named regarding their role during translation. The first binding site is the aminoacyl site or A-site, which is the place where a new,

charged tRNA binds and brings the corresponding amino acid to the reaction. At the P-site or peptidyl site a tRNA bound to the polypeptide chain is located. The E-site is the exit site where the former P-site located tRNA exits the ribosome and gets recycled in the cytosol.

The reaction cycle starts with the selection of the right, charged tRNA corresponding to the codon of the mRNA. The corresponding amino acid that is delivered by this tRNA gets bound to the amino acid that is connected to the tRNA located at the P-site. This process is mediated by the peptidyl-transferase activity of the LSU and subsequently brings the growing polypeptide from the P-site tRNA to the A-site tRNA. Upon a conformational change, the P-site tRNA gets moved to the E-site and exits the ribosome. The A-site tRNA loaded with the polypeptide moves to the P-site and the growing protein chain proceeds through the polypeptide exit tunnel of the LSU. At the end of the tunnel proteins like chaperones or targeting factors bind the nascent chain and help to fold the protein or target it to its desired destination. The mRNA is also shifted by this process leading to the exposure of a new triplet of bases. This starts the next round of the translation cycle by choosing the right charged tRNA from the pool and locating it to the A-site.

1.3 Mitochondrial ribosomes

Although the process of translation is conserved among species mitoribosomes became specialized during evolution. The proteins they synthesize are in most cases very hydrophobic membrane proteins. This led to several structural and functional changes. Thus, the structure and molecular composition of mitoribosomes differs a lot from bacterial and also from cytosolic ribosomes [18] [19] (Figure 2).

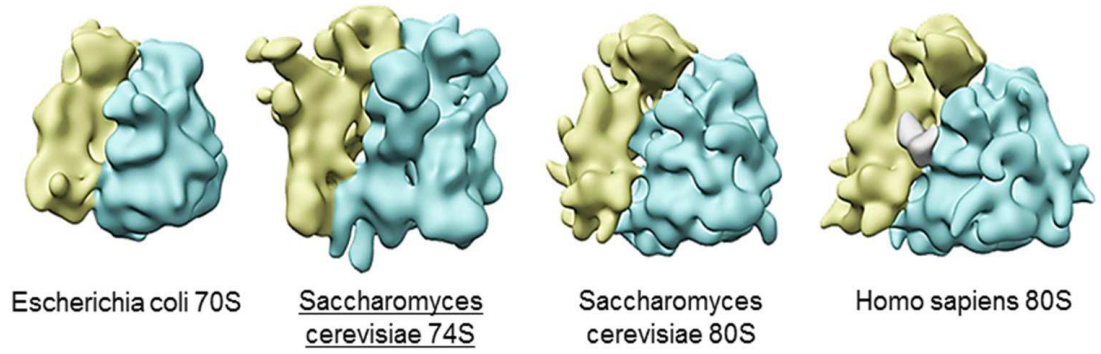

Figure 2: Structural comparison of different ribosomes. Structures of the bacterial 70S ribosome, the yeast mitochondrial 74S ribosome, the yeast cytosolic 80S ribosome and the mammalian cytosolic 80S ribosome (taken from [18]).

1.3.1 Structural changes

The yeast mitochondrial ribosome forms a particle of 74S with the large subunit of 54S and the small subunit of 37S. With an overall molecular weight of 3MDa this is an increase of about 30% compared to the bacterial ribosome [20]. The LSU is composed of a mitochondrial encoded 21S rRNA and additional 46 nuclear encoded proteins resulting in a molecular mass of 1.9MDa [21] [22]. The 21S rRNA consist of 3296 nucleotides and forms eleven additional expansion segments (ES) compared to the bacterial ribosome. The number of nucleotides therefore increased compared to bacteria resulting in 392 additional nucleotides. The sedimentation coefficient of 21S on the other hand is lower than the 23S of the bacterial LSU rRNA. This suggests that although larger than the bacterial LSU rRNA, the 21S rRNA in yeast mitoribosomes is packed tighter [23]. This is

supported by the finding that all mitoribosome-specific proteins except for mL44 and mL49 are found to interact with rRNA expansions that where not present in bacteria.

The SSU contains the 15S rRNA and approximately 35 nuclear encoded proteins [24]. In addition, the mitochondrial encoded ribosomal protein uS3, also known as Var1, is part of the small subunit. This composition results in a molecular weight of 1.1MDa [24]. The 15S rRNA contains 107 additional nucleotides in comparison to bacterial ribosomes. This also results in mitoribosome-specific RNA-expansions and remodeling of the subunit´s architecture. For example, a prominent protuberance is formed close to the mRNA exit by the proteins mS42 and mS43 (Rsm26+Mrp1).

In general, many mitoribosome-specific proteins gained expansions at either their N- or C-terminus. These expansions are mainly formed by prolonged tails or additional loops. Many of these extensions that where not present in bacteria where found to contact extensions of neighboring proteins. This results in a total increase of protein-protein contacts especially in the 54S subunit compared to the bacterial ribosome. Each mitoribosomal protein has on average 4.5 neighbors compared to 1.5 neighboring proteins in bacteria. These new interactions might be necessary to bridge different functional sites of the LSU, especially in regions where the function of the 5S rRNA has been replaced. In addition, some of the extensions expose a high basic charge probably interacting and neutralizing the negative charged backbone of the RNA. This might play a role in folding and stabilizing the secondary structure of the rRNA.

Central protuberance

The 5S rRNA, which is normally located at the central protuberance (CP) of the large mitoribosomal subunit is absent in yeast mitoribosomes [23]. It is replaced by two RNA extensions of the 21S rRNA (82-ES and 84-ES1) forming a remodeled central protuberance of the yeast mitoribosome. Interestingly, the 5S rRNA in mammalian mitochondrial ribosomes is replaced by a tRNA encoded by the mitochondrial genome, in particular by the $tRNA^{Val}$ in human mitoribosomes [25]. Furthermore, mitochondria-specific proteins locate at the central protuberance of yeast mitoribosomes. This results in an increased size of the protuberance compared to other mitoribosomes and a three-fold increase in size compared to the bacterial CP. In addition, the yeast mitoribosomal CP lacks two 5S rRNA binding proteins that are found in bacteria. These proteins got replaced by mitochondria-specific proteins mL38, mL40 and mL46. Of note is that these proteins together with the RNA extension segments do not mimic the 5S rRNA but instead occupy this space and build a new central protuberance structure in yeast mitoribosomes. Still, the function of the CP is not fully understood but it is thought to facilitate communication between the different functional sites of the mtLSU and mtSSU [26 27].

Membrane facing protuberance

The membrane facing protuberance represents an additional expansion segment of the mitoribosome compared to the bacterial large subunit. It is not present in the yeast cytosolic ribosome. In line with the remodeling of the central protuberance the membrane facing protuberance is enriched in mitochondria-specific proteins and RNA extensions. It is located adjacent to the mouth of the polypeptide exit tunnel and, together with the inner membrane protein Mba1, represents one of two binding sites of the mitoribosome to the membrane [28 29]. Structural studies suggest that the binding via Mba1 aligns the exit tunnel in a way that the growing polypeptide chain can directly interact with the mitochondrial inner membrane insertase Oxa1 [30] enabling a co-translational insertion into the membrane [31]. The mammalian homologue Mrpl45 was found on the same position as Mba1 but it is unclear if it fulfills the same

function of anchoring the ribosome to the membrane. The second binding site of the mitoribosome to the membrane was thought to be built by RNA-extensions 0-ES1 and 0-ES2 of the membrane facing protuberance. Instead, it has been shown to be mediated by the 21S rRNA extension 96-ES1 which is not part of the membrane facing protuberance [21] .

Polypeptide exit tunnel

The exit tunnel of the mitochondrial ribosome has also undergone drastic structural changes. While the exit tunnel in bacterial and cytosolic ribosomes is mainly formed by RNA, the mitoribosomal exit tunnel is mostly built up by mitochondria-specific proteins. The exposed surface of the proteins forming this tunnel is largely hydrophobic suggesting an adaptation to the production of membrane proteins by mitoribosomes. Alignment of the bacterial ribosomal exit tunnel path with the mitoribosome showed that this pathway is blocked by an extension of the mitochondria-specific protein uL23. Thus, the polypeptide exit tunnel in yeast mitoribosomes follows a different route through the 54S subunit resulting in a tunnel exit ~35Å away from the original exit in bacterial ribosomes. While the tunnel path starting at the peptidyl transferase center (PTC) and ending at the tunnel exit is about 100Å in length in bacteria, the mitoribosomal exit tunnel is also shortened to a length of approximately 60Å.

The exit tunnel entrance in mitochondrial ribosomes also changed in structure. An additional AU-base pair of the rRNA narrows the entrance by about 8Å and is not found in bacteria. This probably explains the resistance of mitoribosomes to macrolide antibiotics [32]. Chemicals like erythromycin are sterically unable to enter the PTC of the ribosome resulting in no sensitivity for such compounds.

The tunnel exit of the yeast mitoribosome is wider than observed in bacteria. This additional space might allow co-translational interaction with assembly factors necessary for proper OXPHOS complex assembly [21 31 33]. Furthermore, there is more space between the ribosome and the membrane compared to a cytosolic ribosome bound to the translocase of the endoplasmic reticulum. This could allow further factors to interact with the emerging polypeptide. These factors might be involved in folding, insertion of the proteins into the membrane or maturation of enzymatic active sites by incorporating prosthetic groups into the active center of these proteins.

1.3.2 Mitochondrial rRNA

The mitochondrial RNA gets expressed as polycistronic precursor molecules which further get processed to yield mature RNAs. In the case of the 21S rRNA, the precursor is a ~5.1kb transcript which contains a 1.2kb intron (p1) as well as three mitochondrial tRNAs ($tRNA^{Thr2}$, $tRNA^{Cys}$, $tRNA^{His}$). The mature 21S rRNA of 3.1kb is formed by excision of the intron and removal of a 3´-end extension of 900bp [34 35]. This processing occurs with the help of Suv3, an RNA helicase that forms the mitochondrial degradosome (mtEXO) together with Dss1 [36]. The mtEXO is the main 3´-5´-exoribonuclease in mitochondria and deletion of either subunit results in attenuated RNA turnover and also affects 5´-3´-processing of mitochondrial RNAs suggesting that both turnover and processing are linked processes.

The 15S rRNA is also part of a precursor together with $tRNA^{Trp}$. However, the single transcript is a 15.5S RNA which contains 80 additional nucleotides on the 5´-end [35]. It is not clear how the processing occurs, but it is tempting to speculate that the additional nucleotides are removed by Pet127 since it is the only known protein in yeast mitochondria with 5´-3´exonuclease activity and might process the 5´-end of the 15S rRNA precursor transcript [37 38].

1.4 Mitochondrial ribosome biogenesis and assembly

The mitochondrial ribosome in yeast is composed of about 80 proteins of which all but one is encoded on the nuclear genome. Thus, all these proteins need to be synthesized on cytosolic ribosomes, get stabilized and targeted to their destination, get imported into the mitochondrial matrix and finally assemble into a functional mitoribosome (Figure 3).

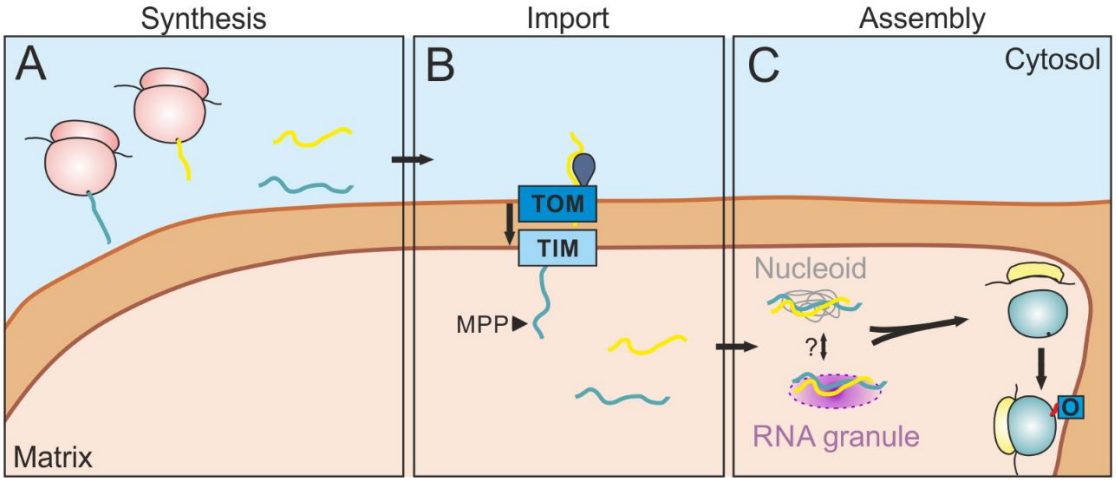

Figure 3: Schematic biogenesis of mitochondrial ribosomes. A: Most of the mitoribosomal proteins get synthesized in the cytosol with a N-terminal presequence guiding these preproteins to the import machinery. B: After binding to the import receptor on the outer membrane the preprotein gets imported into the matrix via the translocase of the outer membrane (TOM) and the translocase of the inner membrane (TIM23) in a membrane potential dependent manner. During the import process the mitochondrial processing peptidase (MPP) cleaves off the presequence. C: The imported MRPs assemble, together with mitochondrial rRNA, close to the nucleoid or RNA granules at the inner membrane to mature subunits. Finally, the subunits associate into the fully assembled mitoribosome and attach to the inner membrane close to the integrase Oxa1 (O).

1.4.1 Synthesis, stabilization and targeting of mitoribosomal proteins in the cytosol

Most of the mitochondrial proteins get synthesized as preproteins or precursor proteins on cytosolic ribosomes. To find their correct destination, the mitochondrial matrix, about 60% of all mitochondrial proteins carry a mitochondrial targeting information at their N-terminus called presequence or MTS (mitochondrial targeting sequence) [39 40]. This presequence is characterized by several common features such as an amphipathic α-helical structure (positive charges on one side hydrophobic amino acids on the other side of the helix), a length of approximately 15-80 amino acids [41] and a predominant but not exclusive localization at the N-terminus of the preprotein. A conserved pattern for presequences is not reported but the presence of rather positive charges and hydrophobic amino acids and the absence of negative charges are well established characteristics. Fusion of presequences of established matrix proteins to the N-terminus of non-mitochondrial proteins efficiently targets these proteins to the matrix [42]. This allows e.g. targeting of the green fluorescent protein (GFP) to mitochondria for microscopy-based localization studies.

Based on the common features of a presequence, computer algorithms such as TargetP have been developed and trained to predict the presence and length of a presequence on mitochondrial proteins or proteins that are assumed to be mitochondrial localized [43].

After synthesis, the preproteins get stabilized and kept in an unfolded, import competent state by chaperones of the Hsp70 and Hsp90 family [44]. Additional factors like co-chaperones and other factors might also be involved. The biochemical properties of the MTS help to localize the preprotein to the mitochondrial outer membrane and to the translocase of the outer mitochondrial membrane (TOM). This post-translational import process is well characterized by *in vivo* and *in vitro* studies for many mitochondrial proteins. Still, the existence of a co-translational import is under debate for many years and supported by studies showing the presence of mRNAs and cytosolic ribosomes on the surface of mitochondria [45 46].

1.4.2 Import of preproteins into the mitochondrial matrix

The first hurdle to be overcome on the way to the matrix is the mitochondrial outer membrane. The entry gate is the so-called translocase of the outer mitochondrial membrane (TOM). This complex is composed of three import receptors (Tom70, Tom20 and Tom22), the pore forming Tom40 [47], and the small Tom proteins (Tom5, Tom6 Tom7) [48]. The initial binding of the preprotein to the TOM complex is mediated by Tom20 via interactions with the hydrophobic surface of the presequence. The presequence is then handed over to Tom22, the central receptor for presequences, which binds to the positive surface of the amphipathic helix. Binding of the presequence stimulates channel activity of the β-barrel protein Tom40 guiding the presequence through the TOM complex into the intermembrane space. The function of the small Tom proteins is not entirely clear, but it is believed that they don´t actively contribute to the import process but rather help during assembly and stabilization of the TOM complex. In the intermembrane space, the IMS-facing receptor domain of Tom22 binds to the preprotein [49]. This receptor thus provides not only a cytosolic binding site for preproteins but also has a second binding domain in the IMS showing the central role of Tom22 during protein translocation into mitochondria. Next, the translocase of the inner mitochondrial membrane (TIM23 complex) helps to transfer the protein over the inner membrane into the matrix. During translocation of a preprotein TOM and TIM could in principle act independent from each other but it was shown that they form a presequence induced TOM-TIM23 super complex [50 51] . The receptor Tim50 binds to the presequence that gets handed over by Tom22. The channel through the inner membrane built by Tim23 and Tim17 opens upon preprotein binding to Tim50 and the protein can be transported through the TIM23 complex. The membrane potential $\Delta\Psi$ generated by the respiratory chain plays an important role during this translocation as its electrochemical gradient provides one of the two driving forces for the import and activates the Tim23 channel [52 53]. The second energy source is provided by adenosine triphosphate (ATP). This energy drives the presequence translocase associated motor (PAM) which is a crucial component of the import machinery [54 55]. Coupled by Tim44 to the Tim23 complex, the mitochondrial chaperone Hsp70 (mtHsp70) binds in an ATP dependent manner to the presequence [56 57]. The co-chaperones Pam16 and Pam18 regulate the hydrolyzation of ATP to ADP resulting in a tight binding of mtHsp70 to the preprotein. The nucleotide exchange factor Mge1 promotes release of ADP [58] which initiates a new reaction cycle of mtHsp70. Based on the Brownian ratchet model the preprotein gets pulled into the matrix by several rounds of mtHsp70 binding to the emerging presequence [59 60]. An interaction of the TIM23-PAM translocation machinery with the respiratory chain super complex III-IV was reported and provides an interesting import system linking the energy dependent import of preproteins to OXPHOS activity and energy availability. Once the presequence reaches the matrix it gets cleaved off by the matrix processing peptidase (MPP) [61] which is a dimeric protease in the matrix. Some proteins get further processed by Icp55 or Oct1 which cleave off one or eight additional residues, respectively [62]. Finally, soluble matrix

proteins get folded with the help of mitochondrial chaperones [63] and the mitochondrial chaperonin Hsp60 and Hsp10 [64] and are released from the TIM-complex (Figure 4).

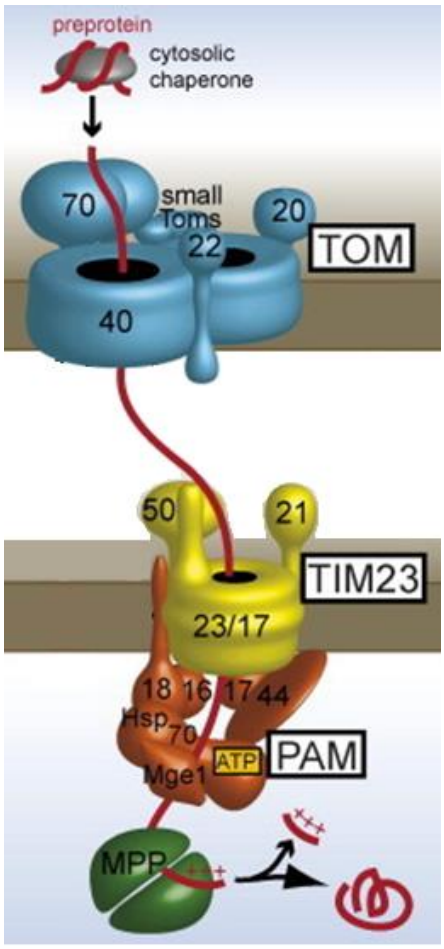

Figure 4: Overview of preprotein import into the mitochondrial matrix. Preproteins get stabilized by cytosolic chaperones and targeted to mitochondria. Interactions with the components of the TOM complex guide the preprotein through the import channel. Subsequently, components of the TIM23 complex bind the preprotein and translocate it into the matrix with the help of the PAM machinery. The mitochondrial peptidase MPP cleaves off the presequence releasing the mature protein (modified from Bohnert et al., 2007).

This import process of preproteins into the matrix is well characterized and understood to a large extend. It has been studied for many mitochondrial proteins in detail but for only 3 mitoribosomal proteins the import has been analyzed and characterized.

One protein that was studied in detail is bL32m (Mrpl32) [65]. This protein gets imported via the TOM-TIM23 super complex and is not matured by MPP in the matrix. Instead, the cysteines present in Mrpl32 have to coordinate a metal ion before it can properly fold. Then the membrane associated m-AAA protease removes the first 71 residues at the N-terminus. Mrpl32 proteins that are not properly folded get instead degraded by the m-AAA protease [66]. The m-AAA protease acts in this way as a quality control checkpoint for mitochondrial ribosome biogenesis.

Another example of a well-studied mitoribosomal protein is mS37 (Mrp10). After translocation through the TOM complex, Mrp10 interacts with the mitochondrial disulfide relay system and gets oxidized. This step depends on the activity of the respiratory chain complexes. The oxidized

Mrp10 is then imported into the matrix and can assemble into the mitochondrial ribosome [67]. This import pathway links mitoribosome biogenesis to the activity of the respiratory chain and can serve as another quality control mechanism for mitochondrial fitness and ribosome biogenesis.

The last example of studied mitoribosomal protein import is bS6m (Mrp17). This protein lacks a classical presequence but instead contains targeting information on the N-terminus, in an area of amino acids 30-60. Its import strongly depends on the membrane potential, but weather Tom receptors are necessary for import is not clear yet. An interaction with mtHsp70 also seems to be absent or negligibly weak (unpublished data).

The import pathways of Mrpl32, Mrp10 and Mrp17 differ a lot from the classical presequence carrying matrix proteins. Still it is unclear whether there were more special import mechanisms present and which additional factors might be involved in the import of mitoribosomal proteins. Future research will address these questions and probably discover more unconventional import pathways in mitochondria.

1.4.3 Mitochondrial ribosome assembly

The step of assembling the imported preprotein together with the mitochondrial made rRNA into a functional ribosome is still mysterious and subject of ongoing research. Important aspects of mitoribosome assembly are the maturation and post transcriptional modifications of the rRNA. Without these essential steps the ribosome formation would not be possible. The place where these steps occur is assumed to be close to or in RNA granules in mitochondria [68]. The RNA granules are found near the nucleoids which contain the mitochondrial DNA and thus are the source of mitochondrial rRNA. This proximity of mitochondrial nucleoids and mitochondrial RNA granules together with imported mitoribosomal preproteins could form a mitochondrial sub compartment for ribosome assembly near or at the inner mitochondrial membrane. Such a sub compartment could indeed make a lot of sense since the place of RNA transcription, maturation and assembly needs to be protected from RNA damage and degradation. Taking these processes together in one place makes it easier for the cell to properly assemble mitoribosomal proteins together with mitochondrial rRNA resulting in functional mitochondrial ribosomes.

In yeast it has been shown that assembly of the small mitoribosomal subunit occurs near the nucleoid. The GTPase Mtg3/Gep3 is found to be associated with the inner membrane near the nucleoid. Mutant strains lacking Mtg3 are unable to mature the 15S rRNA and therefore cannot assemble the SSU [69]. One reason that was hypothesized is fast delivery of fresh synthesized mRNA to the small subunit. This could help to stabilize and protect the mRNA from degradation. This hypothesis is supported by studies that identified additional mitoribosome assembly factors especially those involved in biogenesis of the large subunit close to RNA granules. The mammalian assembly factor DDX28 is involved in maturation of the rRNA by interacting with the 16S rRNA and thus contributes to LSU assembly [70].

DEAD-box RNA-helicases are well known assembly factors of bacterial and cytosolic ribosomes. The mitochondrial protein Mrh4 contains such a DEAD-box motive [71] and is thus a good candidate. Also, GTPases are well established factors involved in ribosome biogenesis. The mitochondrial GTPase Mtg1 is found to be involved in late stage assembly of the LSU [72]. Deletion of either of the two proteins mentioned leads to the accumulation of assembly intermediates that lack only few mitoribosomal proteins.

In general, cells lacking functional mitoribosomes tend to lose their mitochondrial DNA and thus the ability to build the respiratory chain complexes necessary for cellular respiration. This phenotype is surprising since mitochondrial translation is not needed for mitochondrial DNA stability and replication. On the other hand, cells that have defects in assembly of one subunit are often still able to build the other subunit. This suggests that the assembly of each subunit occurs independent of the other. When and how the small and large subunit assemble to a functional ribosome and whether an mRNA is already associated to the small subunit is still not clear.

The studies by Amunts et al. 2014 [21] and Desai et al. 2017 [24] that revealed the near atomic structure of the yeast mitochondrial ribosome helped to better understand the exact composition and architecture of the mitoribosome and the location of the different mitoribosomal proteins to each other and to the remodeled ribosomal RNA in the mature mitoribosome. This understanding was necessary to design new experimental studies to further elucidate the steps of mitoribosome assembly.

1.5 Aim of this work

The mitochondrial ribosome is a conserved enzymatic machinery among eukaryotic cells. The abundance of mitoribosomes compared to cytosolic ribosomes within a single cell is however very low. Also, the contribution of the mitochondrial encoded and on mitoribosomes synthesized proteins to the whole cell proteome is assumed to be less than 0,001% [73]. Still, the importance of mitoribosomes for cell homeostasis and energy metabolisms is obvious. Furthermore, many age-related diseases are connected to mitochondrial dysfunctions which are linked to translation defects and alterations in processes involved in mitochondrial protein synthesis. Thus, learning more about the mitochondrial translation machinery can help to understand the causes of diseases like leigh-syndrome and others.

The biosynthesis of mitochondrial ribosomes is thought to be a very complex process. For the cytosolic ribosome, the assembly process has been described based on studies with in vitro reconstitution experiments. For the mitochondrial ribosome such a system is not available, and it is difficult to imagine that such a system could be established.

In this work, this problem will be addressed by using an inducible in vivo system in yeast. The gene of the ribosomal RNA polymerase Rpo41 was put under an inducible promoter. With this system it is possible to control the production of the ribosomal RNA and thus of the mitoribosome biosynthesis. With the help of density gradient centrifugation and in vivo translation experiments the effects of switching off and on the mitochondrial translation system should be addressed. After establishing this tool in yeast, it should then be used in a mass spectrometry based “complexome profile” experiment. The resulting data can provide further insight into the process of ribosome biosynthesis, the composition of assembly intermediates and help to identify new, so far unknown assembly factors of the mitochondrial ribosome in yeast.

2. Results

The biosynthesis of mitochondrial ribosomes is a complex process that is difficult to address. In contrast to the cytosolic ribosome, an *in vitro* reconstitution system for investigation of the assembly pathway is not available. This might be caused by the fact that the mitoribosome is tethered to the inner membrane and already the initial assembly steps of involving rRNA and early binding MRPs were shown to take place in a state bound to the inner mitochondrial membrane.

Previous studies on mitoribosome biogenesis relied on mutant cells where different mitoribosomal proteins were knocked out and the assembly process thus was halted at a certain stage. Furthermore, biochemical approaches such as immunoblotting were applied to evaluate the results which only detected a small number of proteins. These studies thus were limited in several aspects and could not yield a full overview of the assembly process.

Therefore, the first step of the study was to establish an *in vivo* system in yeast where the biosynthesis of mitochondrial ribosomes is controllable by an inducible promoter of a single gene. A good candidate to choose for this system is the mitochondrial RNA polymerase Rpo41. The rRNA represents the scaffold of the whole ribosome and the assembly is prevented once Rpo41 and thus the rRNA is absent. The promoter used in this study is the promoter of the *GAL10* gene. The expression of *GAL10* strongly depends on the presence of galactose and leads to a fast and strong response of the promoter to galactose but is instead not expressed when glucose or other carbon sources are present. The endogenous *RPO41* promoter was replaced by homologous recombination. Together with the *GAL10* promoter, a *HIS3* cassette was brought into the yeast strain to select for the correct mutant cells (see Figure 5).

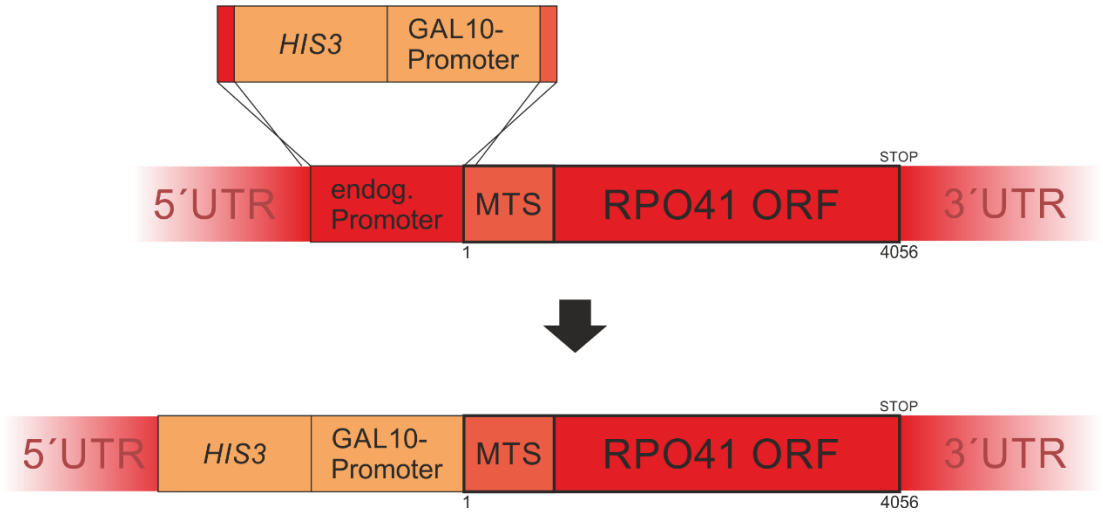

Figure 5: Homologous recombination strategy. The endogenous *RPO41* promoter was replaced by a HIS3-*GAL10*-promoter cassette via homologous recombination. Positive transformants were selected on agar plates lacking histidine.

2.1 Rpo41 is essential for physiological functions of mitochondria

2.1.1 Depletion of Rpo41 leads to respiratory deficient cells

With the *GAL10*-promoter construct introduced into the yeast strain the effect on cell growth was addressed. Yeast cells prefer growth on fermentable carbon sources like glucose where respiration is dispensable. On glycerol, yeast cells depend on the TCA cycle and the respiratory chain to metabolize this carbon source for energy production. Thus, cells from a culture with galactose and therefore with functional mitoribosomes should be able to grow when spotted on plates with glycerol as carbon source while cells from a culture with glucose should not. Indeed, the mutant strain was only able to grow on glycerol plates when the preculture was grown in galactose-containing medium, while the glucose preculture didn´t grow (Figure 6). On glucose plates all strains grew irrespective of their preculture´s carbon source.

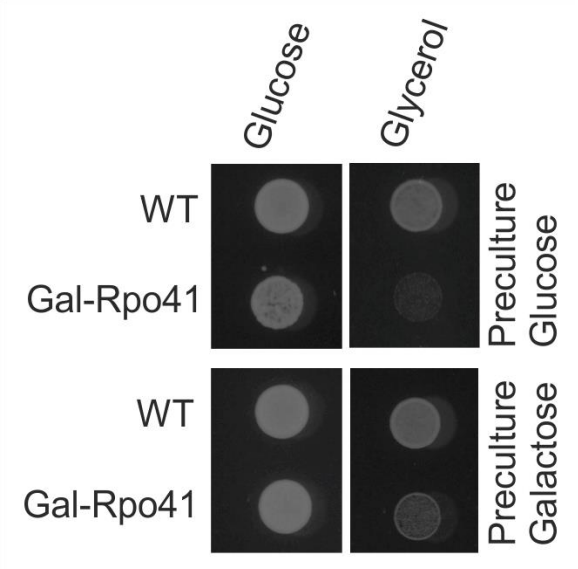

Figure 6: Cellular respiration is inhibited upon Rpo41 depletion. WT and Gal-Rpo41 cells were grown either in glucose or galactose medium for 48 h. 1 OD_{600} cells from logarithmic growing culture was harvested, washed with water and spotted on plates with glucose or glycerol as carbon source. Plates were incubated at 30°C for 48 h.

The results show that the downregulation of Rpo41 with the *GAL10*-promoter leads to a respiratory deficient phenotype. This fits to the assumption that depletion of the RNA polymerase leads to a depletion of all mitochondrial RNAs including mRNA and rRNA and thus loss of mitochondrial ribosomes. Without mitoribosomes, the core components of the respiratory chain cannot be synthesized and therefore the whole respiratory chain is defective. This results in the inability to grow on respiratory medium.

2.1.2 Mitochondrial translation can be efficiently controlled in the *GAL-RPO41* strain

To further address the effect of Rpo41 depletion on yeast cells, mitochondrial translation was monitored. To this end, an *in vivo* labeling experiment was performed. While the cytosolic protein biosynthesis was blocked by addition of cycloheximide, newly synthesized mitochondrial encoded proteins where labeled with [^{35}S]methionine. Cell lysates were subsequently separated by SDS-PAGE, transferred to a nitrocellulose membrane by Western blotting and visualized by autoradiography. The wild-type strain gave the characteristic band pattern for the eight mitochondrial encoded proteins in yeast on either glucose or galactose with only minor differences in band intensities for Cox3 and Atp8/Atp9 (Figure 7 left half). In contrast, the mutant

strain Gal-Rpo41 showed almost no translation products for the glucose culture. Only a few weak bands where detected probably arising from little mitochondrial mRNA and mitochondrial ribosomes left after Rpo41 depletion. The galactose culture instead showed the same translation pattern as the wild type with all eight proteins synthesized to a similar level as the wild type did on galactose (Figure 7 right half). This suggests that the expression of Rpo41 under control of the *GAL*-promoter leads to functional mitochondrial ribosomes and that the level of mitoribosomes seems to be comparable to the wild type situation as the protein synthesis is not affected.

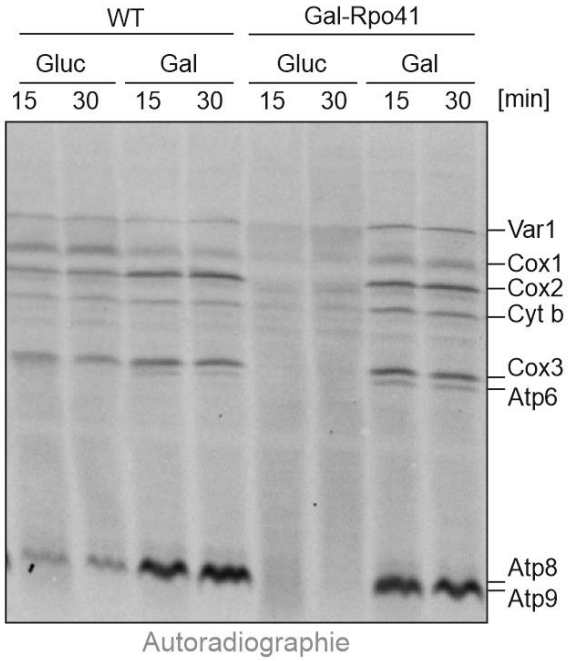

Figure 7: Mitochondrial translation correlates with Rpo41 expression. Cells of WT and Gal-Rpo41 were grown in glucose or galactose medium for 48 h. In logarithmic growth phase cytosolic translation was blocked with cycloheximide and mitochondrial translation products were labeled by addition of [^{35}S]methionine for 15 and 30 min. Samples were analyzed by SDS-PAGE followed by autoradiography.

To further investigate the effect of expressing Rpo41 under Gal-promoter on the levels of mitochondrial ribosomes and the mitochondrial rRNA, quantitative real-time PCR (qRT-PCR) was performed. The *GAL*-promoter is known for a strong expression of the respective gene when galactose is present. One question was therefore how the expression level of Rpo41 on galactose would be compared to the wild type on galactose which would serve as control conditions. Furthermore, it was not clear how the mitochondrial rRNA levels would respond upon changes in Rpo41 levels.

The transcription levels of Rpo41 were approximately 30-fold increased, compared to wild-type levels on galactose (Figure 8a). This is in line with former observations of gene expression under the *GAL10*-promoter where expression levels of 20 to 50-fold compared to the wildtype situation were observed. On glucose, Rpo41 levels where significantly reduced to ~20 % of the wild type. For the mitochondrial 21S and 15S rRNA no significant changes were observed in the Gal-Rpo41 strain on galactose. Both rRNA levels were comparable to the wild-type conditions with only a slight, not significant increase. On glucose, the effect of Rpo41 depletion on rRNA levels was remarkably strong. Both mitochondrial rRNAs were decreased to levels below 10% of the wild type (Figure 8b+c). This is in line with the results from the *in vivo* translation experiment where very little translation was observed for the mutant strain on glucose (Figure 6). The levels

of mitochondrial rRNA together with the translation defect suggest that the mitoribosomes are nearly completely depleted and therefore the mitochondrial translation is absent.

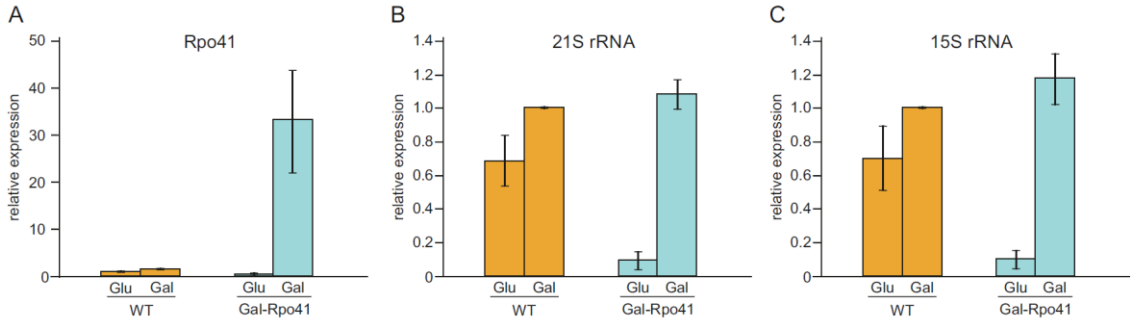

Figure 8: Mitochondrial rRNA levels are reduced upon depletion of Rpo41. Cells of WT and Gal-Rpo41 were grown in glucose or galactose medium for 48 h. Cells from mid-log phase culture were harvested, RNA was isolated, and cDNA synthesized. Gene expression was measured by qRT-PCR. The means and standard deviations from n=3 independent biological replicates are shown.

Interestingly, a reduction of *RPO41* mRNA and mitochondrial rRNA levels is also observed for the wild-type strain on glucose. Lowered levels of Rpo41 expression would also lead to decreased levels of mitochondrial rRNA. Furthermore, the glucose repression mechanism which in response to glucose as a carbon source reduces mitochondrial gene expression and biosynthesis and might contribute to the reduced levels of rRNA.

2.1.3 Rpo41 is essential for mitochondrial DNA-maintenance

The mitochondrial RNA-polymerase Rpo41 is not only needed to produce mitochondrial tRNAs and rRNAs but in addition synthesizes small RNA-primer molecules for mtDNA replication [74]. The depletion of Rpo41 could therefore also lead to a loss of mitochondrial DNA. To test this, the DNA of wild-type cells, Gal-Rpo41 cells and mtDNA-deficient cells (*rho*^{0} cells) were stained with 4',6-Diamidin-2-phenylindol (DAPI) and observed in a fluorescence microscope (Figure 9).

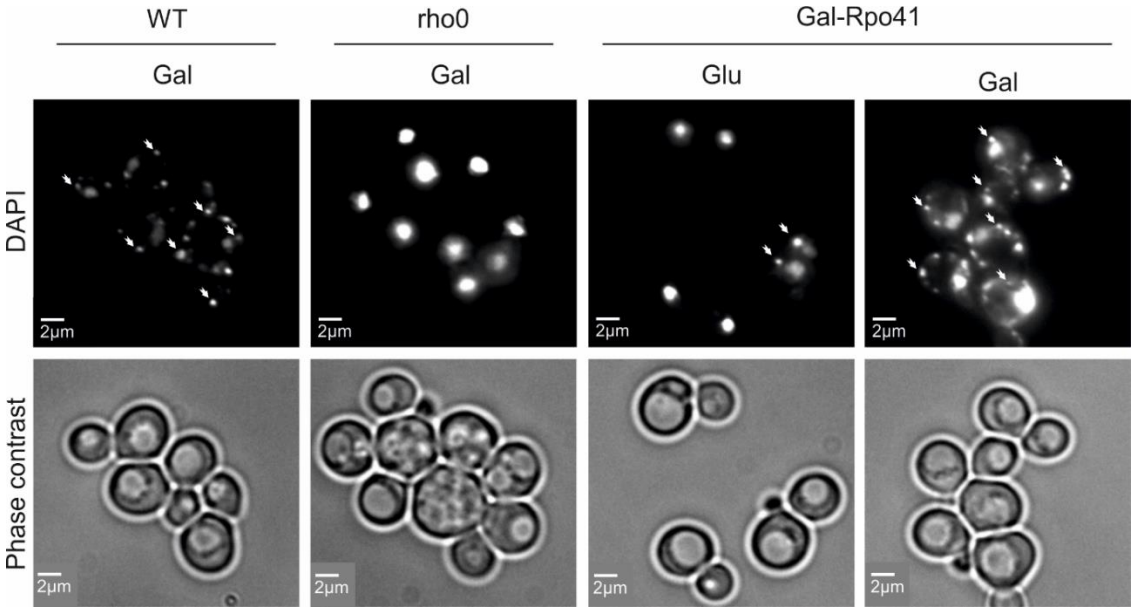

Figure 9: Rpo41 expression directly affects mtDNA levels. Cells were grown for 48 h in glucose or galactose medium as indicated to log phase. DNA was stained with 4',6-Diamidin-2-phenylindol (DAPI) and cells were observed by fluorescence microscopy.

The wild-type cells displayed an equal distribution of small DNA puncta which represent mitochondrial DNA (highlighted with arrows). In contrast, the rho0 cells only contained one prominent DNA structure which represents the nuclear genome while mtDNA was completely absent. For the Gal-Rpo41 strain grown on glucose the pattern was comparable to the *rho*^{0} cells. Many of the observed cells also contained only the nuclear DNA structure while in a few cells some mitochondrial DNA was still present (arrows). This confirms the assumption that depletion of Rpo41 on glucose directly affects the DNA maintenance and leads to a loss of mitochondrial genome. However, the observation that some cells still contained mitochondrial DNA suggest that a recovery might be possible and that the levels of mtDNA upon Rpo41 depletion can be restored. Cells of the Gal-Rpo41 strain grown on galactose displayed a pattern similar to the WT with an equal distribution of mtDNA puncta in all observed cells. Taken together, the results show a direct correlation of mtDNA maintenance with Rpo41 expression whereas increased levels of Rpo41 have no effect on mtDNA abundance. The data further suggest a certain time frame in which the processes of depletion and reinduction must take place since mitochondrial DNA cannot be recovered once it is completely lost.

2.2 Control of mitochondrial ribosome biogenesis in Gal-Rpo41 cells

2.2.1 Mitochondrial translation can recover from ribosome depletion

The previous results showed that the initial idea of generating the Gal-Rpo41 strain enabling a system to directly control mitochondrial ribosome biogenesis was successful. It was shown that upon depletion of Rpo41 by growing cells on glucose the mitochondrial rRNAs were significantly decreased and the mitochondrial translation machinery was efficiently depleted (Figure 7+8). To study mitoribosome biogenesis it is essential that the system is not only capable of shutting down the mitochondrial translation system but that the reverse can also take place. This would mean that a culture initially grown on galactose, shifted for a certain time to glucose for depletion of Rpo41 and loss of mitochondrial translation and then switched back to galactose would re-induce Rpo41 expression and finally mitochondrial translation. To address this hypothesis, a translation experiment was performed, and the mitochondrial translation was monitored by incorporation of radiolabeled [^{35}S]methionine followed by autoradiography. WT and Gal-Rpo41 cells were inoculated in galactose medium, shifted for 48 h to glucose and then brought back to galactose. Samples were taken after different timepoints of switch back to galactose, mitochondria were isolated, and the mitochondrial translation was monitored using an *in organello* translation approach (Figure 10).

For the wild-type strain, no major differences between different conditions and timepoints were observed. Although the translation seems to be most efficient when permanently grown on galactose, also the cells on glucose gave the characteristic 8 bands profile of mitochondrial translation in yeast with only slightly decreased signal intensities for Atp8/Atp9 as seen before (Figure 7). The samples of the time course after reinduction with galactose also showed a normal translation pattern with some minor differences for Cox1 and Atp8/Atp9 translation products.

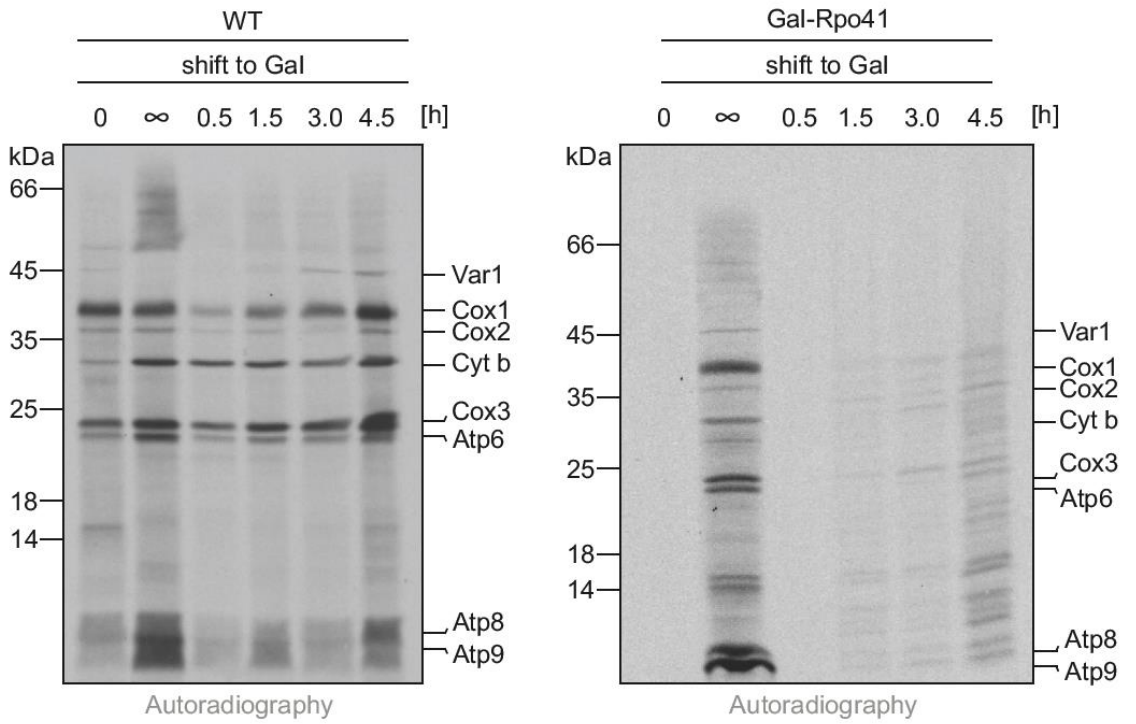

Figure 10: Mitochondrial translation partially recovers after reinduction of Rpo41. WT and Gal-Rpo41 cells were grown in glucose medium for 48 h to log phase and shifted to galactose for the indicated timepoints. Mitochondria were isolated from the respective cultures and mitochondrial translation products were labeled by addition of [^{35}S]methionine for 15 min. Samples were analyzed by SDS-PAGE followed by autoradiography.

The samples of the Gal-Rpo41 strain also confirmed some results observed before. The cells permanently grown on galactose gave a translation pattern like the wild type situation whereas the culture shifted for 48 h to glucose was unable to perform mitochondrial translation. The samples taken at different timepoints after shift back to galactose thus also showed impaired mitochondrial translation. After 30 minutes still no translation was visible. 1.5 h after reinduction faint signals were visible that get stronger after 3 h and 4.5 h but the pattern differs a lot from the normal translation products. Many smaller translation products can be observed that don´t correspond to any of the 8 mitochondrial encoded proteins. The source for these abnormal translation products could be not spliced or partially spliced transcription intermediates that got produced upon Rpo41 expression. The shift from glucose to galactose does not only lead to a reinduction of Rpo41 and therefore the mitochondrial ribosome but rather changes the whole cellular energy metabolism leading to increased mitochondrial biosynthesis and thus burdens the cell with many transcriptional and translational changes. Therefore, it is likely that adaptations to changed carbon sources have a big impact on cellular homeostasis which is best described during the diauxic shift of yeast cells when they change metabolism from fermentation to respiration. A WT cell can tolerate the shift from glucose to galactose and the metabolic changes associated with it, but in Gal-Rpo41 the recovery from depleted mitoribosomes and reduced mtDNA abundance increases the challenge for the cell to adapt to the new carbon source.

In order to compare the constitution of mitoribosomes in WT and Gal-Rpo41 cells upon reinduction by shift from glucose to galactose, density gradient centrifugation was applied and the migration pattern of mitoribosomal proteins of WT and mutant mitochondria was analyzed.

Mitochondrial lysates were loaded on continuous sucrose gradients, centrifuged in an ultra-centrifuge, split into equal fractions and finally analyzed by western blot (**Figure 11**).

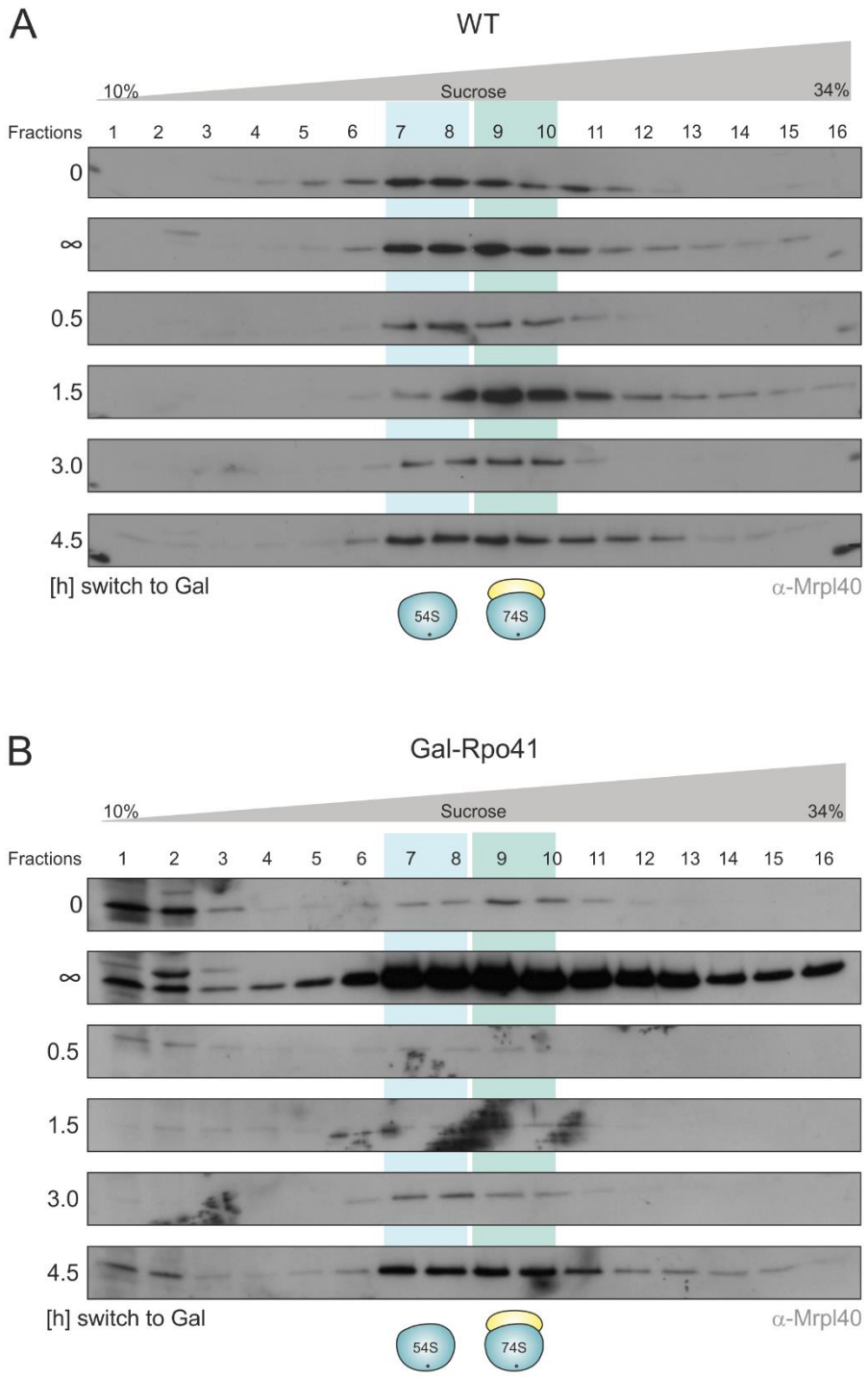

Figure 11: Mitoribosomal constitution is not altered in Rpo41 cells. Sucrose gradient sedimentation analyses of mitochondrial extracts prepared from WT and Gal-Rpo41 cells grown for 48 h in glucose medium and shifted to galactose for the indicated timepoints. Mitochondria were solubilized under low salt conditions, loaded on a linear 10-34% sucrose gradient and centrifuged for 4.5 h at 33,000 rpm in a Beckmann SW41 rotor. Fractions were TCA-precipitated and analyzed by Westernblot using α-Mrpl40 antibody.

Probed for uL24/Mrpl40 which is a protein of the large subunit, the migration pattern of the 54S subunit and the 74S mitoribosome were observed. The wild-type samples displayed an equal distribution pattern from fraction 6 to fraction 12 in all conditions, with the most prominent signal in fractions 8 to 10. The applied experimental conditions with low salt concentration promote a stable association of the small and large ribosomal subunits. Therefore, the migration pattern suggests that fractions 7 and 8 contain the free, soluble 54S subunits while fractions 9 and 10 contain the assembled 74S mitoribosome. The samples from Gal-Rpo41 mitochondria instead displayed results in line with the findings mentioned before. As seen in the translation time course experiment (Figure 10) samples taken from the strain grown on glucose were severely affected by the Rpo41 depletion displaying only very weak signals for the fractions that contain ribosomal subunits and assembled ribosomes in the WT. Instead, the soluble fractions 1 and 2 contained most of the probed protein indicating impaired mitoribosome assembly. The migration pattern of the sample continuously grown on galactose was comparable to the WT situation with signal peaks at fractions 8 to 10, speaking for normal ribosome constitution. However, signal intensity was much stronger and distributed over the entire gradient. This indicates problems in ribosome assembly which results in soluble mitoribosomal proteins in the fractions of lowest density, as well as aggregated forms of assembly intermediates found in fractions of high density. Upon reinduction with galactose for 0.5 h and 1.5 h, the signal was still very weak, in line with the poor translation observed in Figure 10. After 4.5 h the signal distribution and intensity recovered to a level comparable to the WT, but again signal was also observed for the fractions of lowest and highest density as seen in the continuously in galactose grown cells. These results support the hypothesis that ribosome assembly is affected.

2.2.2 Time of depletion is critical for recovery of the mitochondrial translation machinery

The previous results demonstrated that depletion of Rpo41 upon growth on glucose for 48 h efficiently eliminates mitochondrial translation and almost completely removes functional mitoribosomes. The reinduction of Rpo41 with galactose for 4.5 h recovered mitochondrial translation, but the ribosome assembly seemed to be partially defective, resulting in aggregated MRPs. Therefore, the question arose if the time of depletion is critical for the cells to recover. To address this question, a time course experiment was performed. Cells were shifted to glucose and the mitochondrial translation was monitored after different timepoints (Figure 12A). The wild-type strain was unaffected by the shift to glucose resulting in a normal translation pattern for all timepoints tested. The mutant strain was able to perform mitochondrial translation within the first 24h with no difference to the WT but then lost the ability to translate mitochondrial encoded proteins at timepoints 42 h and 48 h. A shift back to galactose after the 48 h timepoint resulted again in a partial recovery of the translation pattern within 4h of reinduction.

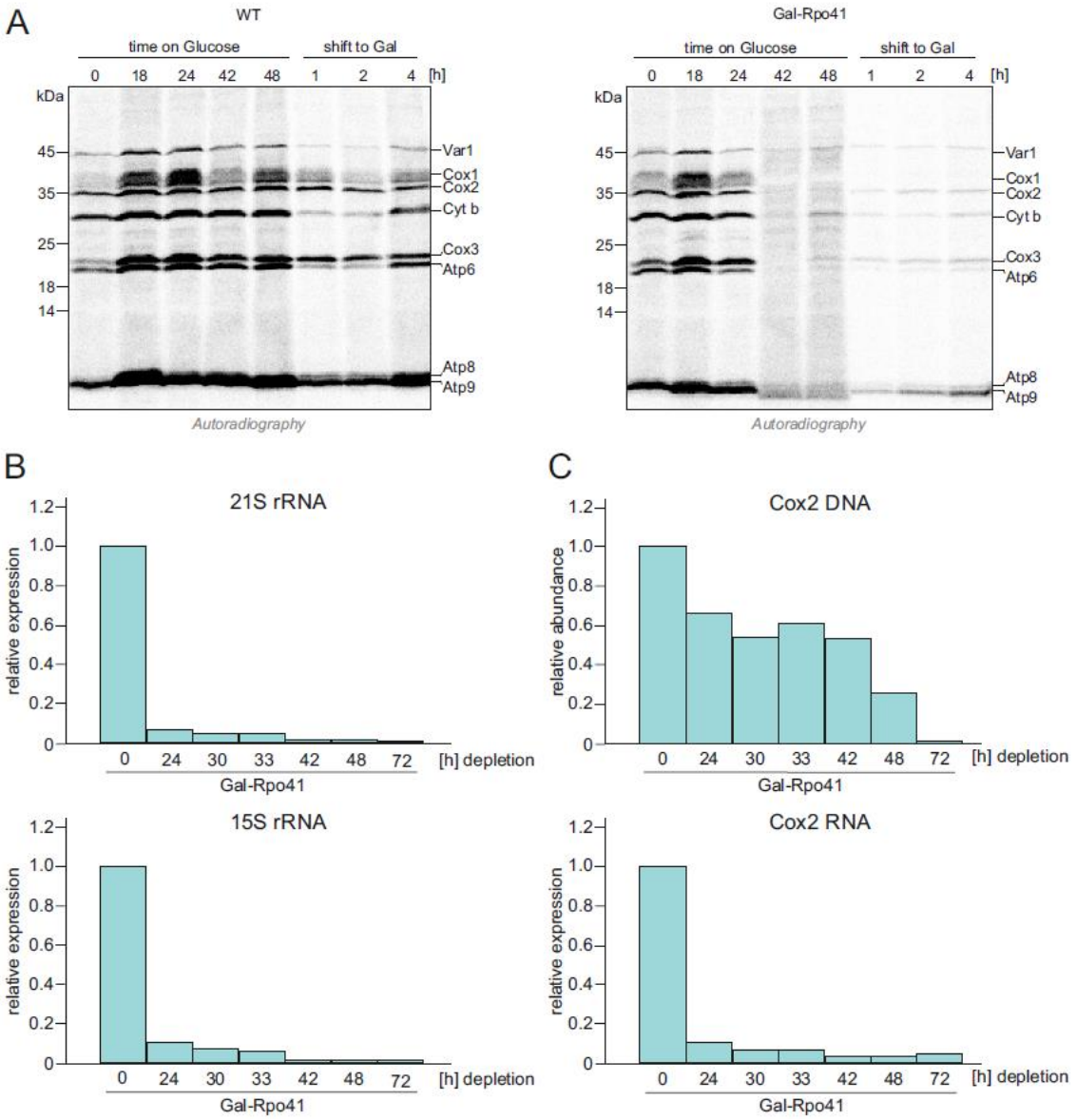

Figure 12: Period of Rpo41 depletion is critical. A: Cells were grown in glucose medium for the indicated timepoints or shifted after 48 h to galactose and further grown for the indicated timepoints. Cytosolic translation was blocked with cycloheximide and mitochondrial translation products were labeled by addition of [^{35}S]methionine for 15 min. Samples were analyzed by SDS-PAGE followed by autoradiography. B: Cells from mid-log phase culture were harvested, DNA and RNA were isolated and gene expression was measured by qRT-PCR.

In line with the loss of mitochondrial translation the mitochondrial 21S and 15S rRNAs and the mitochondrial *COX2* mRNA were significantly reduced within the time course (Figure 12B+C). The mitochondrial DNA monitored by the Cox2 gene decreased slower than the RNA but was also lost over time resulting in a *rho*^{0}-like situation as observed with microscopy (Figure 9). Taken together these results suggest a defined timeframe for Rpo41 depletion where mtDNA is still present and the mitochondrial translation machinery can recover from the depletion. Furthermore, the time frame for full recovery seems to be longer than 4 h and needs to be extended for further experiments.

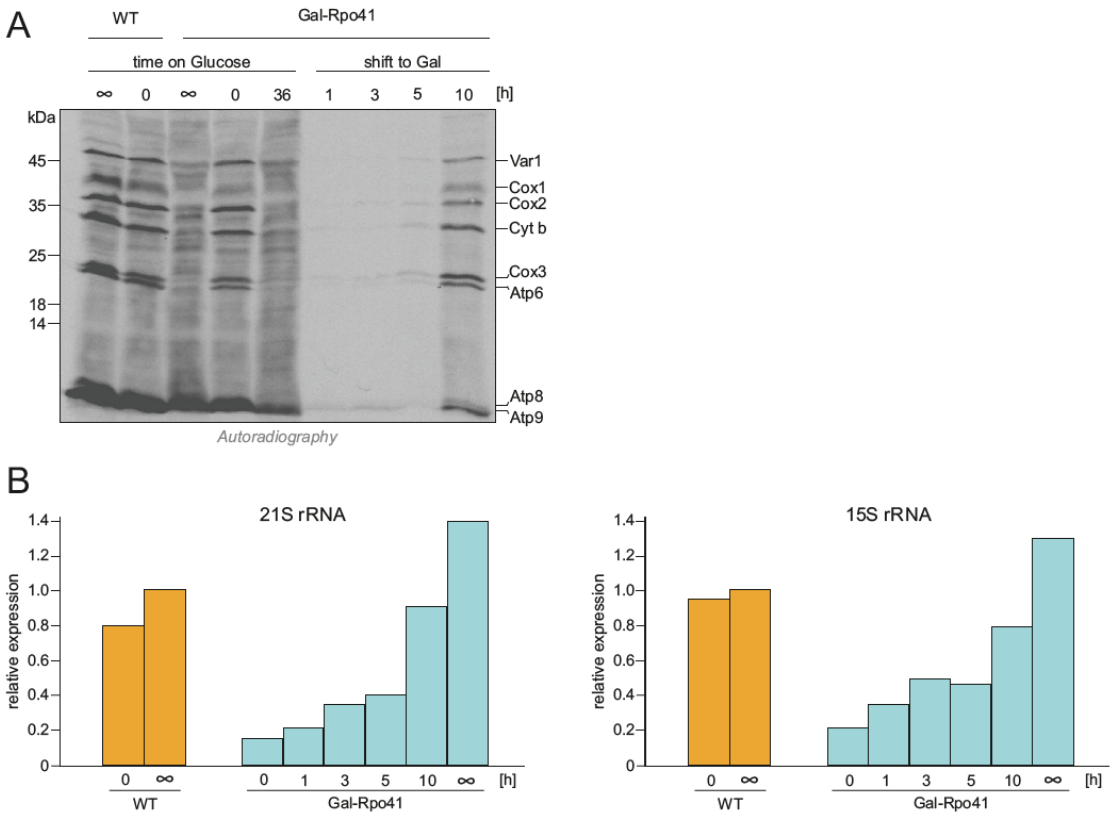

Figure 13: Defined depletion time ensures full recovery of mitochondrial translation and rRNA levels. A: Cells were grown in glucose medium for the indicated timepoints or shifted after 36 h to galactose and further grown for the indicated timepoints. Cytosolic translation was blocked with cycloheximide and mitochondrial translation products were labeled by addition of [^{35}S]methionine for 15 min. Samples were analyzed by SDS-PAGE followed by autoradiography. B: Mid-log phase culture grown for 36 h in glucose and shifted for the indicated timepoints to galactose were harvested, DNA and RNA were isolated and gene expression was measured by qRT-PCR.

Based on these findings, 36 h was chosen as the timepoint for Rpo41 depletion and the reinduction time was increased to a timeframe of 10 h. These parameters were tested by *in vivo* translation and qRT-PCR experiments. Under these conditions, the mitochondrial translation was strongly reduced upon Rpo41 depletion but recovered during the 10 h time course of reinduction to wild-type levels (Figure 13A). The mitochondrial rRNA was also significantly reduced but recovered during the timeframe to ~80% of WT (Figure 13B).

2.3 Complexome profiling reveals a building-block model for mitoribosome assembly

2.3.1 Establishing complexome profiling as a method to determine complex composition and assembly in mitochondria

With the previous results, it was shown that the Gal-Rpo41 strain established a powerful tool to manipulate the mitochondrial protein biosynthesis machinery. Depletion of Rpo41 efficiently decreased mitochondrial rRNA levels and impaired mitochondrial translation. Moreover, a recovery of the mitochondrial translation machinery and therefore of mitochondrial translation upon reinduction with galactose was observed. This strain was thus assumed as an appropriate tool to further study the mitoribosome biogenesis.

As mentioned in the beginning, former studies on mitoribosome biogenesis were limited in several experimental aspects such as immunoblotting and detection of only a small set of MRPs to collect their data. Therefore, Gal-Rpo41 mitochondria were used to generate complexome profiles in collaboration with the group of Prof. Ulrich Brandt in Nijmegen, Netherlands. This powerful technique monitors the abundance of proteins in a blue native gel by mass spectrometry. The gel is therefore cut into equal slices, in the following case into 60 individual slices, and proteins are measured by mass spectrometry for each slice separately. Plotting the abundances in a heat map followed by hierarchical clustering of protein groups based on similar migration patterns gives information about the composition and association of individual protein complexes found in these mitochondria (Figure 14). This technique thus delivers an overview over all known components of certain protein complexes and enables to search for new, unknown components.

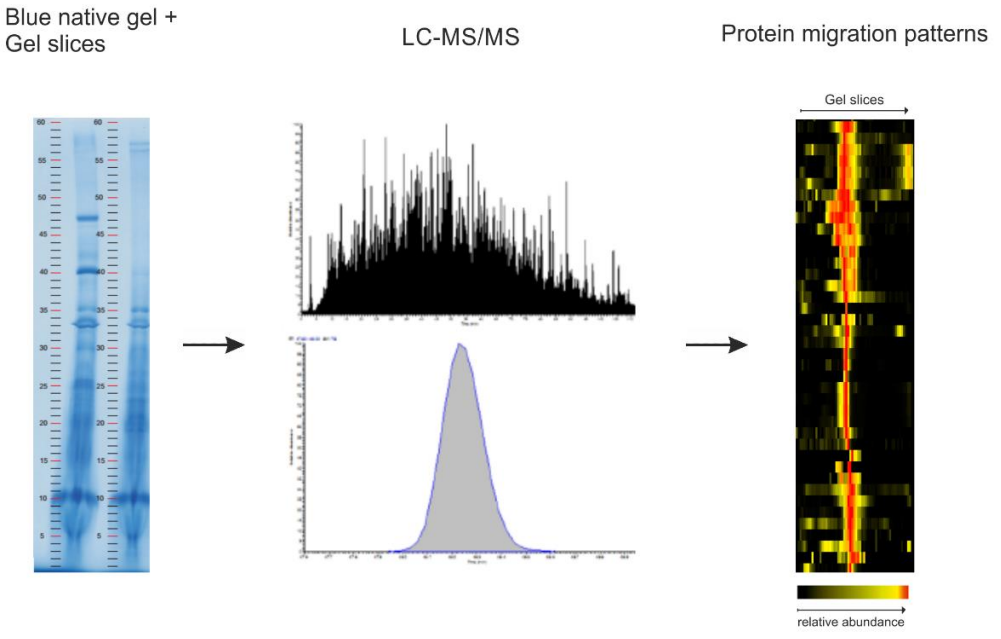

Figure 14: Schematic illustration of the workflow for complexome profiling. Protein complexes were separated via blue-native PAGE according to their size. The gel is cut into slices of even size and each slice is processed separately by in-gel tryptic digestion followed by mass spectrometry. Migration patterns can be reconstructed by combining the identified relative protein abundance from each individual MS analysis.

Gal-Rpo41 mitochondria isolated from a culture continuously grown on galactose were used as control samples and a complexome profile was generated. The profiles of the OXPHOS complexes II, III, IV and V were observed (Figure 15) to check if the applied experimental approach is suited to investigate protein complex formation in mitochondria.

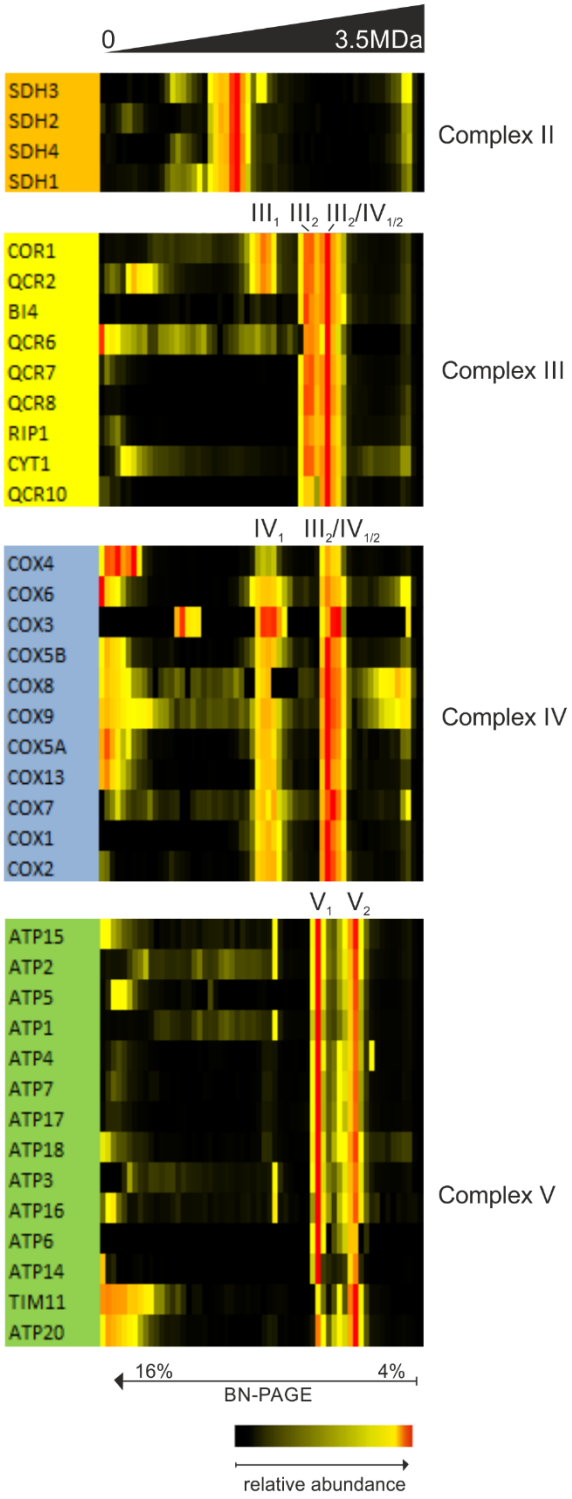

Figure 15: Complexome profiling heatmap of OXPHOS complexes II, III, IV and V under steady state conditions. The migration profiles of components of OXPHOS complexes were assembled manually and color coded by normalizing the relative abundance for each protein separately.

Complex II is composed of the 4 nuclear encoded proteins Sdh1-4 and was identified as a complex with a mass of approximately 135 kDa in line with the calculated molecular weight of 142 kDa. Components of complex III were found in two high abundance peaks reflecting the complex III dimer (III_2) of 490 kDa and the complex III/complex IV super complexes with either a III_2/IV_1 or III_2/IV_2 stoichiometry of 695 kDa or 900 kDa, respectively. The complex III monomer was only weak detected with signal for some proteins like Cor1 and Qcr2 indicating that the majority of complex III assembles either into a homodimer or a super complex with complex IV. Complex IV components thus displayed a similar migration pattern like complex III resulting in the complex III/complex IV super complexes III_2/IV_1 or III_2/IV_2. In addition, a stable complex IV monomer of ~205 kDa was detected and several components of complex IV namely Cox4, Cox5A/B, Cox6, Cox8, Cox9 and Cox13 were also found as soluble proteins in the low molecular weight range. Components of complex V were detected in both monomeric (600 kDa) and dimeric form (1200 kDa) with an equal distribution of approximately 1 to 1 ratio under these conditions. Former studies on complex V also describe the presence of both monomeric and dimeric forms and even oligomeric forms of complex V have been shown. However, the dimeric form has been described as the predominant form and the monomer was shown to be less abundant. This is in contrast with the finding of a 1 to 1 ratio in the complexome profiling and might have several reasons. However, the overall composition of the OXPHOS complexes is not altered and the samples thus can build the basis for further experiments. In summary, these observations reflect the steady state conditions of the Gal-Rpo41 strain grown on galactose and, concluded from the results shown before, assumed as a wild-type like situation.

Next, a time course experiment with Rpo41 depletion for 48 h followed by reinduction for 4.5 h was performed and complexome profiles for OXPHOS complexes were generated (Figure 16). Before reinduction (0 h) only complex II and partially complex V were present while complex III and IV were completely absent.

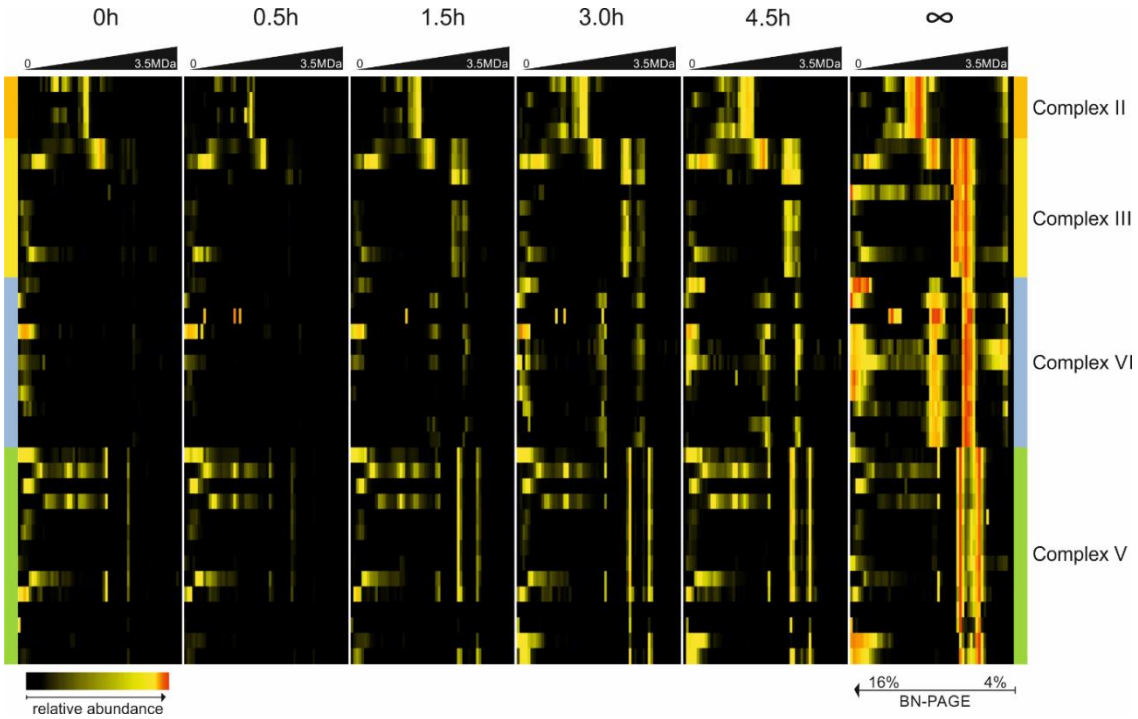

Figure 16: Complexome profiling heatmaps of OXPHOS complexes II, III, IV and V in a time course of 4.5 h of Rpo41 induction. The migration profiles of components of OXPHOS complexes were assembled manually and color coded by normalizing the relative abundance over control and all timepoints for each protein separately.

At timepoint 0.5 h no changes were observed compared to the 0 h sample. Complex III recovered upon reinduction within the 4.5 h timeframe with weak signals detectable already after 1.5 h. Complex IV was also reconstituted within the time course but to a lower level than complex III which is seen by very faint signals after 1.5 h and also still weak signals after 3.0 h of galactose induction. After 4.5 h, all complexes/super complexes are present, but the overall abundance is lower compared to the control condition (denoted with ∞). Complex V was already present before reinduction (0 h) as both monomer and dimer although with extremely low abundance. During the induction time the abundance increased comparable to complex III and IV. Taken together the complexome data of the respiratory chain complexes showed that Gal-Rpo41 cells grown on galactose medium exhibit normal OXPHOS composition with all known complexes and super complexes. Depletion of Rpo41 significantly diminished levels of complex V and complex III and IV were entirely absent. Upon reinduction of Rpo41 all respiratory chain complexes recovered to a similar extend but within the 4.5 h timeframe not to the steady state levels of the control sample. Complex II levels were also reduced upon glucose mediated depletion of Rpo41 but in contrast to complexes III, IV and V, complex II was still clearly present at timepoint 0 h. This fits to the circumstance that complex II is exclusively composed of proteins encoded by the nuclear genome. Complexes III, IV and V though contain core components encoded by mtDNA and thus are strongly affected by depletion of Rpo41. Therefore, it can be concluded that complexome profiling is an appropriate method to monitor complex formation in Gal-Rpo41 regulated mitochondria.

2.3.2 A stable subcomplex assembles during 37S biogenesis

Observation of the respiratory chain complexes in complexome profiles nicely showed the response of mitochondrial protein complex formation upon Rpo41 depletion and reinduction. Furthermore, the results showed that generating complexome profiles is a well-suited technique to monitor complex formation in a time course approach which is a prerequisite to study mitoribosome biogenesis. Therefore, the complexome profiles of mitoribosomal proteins were extracted from the dataset to assess the complex composition of mitochondrial ribosomes after Rpo41 depletion and reinduction. The steady state control conditions from the galactose culture were used and the MRPs of the 37S subunit were plotted (Figure 17). The peak of highest protein abundance represents the fully assembled small ribosomal subunit with a molecular weight of ~1.5 MDa. This is 400 kDa more than reported for the 37S subunit but might reflect the experimental inaccuracy of mass estimation from a BN-PAGE. Many 37S MRPs were also found with high abundance in low molecular mass fractions, indicating a pool of soluble, unassembled mitoribosomal proteins. Furthermore, a group of 9 proteins (Mrp2, Mrps9, Rsm7, Rsm10, Rsm23, Rsm24, Rsm27, Sws2 and Var1) was exclusively found at the 1.5 kDa peak of the fully assembled 37S. This might suggest a different role for these proteins during complex formation compared to the protein group that is also found in a potential soluble pool. However, an unexpected second peak of high protein abundance for a cluster of 6 proteins with a mass of ~200 kDa was found. This subcomplex of the 37S subunit is composed of Mrp1, Mrp4, Mrp51, Rsm18, Rsm25 and Rsm26, and is hereafter referred to as SC_{200} (subcomplex of 200 kDa).

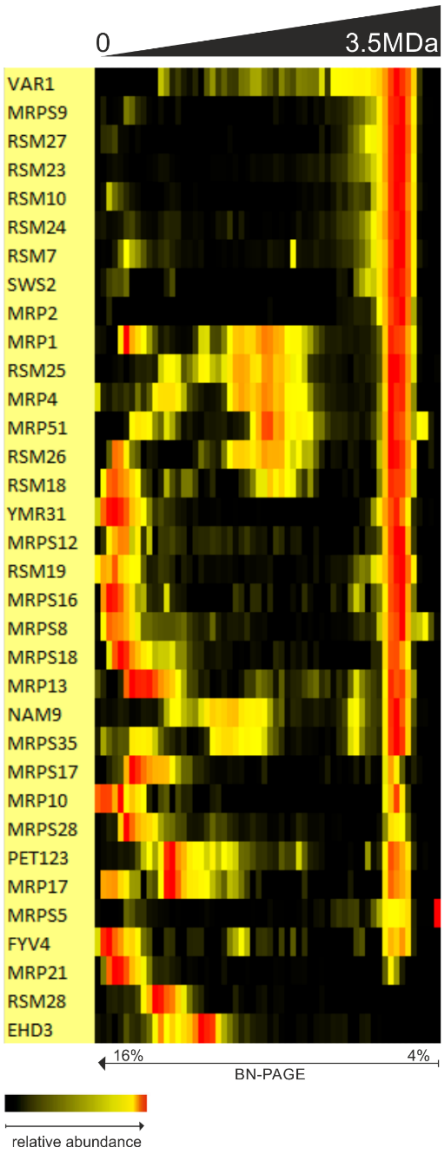

Figure 17: Complexome profiling heatmap of mitoribosomal proteins forming the 37S subunit under steady state conditions. The migration profiles of 37S MRPs were assembled manually and color coded by normalizing the relative abundance for each protein separately.

The finding of differently migrating protein groups and the SC_{200} under steady state conditions was an interesting observation and was further addressed. To this end, the data of the time course experiment with Rpo41 depletion for 48 h followed by reinduction for 4.5 h (shown for OXPHOS in Figure 16) were used to generate complexome profiles for the 37S MRPs (Figure 18). Upon Rpo41 depletion at timepoint 0 h the abundance of nearly all 37S MRPs was strongly reduced and the 37S peak as well as the 200 kDa subcomplex were entirely absent. After 0.5 h and 1.5 h of reinduction, only slight increases of abundances for the group that is found as soluble proteins and highlighted in red were observed. At 3 h, the signal for this group further increased and in addition, the SC_{200} appeared (proteins marked in yellow). After 4.5 h, also the peak for the fully assembled 37S subunit starts to emerge but is mainly seen for the protein group highlighted in green. This is a strength of the complexome profiling technique since the detection of some proteins of the 37S subunit at the 1.5 MDa peak indicates that all other 37S MRPs are also assembled into a mature 37S particle.

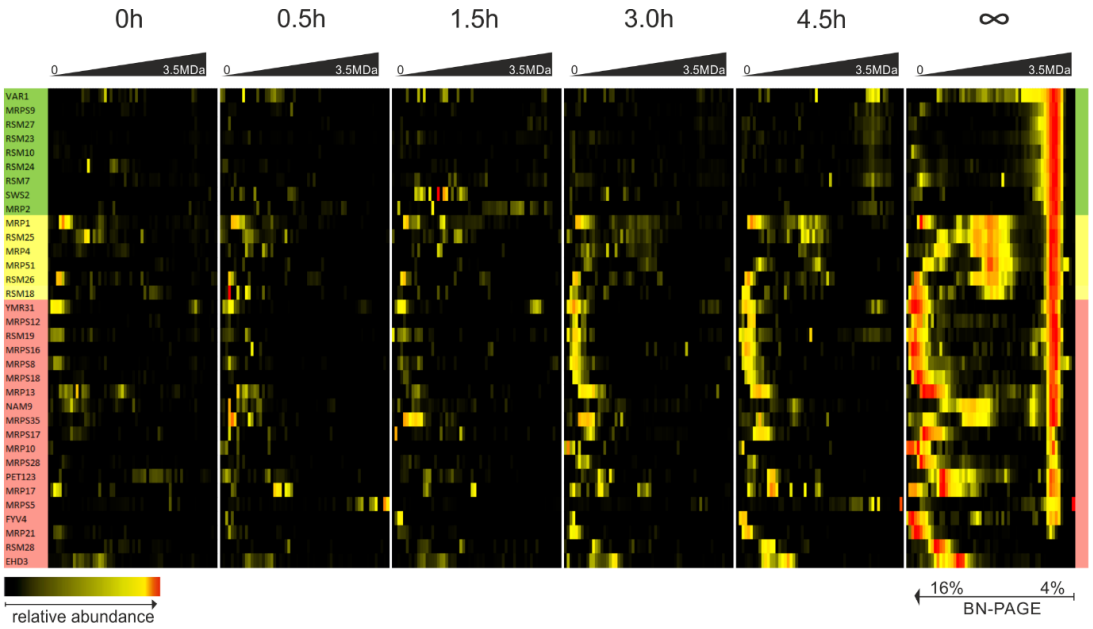

Figure 18: Complexome profiling heatmaps of mitoribosomal proteins forming the 37S subunit in a time course of 4.5 h of induction. The migration profiles of 37S MRPs were assembled manually and color coded by normalizing the relative abundance over control and all timepoints for each protein separately. Proteins were grouped based on their migration profile and colored regarding their respective group.

Otherwise the detected proteins would not migrate at the molecular weight of the assembled small subunit. The SC_{200} signal increases further at 4.5 h indicating that the involved MRPs predominantly assemble into the subcomplex rather than directly associating with a 37S assembly intermediate (Figure 19). All this together shows that the small mitoribosomal subunit is efficiently depleted upon glucose repression of Rpo41 and that reinduction leads to a partial recovery as suggested by translation experiments before. Furthermore, the MRPs that incorporate into the 37S subunit were classified into three different protein groups based on their migration pattern. In addition, a stable subcomplex was identified which is composed of proteins belonging to one of the classified groups and is also present under control conditions suggesting a direct function during 37S subunit assembly.

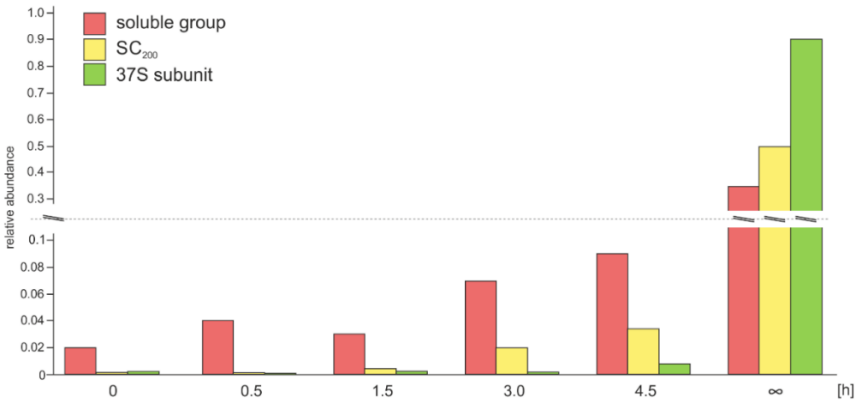

Figure 19: SC_{200} forms faster than the fully assembled 37S subunit during reinduction. The relative abundances of proteins from the soluble group, the SC_{200} forming group and the full assembled 37S subunit were summed to a mean value and plotted for every timepoint of reinduction. Please note that the y-axes is displayed discontinuously and highlighted by a dashed line.

The finding of the 200 kDa subcomplex was unexpected and not reported in former studies yet. Thus, it was interesting to see the exact localization of the proteins contributing to SC_{200} in the 37S subunit. To this end, the structure of the 37S subunit was modelled based on the structure published by Desai et al. 2017 using the UCSF Chimera software. The three protein groups identified in the complexome profiles were color-coded in yellow, green and red as shown in Figure 17. Indeed, the proteins forming the potential subcomplex, displayed as yellow spheres, are located in a cluster with broad protein-protein contacts among each other and additional protein-rRNA contacts. (Figure 20). Also, the proteins found exclusively in the assembled 37S subunit (green spheres) cluster together in the ribosome structure and seem to build a specific element of the small subunit. The proteins that were found either assembled in the 37S subunit or soluble in a free pool were depicted as red ribbons. These proteins are distributed all over the structure of the small subunit and display interactions among each other as well as to proteins of the other groups and to the 15S rRNA.

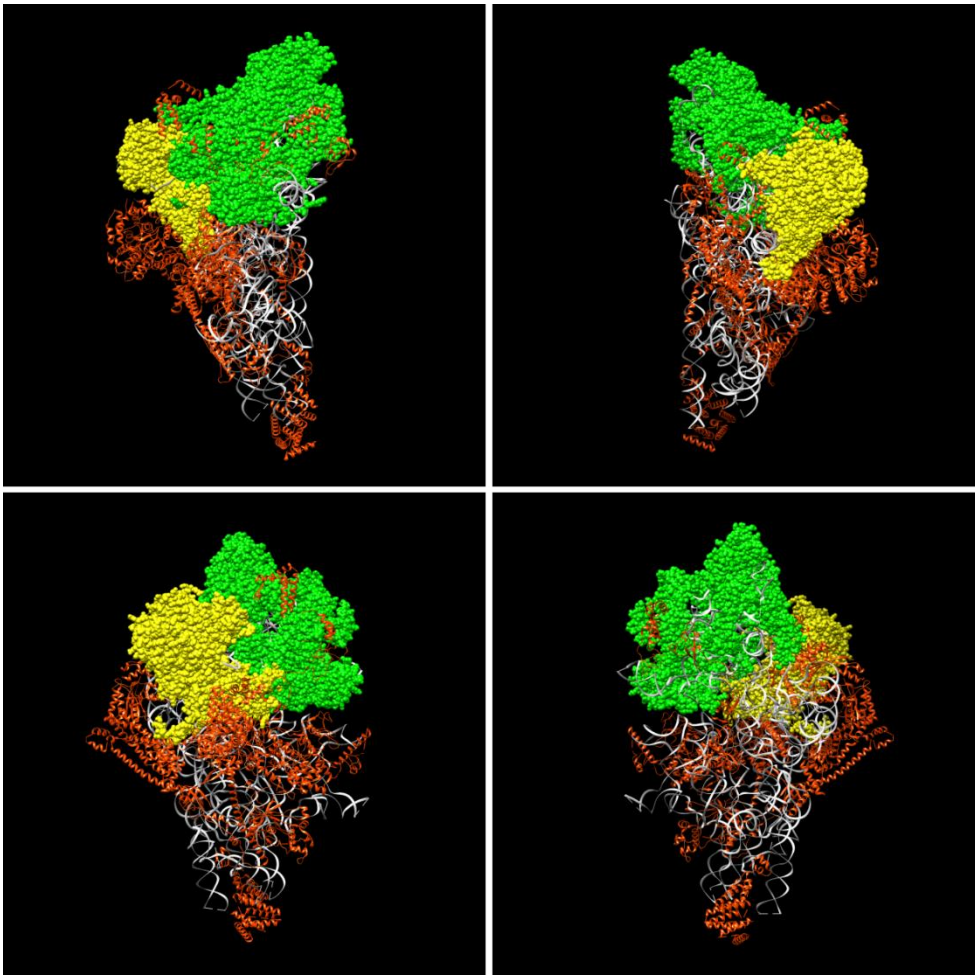

Figure 20: Structure of the 37S subunit. Protein groups assigned from complexome data were depicted as green and yellow spheres or red ribbons and the 15S rRNA is represented as grey ribbon (modified from Desai et al. 2017).

Taken together, these results suggest the existence of a so far undescribed subcomplex that is directly involved in the 37S subunit biogenesis, stably assembles under steady state conditions and forms initially during mitoribosome biogenesis before incorporation of the whole subcomplex into the assembling small subunit.

2.3.3 Characteristic structures of the 54S subunit are built by preassembled subcomplexes

The assembly of the large ribosomal subunit in yeast was recently described in a publication as a hierarchical incorporation of protein clusters and modules. Thus, it was of special interest to investigate the assembly pathway of the 54S subunit. To this end, complexome profiles were generated for the steady state control conditions from galactose culture and proteins of the large ribosomal subunit were plotted in a heatmap (Figure 21). As seen for the small subunit, a peak of high protein abundance was found representing the assembled 54S subunit with a mass of ~2.4 MDa. This molecular weight is approximately 500 kDa more than expected from literature but as already seen for the 37S subunit might reflect the experimental inaccuracy of mass estimation from a BN-PAGE. Another possibility would be the association of additional, so far unidentified proteins of the LSU that cause the increase in mass, although this case seems rather unlikely. Furthermore, many proteins of the 54S subunit were found in a second peak of high abundance with low molecular masses in a range of 15-30 kDa. This fits to the size of most of the yeast MRPs and suggests that these proteins are found in a soluble unassembled pool, in addition to their assembled state in the mature 54S subunit. A group of six proteins, Mrpl3, Mrpl15, Mrpl20, Mrpl23, Mrpl49 and Mrpl51 had no or only little abundance in the low molecular range and were mostly found in the 2.4 MDa complex. Of note was the migration pattern of Mrpl4, Mrpl27, Mrpl40 and Mrp20. In addition to their assembled state in the 54S peak they were found in a potential subcomplex of 124 kDa (SC_{124}) which matches the summed calculated molecular weight of these MRPs. A second potential subcomplex was built by Mrpl7, Mrpl11, Mrpl17, Mrpl28 and Mnp1 adding up to a molecular weight of around 130 kDa (SC_{130}).

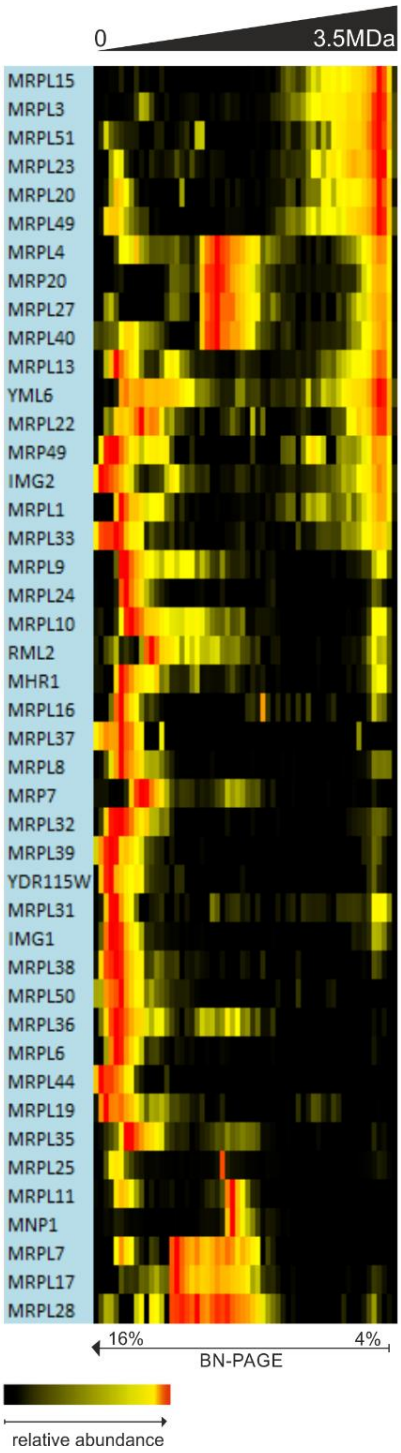

Figure 21: Complexome profiling heatmap of mitoribosomal proteins forming the 54S subunit under steady state conditions. The migration profiles of 54S MRPs were assembled manually and color coded by normalizing the relative abundance for each protein separately.

To follow the temporal assembly of the large subunit, the time course data were used to generate complexome profiles (Figure 22). At timepoint 0h the abundance of all plotted MRPs was strongly decreased and the peak for the assembled 54S subunit as well as the peak for the potential 124 kDa subcomplex was absent. The signal of the 130 kDa subcomplex was also significantly decreased, however it was still present to a minimal extend. Within 1.5 h of reinduction only slight increases of abundances were observed, most prominently for the group that is found as soluble proteins and highlighted in red. At 3 h the signal for this group further

increased and in addition the 124 kDa and 130 kDa subcomplexes slightly appeared (proteins marked in purple and green, respectively). At timepoint 4.5 h abundances of the protein groups red, purple and green further increased and also slight signals for the yellow group became visible indicating the presence of full assembled 54S subunits as the proteins of the yellow group were exclusively found in the 2.4 MDa peak of the assembled LSU.

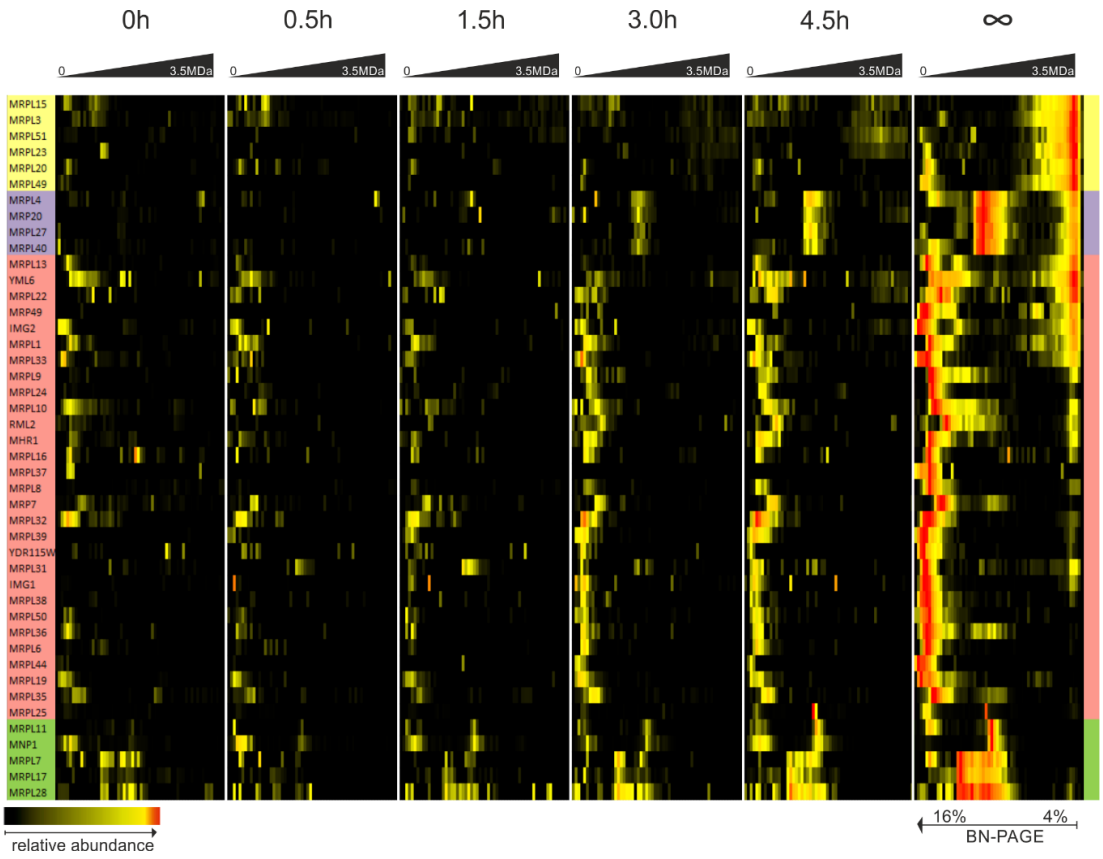

Figure 22: Complexome profiling heatmaps of mitoribosomal proteins forming the 54S subunit in a time course of 4.5 h of induction. The migration profiles of 54S MRPs were assembled manually and color coded by normalizing the relative abundance over control and all timepoints for each protein separately. Proteins were grouped based on their migration profile and colored regarding their respective group.

In summary, the data show that the 54S subunit is efficiently depleted upon Rpo41-repression and partially recovers at 4.5 h of reinduction. Furthermore, the MRPs of the 54S subunit were classified into 4 major groups based on the migration pattern observed in complexome profiles. Two of these groups seem to build stable subcomplexes, SC_{124} and SC_{130}, which both appear to assemble prior to their incorporation into 54S assembly intermediates (Figure 23).

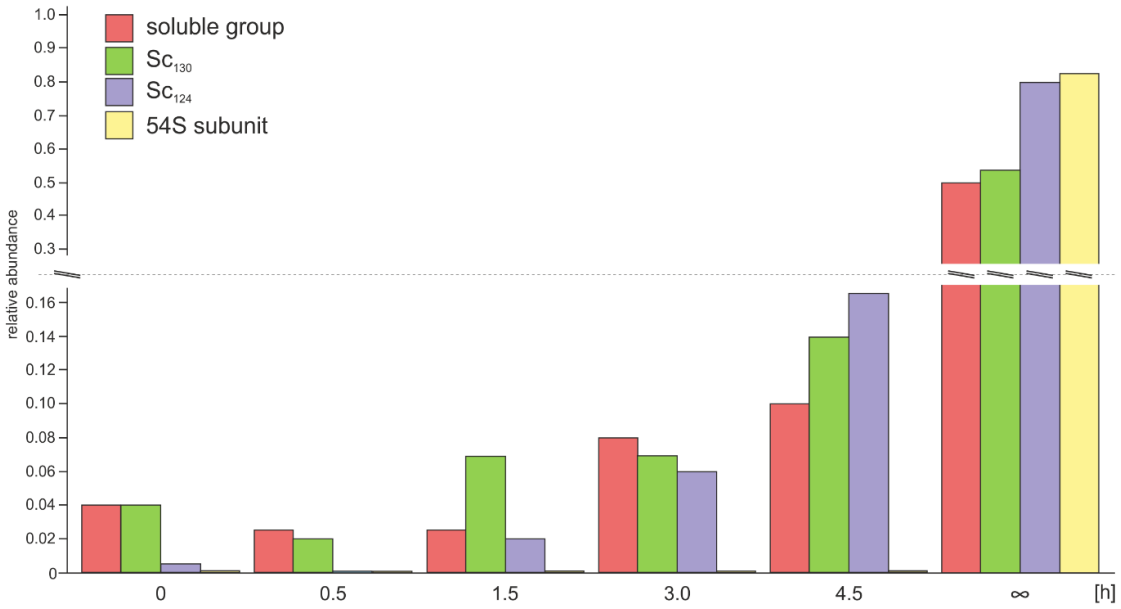

Figure 23: SC_{124} and SC_{130} form before the fully assembled 54S subunit emerges during reinduction. The relative abundances of proteins from the soluble group, the SC_{124} and SC_{130} forming groups and the full assembled 54S subunit were summed to a mean value and plotted for every timepoint of reinduction. Please note that the y-axes is displayed discontinuously and highlighted by a dashed line.

Zeng et al. described the assembly pathway of the large mitoribosomal subunit as a hierarchical process in which protein clusters were assembled prior to their incorporation into the 54S subunit [75]. The protein clusters found in the complexome profiles of the large subunit fit well to the proposed model and contain mainly the same proteins as suggested by the authors. Still, the role of these clusters in the structure of the ribosome and a potential function was not entirely clear. To address this question, the structure of the 54S subunit was modelled based on the structure published by Desai et al. 2017 [24] using the UCSF Chimera software and the localization of the protein clusters in the overall structure was analyzed. To this end, the respective proteins were highlighted in colors of their corresponding groups assigned to in complexome profiles (Figure 24). The proteins of the yellow, purple and green groups were displayed as spheres and all clustered together, each group in a different position on the 54S structure. The yellow group proteins, which are the ones predominantly found in the assembled state, represent the membrane facing protuberance of the mitoribosome which is involved in anchoring the subunit to the inner mitochondrial membrane. The proteins of the purple group, giving rise to the 124 kDa subcomplex, are found at the position where the protein exit tunnel of the ribosome is located. Finally, the proteins of the 130 kDa subcomplex (green group) most likely form the central protuberance of the LSU which is thought to be important for interactions between small and large subunit. The proteins that were found either assembled in the 54S subunit or soluble in a free pool were depicted as red ribbons. These proteins are distributed all over the structure of the large subunit and display interactions among each other as well as to proteins of the other groups and to the 21S rRNA.

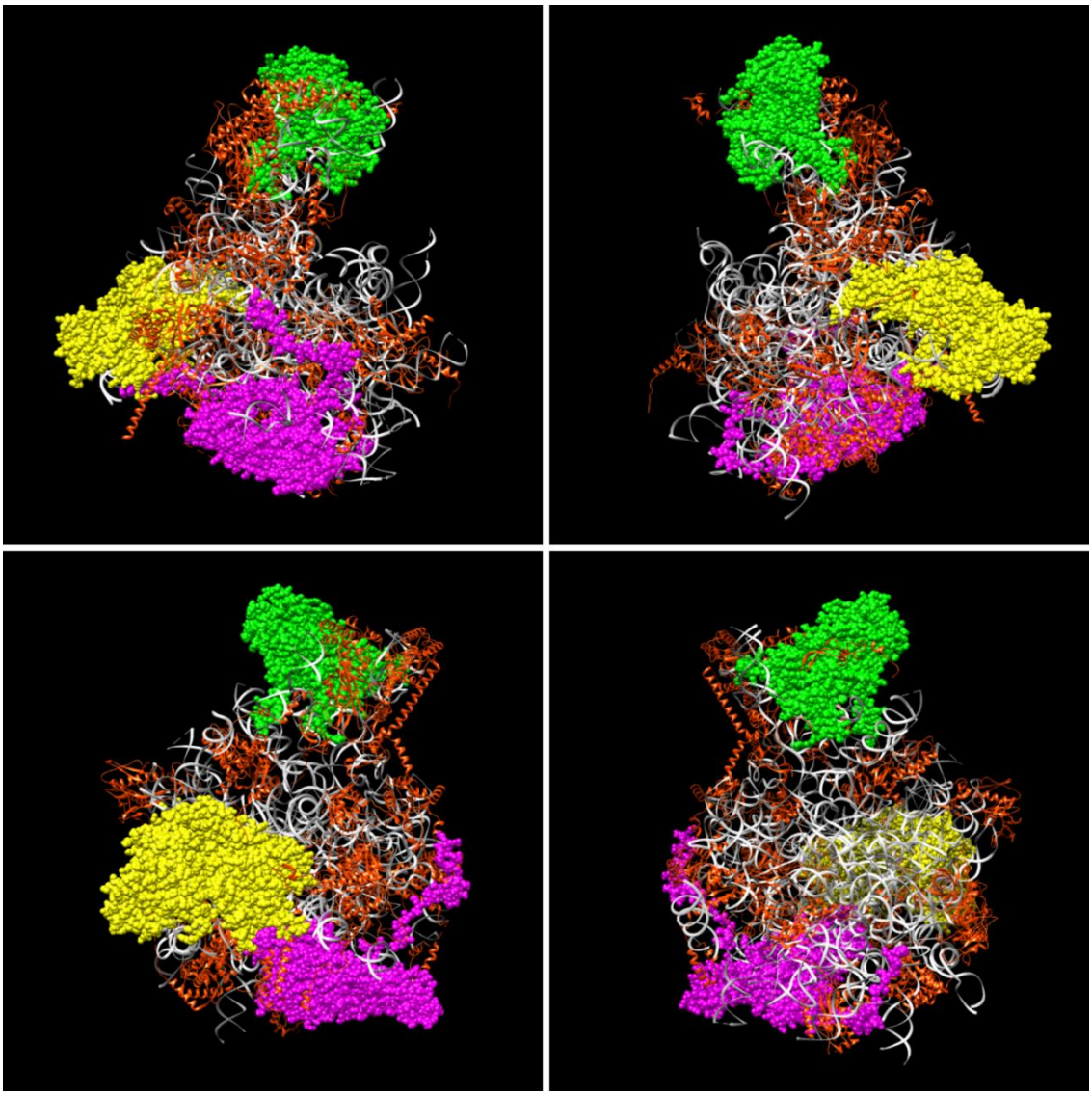

Figure 24: Subcomplexes SC_{124} and SC_{130} form characteristic structures of the 54S subunit. Protein groups assigned from complexome data were depicted as purple, green and yellow spheres or red ribbons and the 21S rRNA is represented as grey ribbon (modified from http://www.rcsb.org/structure/5MRC).

In summary, the presented results suggest the existence of two stable subcomplexes, each forming a characteristic structure of the large subunit, stably associating under control conditions, and forming initially prior to the assembly into the LSU. Furthermore, proteins forming the membrane facing protuberance were found almost exclusively in the assembled state suggesting a special role of this group during ribosome biogenesis.

3. Discussion

The aim of my thesis was to study the mitochondrial ribosome in yeast and in particular the process of mitoribosome biogenesis. To unravel this to date unclear process, I engineered a genetically modified yeast strain in which the mitochondrial RNA polymerase Rpo41 is under control of an inducible *GAL10* promoter. Reversible depletion of the RNA polymerase directly affects mitoribosome biogenesis since the mitochondrial rRNA builds the scaffold for ribosome assembly. I investigated the impact of Rpo41 depletion on the cellular and especially on mitochondrial physiology. Furthermore, I tested the response of cells in which Rpo41 was depleted for a certain time and then reinduced for different timepoints. Finally, I used the Gal-Rpo41 strain in a time course experiment of depletion and reinduction and analyzed the formation of mitochondrial ribosomes with a mass spectrometry based complexome profiling approach.

3.1 RNA processing and modification in mitochondria

The mitochondrial DNA in yeast encodes the RNA component of the RNase P (*RPM1*). Besides the mitochondrial encoded *RPM1*, RNase P consists of the nuclear encoded protein Rpm2 which is synthesized in the cytosol and gets imported into the matrix [76]dss. Thus, active RNase P is both dependent on cytosolic protein biosynthesis as well as the polymerase activity of Rpo41. Depletion of Rpo41 thus leads to multiple impaired processes in mitochondria which lead to much more complex impacts than simply a depletion of the mitochondrial ribosome. For example, impaired tRNA maturation caused by defective RNase P subsequently affects mitochondrial translation which results in impaired mitochondrial protein synthesis and thus defects in respiratory chain complexes.

In human patients several mutations in the mitochondrial tRNA gene *MT-TV* encoding for $tRNA^{Val}$ have been found causing mitochondrial disorders [77]. Nucleotide variants like G1606A affecting the acceptor stem of the tRNA, T1658C leading to changes in the T-loop structure of the tRNA or C1623T affecting a base pair in the dihydrouridine loop results in severe mitochondrial diseases. Clinical manifestations of mutations on mitochondrial $tRNA^{Val}$ include adult onset complex neurologic syndrome such as hearing loss, ataxia and dementia, multiple neonatal deaths and, in surviving children, Leigh syndrome or MELAS (mitochondrial myopathy, encephalopathy, lactic acidosis, and strokelike episodes) [78] [79]. In many of the patients suffering from $tRNA^{Val}$ mutations respiratory chain deficiency was observed indicating the direct effect of impaired mitochondrial translation on OXPHOS and subsequently, on a global view, the health of a patient.

The assembly process of mitochondrial ribosomes observed in Gal-Rpo41 with complexome profiling showed that it takes more than 4.5h to recover from Rpo41 depletion and reach mitoribosome levels comparable to steady state conditions. Upon reinduction of the RNA polymerase, the mtDNA gets transcribed from 11 distinct promoters [80], giving rise to the polycistronic RNA precursors as mentioned before. Thus, not only mitochondrial rRNA gets transcribed but also all the other RNAs needed for proper mitochondrial protein biosynthesis. This might be one reason why the recovery time is much longer than expected.

Ribosome formation in bacteria was shown to occur within minutes [81] [82] and a comparable timeframe was assumed to be sufficient for mitoribosome assembly. However, the recovery from Rpo41 depletion challenges the mitochondrial ribosome synthesis on several aspects and

thus seems to take much longer than the generation of ribosomes in bacteria like *E. coli*. Furthermore, rRNA processing and mitoribosome assembly might occur simultaneously and thus, components involved in both processes might compete with each other. In addition to the RNA processing, mitochondrial rRNA undergoes post-transcriptional modifications to form mature rRNA. In contrast to the cytosolic ribosomal RNA, the yeast mitochondrial rRNA is scarcely modified. For the 15S rRNA there is one pseudouridylation site [83] known and for the 21S rRNA there are three modification sites shown to be present [84 85]. These modification sites are located at the peptidyl transferase center (PTC) of the ribosome in a highly conserved region among human, mouse and gram-negative bacteria. This site has a functionally important role during peptide bond formation and indicates the importance of post-transcriptional modifications on mitochondrial rRNA. In contrast to the yeast 15S rRNA, the human 12S rRNA contains five methylations. Two methylated adenines (A936 and 937) locate at the 3´end of the RNA which is a region conserved in all domains of life. This region builds the mRNA decoding center and binding site for the LSU suggesting an important function for translational regulation. Knock out of the human methylase TFB1M which mediates these modifications leads to embryonic lethality as well as impaired ribosome assembly and consequently impaired translation in mitochondria [86]. These deleterious effects further indicate the necessity of correct maturation of the ribosomal RNA in mitochondria including post-transcriptional modification and processing. Spatial limitations could restrict access for modifying enzymes and assembly factors to the rRNA and therefore further increase assembly time.

In addition to the afore mentioned processes that influence the assembly time of mitoribosomes, the presence of the *VAR1* gene on the mitochondrial DNA encoding the small subunit protein Var1 might have an impact on the assembly time. Mitoribosomes can therefore be denoted as autocatalytic, since functional mitoribosomes are necessary to produce new functional mitoribosomes by synthesizing the mitoribosomal Var1 protein. A strong depletion of mitoribosomes like seen in the Gal-Rpo41 samples would thus lead to a long “lag phase” where only few mitoribosomes can be fully assembled. After some time, when more fully assembled mitoribosomes accumulate, the biosynthesis would be able to occur in a rapid “log phase” yielding higher levels of mitoribosomes. Thus, it is difficult to estimate the correct timeframe in which mitoribosomes assemble. Assuming that the assembly process is still comparable to the process in bacteria and considering that the mitoribosome is more complex than the bacterial ribosome, a time frame of minutes would still be likely to be sufficient for mature mitoribosome formation.

In Gal-Rpo41 yeast cells it is not surprising that depletion of the RNA polymerase has a direct impact on cellular growth and diminishes mitochondrial translation. However, it is astonishing that the cells can tolerate the time of depletion quite well without taking severe damage and recover after some time of reinduction, finally displaying a partially wild type like phenotype. The levels of mitochondrial DNA are comparable to the wild type in Gal-Rpo41 cells grown on Galactose as shown in Figure 9. However, cultures grown in glucose displayed a *rho*^{0}-like phenotype with almost complete loss of mtDNA. Reinduction of the Gal-promoter and therefore of Rpo41 enables the synthesis of mtDNA and could finally rescue the phenotype in these cells. Together with the observation that mitochondrial rRNA levels are also stable upon Rpo41 overexpression several possible mechanisms can be imagined. One possibility is that the levels of mtDNA and rRNA are balanced by degradation of excess copies of mtDNA and rRNA that are produced by elevated levels of Rpo41. The mitochondrial degradosome mtEXO as the main 3´-5´-exoribonuclease in mitochondria is responsible for RNA turnover and might rapidly degrade RNA molecules that are synthesized in excess by Rpo41. Another possibility would be that

elevated levels of RNA primer synthesized by increased Rpo41 levels might not necessarily increase DNA replication since other factors like the DNA polymerase might be limiting. Also possible is that RNA synthesis and DNA replication are controlled by additional co-factors of the respective polymerase such as Mtf1 which is known as a mitochondrial transcription factor interacting with the polymerase Rpo41 and mtDNA.

3.2 Being at the right place at the right time: Spatial distribution of mitoribosome assembly

A hallmark of ribosome biogenesis is the compartmentalization of this process. Biogenesis of cytosolic ribosomes starts in the nucleus where the rRNA initially gets transcribed. The assembly then proceeds in the nucleolus where ribosomal proteins and assembly factors, that initially got synthesized in the cytosol and then translocate to the nucleolus, assemble onto the pre-rRNAs to form pre-particles of the small and large subunit. Upon nuclear export, cytoplasmic maturation finally yields the mature 40S and 60S subunits which subsequently associate into translation competent 80S particles [87].

A breakthrough in understanding mitoribosome assembly was the identification of distinct foci in mitochondria where assembly takes places. The available data suggests that the nucleoid and the RNA granules are the hotspots where mitoribosomes are assembled. The nucleoid is a complex structure containing mitochondrial DNA and proteins involved in DNA maintenance, replication, and transcription [88 89 90 91]. Furthermore, mitochondrial RNA processing enzymes like RNase P and mitoribosomal proteins associate with nucleoids or foci close to nucleoids to initiate RNA processing and mitoribosome assembly [11]. RNA granules are found in close proximity to the nucleoid [92] most likely representing the foci where RNA processing enzymes and MRPs are also found [93]. RNA granules accumulate mitochondrial RNAs for processing, storage, sorting and translation [94 95 68]. The overlapping pool of proteins associated with either mitochondrial nucleoids or RNA granules reflects their proximity, the lack of membranous boundaries sealing these compartments and their connection during mitoribosome assembly. Labeling experiments of newly transcribed RNAs showed that many RNA granules co-localize with mitochondrial DNA within a short pulse time but after longer chase periods the stained foci become distributed randomly. Thus, assembly of mitochondrial ribosomes might initially start at or close to nucleoids possibly in a co-transcriptional process like in bacteria. Protein complexes like the fatty acid synthase (FAS) or the aminoacyl-tRNA synthetase have been shown to assemble in a co-translational process potentially due to high misfolding propensities of some subunits [96]. The co-transcriptional assembly initiation of mitoribosomes might reflect this problem for rRNA, that is prone to misfolding and degradation and thus gets stabilized by the initial binding MRPs to ensure correct folding. The assembly then proceeds in RNA granules where ribosome formation is completed. The sub-compartmentalization of this process in the matrix is thus reminiscent of cytosolic ribosome biogenesis and the RNA granules have therefore been proposed to be termed “the mitochondriolus” since they exhibit equivalent features of the nucleolus [70 97].

In the complexome profile of the time course experiment (Figure 18), assembly of the SSU seemed to occur faster and abundances of SSU MRPs seemed to recover stronger than observed for the LSU. Upon Rpo41 depletion, all mitochondrial RNAs are strongly reduced or even absent as seen with qRT-PCR analysis (Figures 8 and 12). Thus, also RNA granules are likely to be decreased or absent and need to be formed *de novo* upon reinduction of Rpo41. If assembly of the SSU proceeds further in nucleoids than the LSU, the dependence on RNA granules for mature

subunit assembly might be less compared to the LSU. A possible explanation for this interesting observation could be, that the RNA granules are absent upon depletion of Rpo41 which leads to a slower recovery rate of the LSU within the timeframe observed in the complexome profile compared to the SSU. In line with this proposed assembly process, taking place at the nucleoid and subsequently at RNA granules, proteomic studies found MRPs from both LSU and SSU to be present at nucleoids and RNA granules [11]. Primary assembly steps of LSU and SSU where shown to take place at the nucleoid and the assembly intermediate is then transferred to RNA granules. However, mitoribosomal proteins of the small subunit are more abundant in nucleoids than MRPs of the large subunit. This suggests that assembly of the SSU might progress further in nucleoids compared to the LSU assembly before intermediates get transferred to RNA granules.

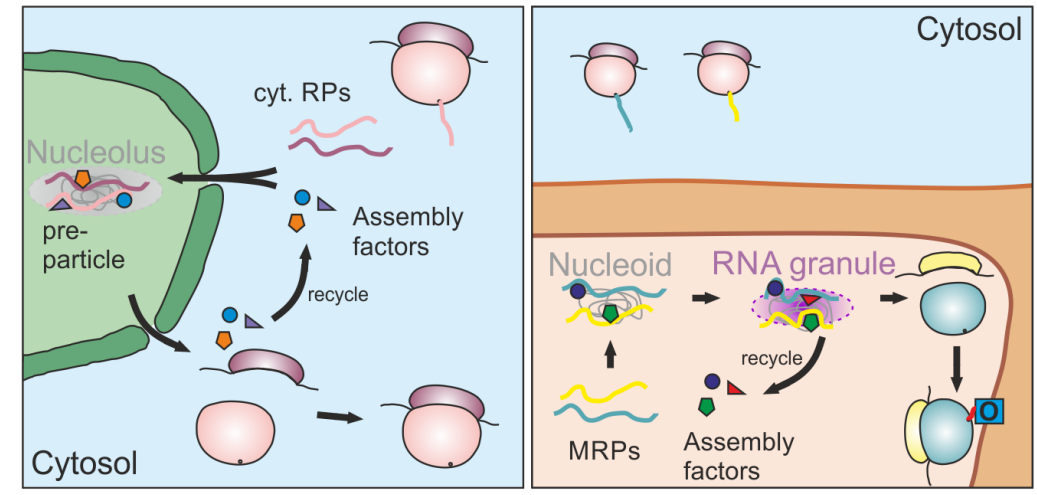

Figure 25: Schematic comparison of cytosolic and mitochondrial ribosome assembly. Cytosolic ribosome biogenesis starts at the nucleolus with formation of ribosomal pre-particles which are subsequently transported to the cytosol where assembly is completed. In mitochondria, mitoribosome assembly starts at the nucleoid and is finalized at or close to RNA granules.

The spatial distribution of assembly taking place at two subcompartments in the matrix might in addition prolong the assembly process. The transfer from nucleoid to RNA granule is so far not well understood [98] and it is not clear if this is an active, probably energy-driven process or passively occurs during assembly and which factors mediate this transfer. However, in contrast to the nuclear/cytosolic localization of the 80S ribosome assembly, the two subcompartments in the matrix are not separated by a membrane which makes it easier for assembly intermediates to diffuse/get transferred from one to the other assembly spot. Still, it is not clear how this transfer occurs, and it will be exciting to study the nucleoid/RNA granule assembly network in more detail in the future.

3.3 Temporal hierarchy and building block model for mitoribosome biogenesis

In yeast mitoribosomes, 26 of the 38 mtSSU proteins and 30 of the 46 mtLSU proteins are homologous to *E. coli* proteins. The remaining 28 proteins are mitochondria-specific MRPs found in yeast and higher eukaryotes. The 74S mitoribosome has a significantly decreased RNA to protein ratio (approximately 1:1) compared to bacterial ribosomes (~2:1). RNA such as the 5S rRNA has been replaced by mitochondria-specific MRPs mL38, mL40 and mL46, and structures like the central protuberance (CP) where extensively remodeled in the yeast mitochondrial ribosome, resulting in the triple volume of the bacterial CP. Furthermore, the polypeptide exit

tunnel is rerouted compared to the bacterial and cytosolic ribosome orienting the exit towards Oxa1, the insertase of the inner membrane, to facilitate co-translational insertion of the mitochondrial encoded proteins into the inner membrane. In addition, a membrane-facing protuberance composed of mitochondria-specific ribosomal proteins and rRNA extensions is formed tethering the mitoribosome to the inner membrane.

In the complexome data for yeast LSU formation, a group of proteins exclusively found in the assembled state was observed (Figure 22). This group is composed of the proteins uL13, bL21, mL43, mL44, mL57 and mL58 (group highlighted in yellow containing proteins Mrpl23, Mrpl49, Mrpl51, Mrpl3, Mrpl15 and Mrpl20). Except for bL21/Mrpl49 all proteins of this group are shown to be involved in forming the membrane facing protuberance binding the mitoribosome to the inner membrane (see structure model in Figure 28).

In vitro reconstitution of *E. coli* LSU assembly [99] indicated that the ribosomal proteins L4, L13, L20, L22 and L24 locate at the 5´end of the 23S rRNA and are essential for the formation of a first assembly intermediate from which the ribosome formation proceeds [99 100]. Studies on yeast 54S mtLSU assembly show that mitochondria-specific proteins mL43, mL44, mL50, mL57 and mL58 bind early on the 5´end of the 21S rRNA probably in a co-transcriptional manner and were shown to stabilize a mitochondria- specific expansion segment of the 21S rRNA. Mutant strains lacking either of the five proteins were further shown to lack 21S rRNA indicating a role in early assembly and stabilization of the rRNA. The proteins uL13, bL21, uL22, uL23 and uL24 bind immediately after the initial five proteins to a domain in the 5´end of the 21S rRNA suggesting being also involved in early assembly steps. The early binding mitospecific proteins mL43, mL44, mL50, mL57 and mL58 form the membrane-facing protuberance tethering the ribosome to the inner membrane, which is a hallmark of mitochondrial ribosomes in yeast. The formation of this characteristic structure of the yeast mitoribosome is followed by assembly of proteins similar to those that initiate ribosome formation in bacteria. This shows that the assembly process in yeast is extended compared to bacterial ribosomes and is caused by the remodeling of the yeast mitoribosome. After formation of this extended ribosome structure, the assembly pathway aligns with the bacterial assembly pathway [101].

These findings suggest that the early binding proteins, initiating the assembly process (yellow group in Figure 22), are only stable when bound to the 21S rRNA. If no assembly intermediate can be formed, these proteins are likely to be degraded by mitochondrial proteases as suggested by studies using mammalian cells. The authors showed that MRPs are synthesized and imported in excess and can be unstable and most likely will be degraded if not assembled into mitoribosomes. This might be part of a control mechanism in mitochondria to ensure proper ribosome formation. If the rRNA is depleted like in Gal-Rpo41 mitochondria, the initial binding proteins might get destabilized and degraded to avoid the formation of defective ribosome intermediates that would never mature into functional 74S particles but instead could cause proteotoxic stress due to misfolding and aggregation [102].

The proteins uL23/Mrp20, uL24/Mrpl40 are found in the complexome data together with uL29/Mrpl4 and mL41/Mrpl27 forming a subcomplex of 124kDa (purple group in Figure 22). These proteins form the polypeptide exit tunnel and are also shown to assemble in early steps of assembly. In contrast to the five initially binding proteins, which are exclusively found in the assembled state, these proteins seem to form a stable subcomplex prior to the incorporation into the LSU. This hypothesis is supported by the time course complexome data, where the formation of this subcomplex can be observed after 3h and 4.5h, whereas the mature 54S subunit is hardly detected at these timepoints. The presence of an rRNA independent protein

cluster composed of proteins forming the exit tunnel was also shown in cells lacking the mtDNA [103] supporting the idea of a building block model in which preassembled protein clusters assemble during ribosome formation.

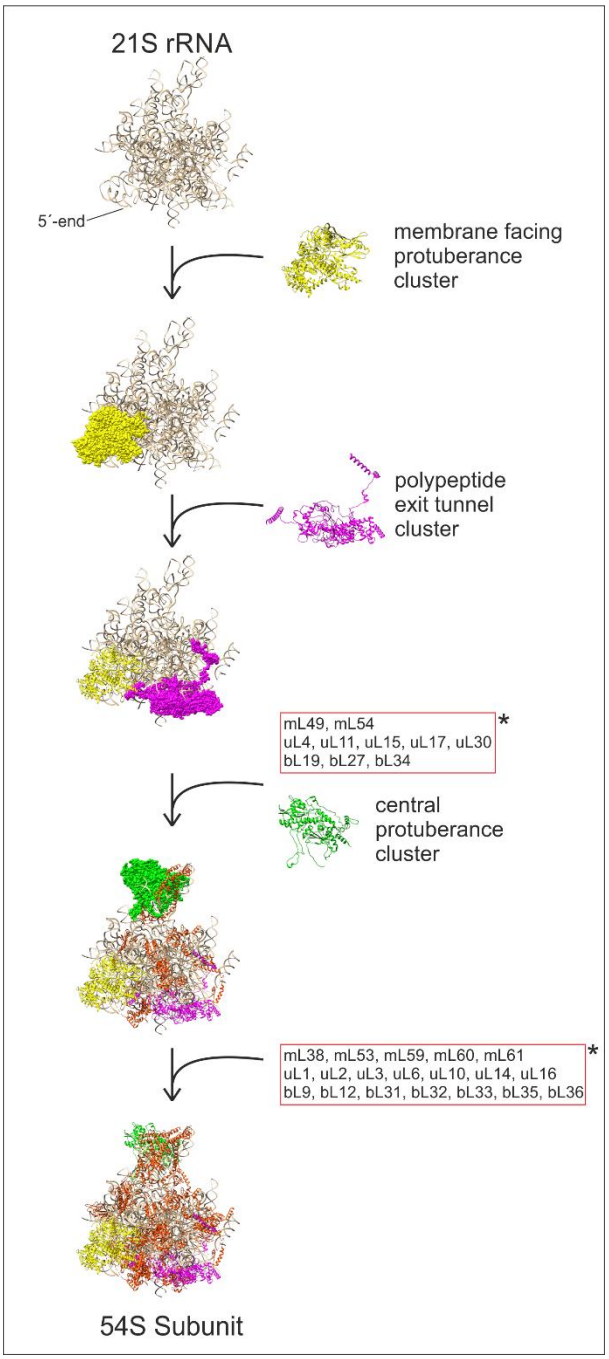

Figure 26: Building block model for ribosome assembly in yeast mitochondria. Schematic representation of proposed building block-based assembly pathway of yeast mitochondrial ribosome LSU. Asterisks indicate assembly steps based on Zeng et al. 2017.

A second building block of preassembled MRPs is built by the proteins uL5, uL10, mL40, mL46 and bL12 (Mrpl7, Mrpl11, Mrpl28, Mrpl17 and Mnp1; green group in Figure 22) forming a subcomplex of 130kDa. These proteins form the central protuberance of the mitoribosome and occupy the space where the 5S rRNA in bacterial is located. In contrast to the subcomplex of 124kDa, these proteins are also stable when the rRNA is depleted as seen in the complexome profile of Gal-Rpo41 mitochondria depleted for 48h (Figure 22 timepoint 0h). Stable clusters of

these proteins where also found in IP experiments and the cluster was only unstable in knock out mutants directly affecting proteins of the subcomplex [104]. Furthermore, it was shown that the proteins of the central protuberance assemble at later stages of mitoribosome assembly. The central protuberance resembles a functional site of mitoribosomes being involved in communication between small and large subunit. Thus, the assembly of this functional site at late stages keeps the area where the CP locates in an unstructured and nonfunctional state. Only after correct assembly of the CP cluster, the LSU can mature into a functional 54S particle. This prevents incompletely assembled subunits from translation activity and thus ensures that only mature 74S ribosomes facilitate protein synthesis in mitochondria. One of the very last functional elements to mature during assembly of "modern ribosomes" is the PTC. This late maturation of the PTC has also been observed in bacteria like *B. subtilis* [105]. Thus, the late maturation of this highly conserved region in ribosomes throughout the different domains of life represents a common feature of ribosome biogenesis. In addition to the late incorporation of the CP subcomplex seen in yeast mitoribosome assembly this process might protect the cell from incompletely assembled and unmatured ribosomes and further ensure that only fully functional ribosomes participate in protein synthesis.

The incorporation of preassembled protein clusters into assembling complexes seems to be a feature that occurs frequently in mitochondria. Guerrero-Castillo et al. [106] showed that complex I assembly is facilitated by incorporation of subassemblies that mirror the modular architecture of complex I. Although the respiratory chain complexes do not contain RNA molecules that build the scaffold of the complex, they contain mitochondrial encoded core protein subunits that are essential for the formation, stability, and function of the complex. Therefore, parallels to the assembly of the mitoribosome can be drawn. The fact that the modular assembly process is found in both complex I and the mitoribosome suggests that it is beneficial for the cell to build these big protein complexes in a building block-based event.

Formation of these building-blocks prior to their incorporation into the ribosome might have several beneficial and important functions. First, the MRPs involved in building these subcomplexes might be unstable if unassembled and present as soluble single proteins in the matrix, as suggested for the initially binding proteins. It is also shown that protein complexes are less vulnerable to proteotoxic stress [107]. Once the proteins are assembled in subcomplexes prior to their incorporation into assembly intermediates they get more resistant to unfolding and degradation caused for example by heat stress. Formation of a preassembled subcomplex and interaction with the binding partners early after import into the matrix could therefore stabilize the proteins and protect them from degradation. Furthermore, the subcomplex would ensure the presence of a larger set of proteins necessary at a certain timepoint during assembly. This could therefore lead to faster assembly than it would be possible if the proteins would attach to the assembly intermediate independently one after the other. Also, during stress situations when stress responses lead to reduced cytosolic and mitochondrial translation [108] the building-block based assembly of the mitoribosome would allow a faster recovery by quickly building up new mitoribosomes once the cell has overcome the stress situation. A second function of the proposed building-blocks could be the folding of the rRNA. By assembling a number of MRPs at one step the rRNA can fold at a larger area than with a single protein binding to it. The folding of the rRNA is thought to occur in a 5´-3´direction during early assembly steps but subsequent assembly steps may not follow the 5´-3´transcription direction and proceed in a more disorganized way. Thus, parts of the rRNA may be exposed to damage causing molecules like reactive oxygen species (ROS) or degrading enzymes for a certain time during transcription.

The assembly of a subcomplex could therefore protect and subsequently fold these stretches of RNA and by this ensure functional mitoribosome formation.

The remaining proteins of the LSU found in the complexome profile in the group of either soluble or assembled proteins (Figure 22 group red) are distributed all over the structure of the 54S subunit. They assemble at different stages of the assembly process and locate predominantly on the surface of the large subunit. This supports the idea that MRPs of both the small and large subunit are present in a soluble pool in the matrix and that this pool supplies ribosome assembly intermediates with unassembled mitoribosomal proteins. Knock-out strains of many of these proteins were shown to retain partial or complete translation capacity indicating that they are dispensable for functional mitoribosomes. What could be their role then? It is tempting to speculate that these proteins might perform other functions on mitoribosomes such as regulatory functions. It is reported that mitochondrial translation is supported by translational activators specific for each mitochondrial encoded gene. Thus, peripheral proteins might serve as binding partners for the translational activators ensuring delivery of the appropriate mRNA to the mitoribosome. This hypothesis is supported by findings of uncharacterized densities in cryo EM studies on mitochondrial ribosomes [18] that could represent these translational activators. The peripheral MRPs could furthermore contribute to translational accuracy or structural stability by stabilizing the ribosome structure.

In a study on bacterial ribosome assembly the authors observed parallel pathways of ribosome biogenesis when depleting an early binding ribosomal protein of the large subunit bL17 [109]. The authors hypothesize that the different pathways of assembly might occur in parallel in a cell and might ensure that blockage of a particular pathway for example by temporal limitation of a ribosomal protein or misfolding of the rRNA can be compensated by alternative pathways until the bottleneck can be relieved. For yeast mitoribosomes such a flexible assembly pathway has so far not been described. The work by Zeng et al.[75] admittedly used MRP deletion strains to dissect the LSU assembly. But in contrast to the work in bacteria they didn´t apply cryo-EM to elucidate the structures of the intermediates that they generated by knocking out individual MRPs. Instead, they used proteomic approaches to identify the composition of the incomplete assembled subunits. Clustering of their data lead to a model of assembly in which steps of early, intermediate, and late assembling proteins were assigned. Still it is possible that such alternative or parallel assembly pathways exists. The import of MRPs into the matrix and supplying them in a sufficient amount during mitoribosome biogenesis is a challenge for the cell and could easily cause stalled or prolonged assembly once this balance is disturbed. Thus, especially for mitoribosome formation such parallel assembly pathways would be greatly beneficial for the cell and might be conserved from bacteria to eukaryotes. It was further shown that some components of the LSU in bacteria depended on bL17 incorporation, including some MRPs and rRNA interactions and that they must form or incorporate downstream of bL17. This fact implies that the assembly is still hierarchical in some regards and might not be completely flexible. This is most likely caused by key points during assembly like folding or modification of highly conserved rRNA domains and can not be circumvented at some point.

Unfortunately, the approach of depleting and re-inducing Rpo41 to follow mitoribosome formation by complexome profiling used in my study is also limited in resolving these potentially existing parallel and flexible assembly pathways. The presented building block-based assembly model might also compete in parts with the parallel assembly hypothesis since the subcomplexes already bear several MRPs that would assemble simultaneously and thus restrict the flexibility of assembling the MRPs involved in building the subcomplexes. Still, the assembly of the very early binding MRPs of the yellow group as well as the later and peripherally binding

proteins of the red group would be candidates for flexible assembly steps. The initial binding proteins are thought to be essential to stabilize the rRNA in a co-transcriptional manner and generate a first stable assembly intermediate. Using several parallel pathways could therefore ensure the proper formation of this first intermediate. The assembly of the peripherally located MRPs might have less importance for functional ribosome formation as suggested by remaining translation competence of knock out strains of these proteins. Thus, a flexible assembly of the MRPs during late assembly steps would also be beneficial for the cell and for final maturation of the mitoribosome.

The knock-out of ribosome assembly factors in bacteria has often little or no effect, thus indicating that they are nonessential. Still they participate in maturation of the essential ribosome. The parallel assembly pathways might explain this finding, indicating that they are partially redundant and assembly steps can be shifted to alternative pathways. This would also suggest that the nonessential co-factors are most likely involved in steps that are comprised of efficient folding and assembly processes. However, essential assembly factors would then be involved in the key points of ribosome formation that represent complicated and error prone folding kinetics, explaining why they are not dispensable. In yeast, also many assembly factors are nonessential as knock-out strains are still viable but lose the ability to respire. Thus, the so far identified co-factors might predominantly be involved in key points of mitoribosome formation that cannot be accomplished by parallel pathways. An interesting question therefore is if in yeast mitochondria additional assembly factors participate in mitoribosome formation, probably also during the hypothesized parallel pathways or weather these processes can be conducted without the help of such co-factors.

Taken together the findings presented in the complexome data not only confirmed the knowledge about the initial assembly steps but extended the available information of later assembly steps by showing the presence of preassembled building blocks that form prior to their incorporation into the assembling mitoribosome. These building blocks form characteristic structures of the yeast mitochondrial ribosome that are not found in bacteria and might demonstrate how the mitoribosome diverged from its bacterial ancestor during evolution.

3.4 Import of the exceptionally large protein Rpo41

The mitochondrial RNA polymerase Rpo41 is a nuclear encoded single subunit enzyme with a molecular mass of 153 kDa. The N-terminus carries a mitochondrial targeting sequence of approximately 30 amino acids and gets imported most likely via the TOM-TIM23 pathway. Based on studies by Morgenstern et al. [110] the protein abundance is ~60 copies per cell what renders Rpo41 a rather rare protein in the cell . Nevertheless, it still fulfills a very important function in mitochondria [74]. Thus, a proper and efficient import of Rpo41 into the mitochondrial matrix is crucial for the cell to maintain mitochondrial homeostasis. Furthermore, upon re-induction of Rpo41 in the Gal-Rpo41 strain, a proper import and functional polymerase activity of Rpo41 is the basis of healthy mitoribosome assembly and subsequently of many of the experiments conducted with this strain. Thus, it is interesting to understand the underlying import mechanisms and consider possible problems occurring when expressing Rpo41.

The TargetP based analysis tool iMLP (iMTS-L predictor service) provides information about potential import signals within the amino acid sequence of a protein[111 43 112]. Backes et al. [113] showed that mitochondrial proteins exhibit internal mitochondrial targeting sequence-like structures (iMTS-L) in addition to their N-terminal presequence which are recognized by

Tom70/71 and increase the import efficiency. The model protein Atp1, which is a subunit of the ATP synthase or complex V, displays three iMTS-L structures at position 160, 315 and 400. Deletion of these stretches strongly decreased the import of Atp1. When applying the iMTS-L predictor tool on the amino acid sequence of Rpo41, only one considerable iMTS-L peak at amino acid 570 can be found (Figure 25). Rpo41 consists of 1351 amino acids which is almost 3-fold the size of Atp1. Still, Rpo41 contains only one iMTS-L structure that might increase import efficiency with the help of Tom70/71 while Atp1 contains three.

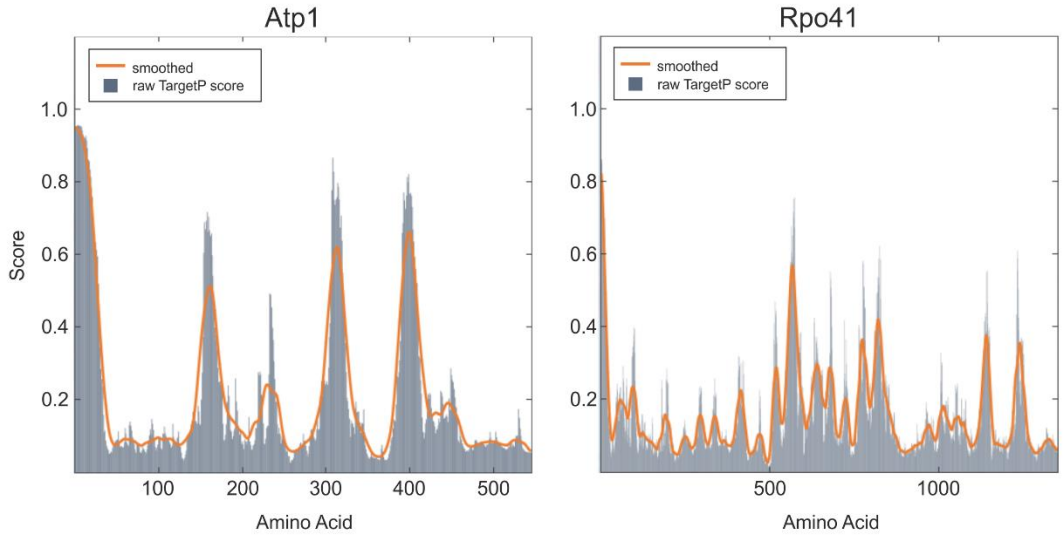

Figure 27: iMTS-L structures in Atp1 and Rpo41. TargetP profiles of Atp1 and Rpo41 were shown as raw TargetP scores and smoothed graphs.

This is remarkable since it was shown that many mitochondrial and also non-mitochondrial proteins contain iMTS-L structures which the cell might have made use of by "inventing" the Tom70/71 receptor that recognizes these structures and increases import efficiency. Especially large proteins might have a higher tendency to premature folding of specific domains which can stall import inside the translocase [114] [108] [115]. Thus, such a large protein like Rpo41 would be a wonderful candidate to exhibit several iMTS-L structures to ensure proper mitochondrial import. However, there is only one potential structure in Rpo41 that could facilitate iMTS-L function and it would need further investigation to clarify if the import efficiency is actually increased by the iMTS-L structure and the help of Tom70/71 or whether it is dispensable for proper import. If the import is independent of Tom70/71 and iMTS-L structures, it would be interesting to investigate if the cell uses other mechanisms to ensure a proper Rpo41 import. Furthermore, there is a general tendency of mitochondrial proteins to be rather small in comparison to cytosolic ones (Figure 26 A). Thus, it is very likely that the cell has different mechanisms for large proteins to ensure proper import.

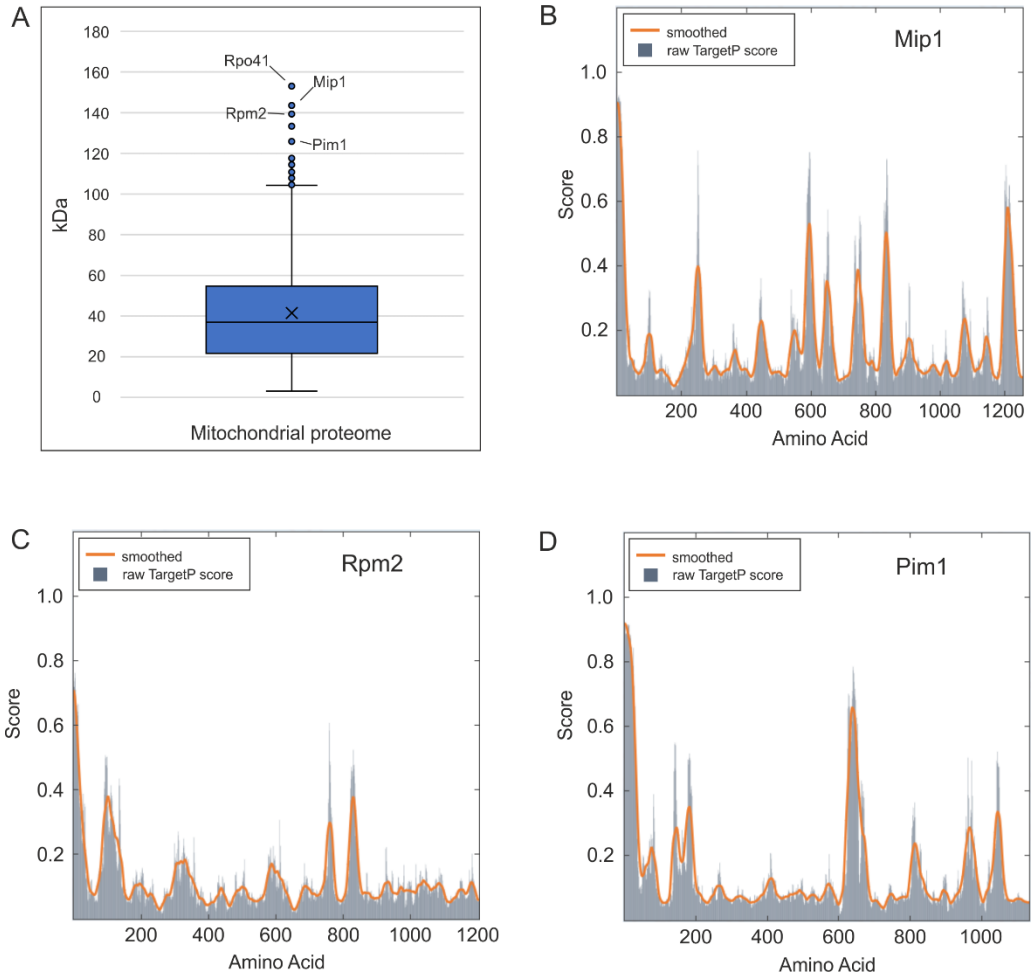

Figure 28: Large mitochondrial proteins display heterogeneous occurrence of iMTS-L structures. A: Boxplot of the molecular weights of the mitochondrial proteome (modified from Morgenstern et al. 2017) shows the tendency of mitochondrial proteins to be rather small (median 37kDa). **B-D:** TargetP profiles of the unusual large mitochondrial proteins Mip1, Rpm2 and Pim1. TargetP profiles were shown as raw TargetP scores and smoothed graphs.

Other examples for large mitochondrial proteins are Mip1, Rpm2 and Pim1. Mip1 is the mitochondrial DNA-polymerase, Rpm2 represents the protein component of RNaseP and Pim1 is a mitochondrial protease involved in degradation of misfolded mitochondrial proteins. These proteins however exhibit considerable different patterns of iMTS-L structures (Figure 26 B-D). While Mip1 displays three internal peaks of high TargetP score, Rpm2 has only one defined peak with a score of 0.6 which might be considered as an iMTS-L. In contrast, Pim1 has also only one iMTS-L structure but the range of high TargetP scores is much broader than in the other two examples probably indicating a stronger influence of this internal signal on the import of Pim1. When considering the protein abundance per cell (based on [110]) Rpm2 is present with ~70 copies while Pim1 is reported with more than 3000 copies per cell. This could in combination with the weak iMTS-L signals indeed suggest the hypothesis, that highly abundant and large proteins might get imported via Tom70/71 interaction with iMTS-L structures whereas low abundant large proteins like Rpo41 and Rpm2 are imported independently of this pathway. Tsuboi et al. [116] suggested that the probability of a co-translational import increases the longer a protein needs to be translated. In case of large proteins, the translation consequently takes longer than for small proteins. Thus, a possibility to ensure proper import of these large proteins might be co-translational import. Since the copy number of the proteins Rpm2 and Rpo41 is anyways very

low, this might be an easy way for the cell to overcome possible problems occurring during import.

The catalytic core of Rpo41 is similar to that of bacteriophage T7 and T3 rendering the polymerase a very ancient molecule[117]. The specificity factor Mtf1 binds to Rpo41 forming a holoenzyme prior to DNA binding. Mtf1 mediates recognition of the promoter region on the DNA and is released from Rpo41 after transcription initiation once a transcript of 13 nucleotides is formed[118]. Mtf1 exhibits a size of 40 kDa and is found with approximately 800 copies per cell. This is more than ten-fold the Rpo41 abundance and raises the question why it is present in such an excess compared to the polymerase. One possibility that could explain the high copy number would be the formation of multimer complexes of Mtf1 binding to Rpo41 and the mitochondrial DNA.

3.5 Mitoribosomes in human diseases

Several severe human diseases are caused by defects in mitochondria and in particular by defective mitochondrial translation. Biochemical characteristics of these diseases are alterations in OXPHOS enzymes which contain mitochondrial encoded subunits. These alterations lead to multisystemic diseases like Leigh syndrome, encephalomyopathy and hypertrophic cardiomyopathy and are often caused by mutations in mitochondrial encoded tRNA genes and nuclear genes encoding mitoribosomal proteins and assembly factors [119] [120] [121]. Especially MRPs involved in early assembly steps are implicated in serious mitochondrial disorders including mitochondria-specific and conserved proteins of both SSU and LSU. A lack of early binding proteins may be more likely to disrupt the mitoribosomal structure and subsequently assembly intermediates. For example, mL44 was found mutated in human patients suffering from multisystem disease with childhood-onset hypertrophic cardiomyopathy. Fibroblasts with mutated mL44 were shown to have lower assembled LSU and 16S rRNA levels. mL44/Mrpl3 was found in the complexome profile exclusively migrating in the assembled fraction of the LSU. As discussed earlier, this group most likely forms an initial assembly intermediate by interacting with the 5´end of the 21S rRNA in a co-transcriptional manner. Mutations in proteins of this group would severely affect the LSU assembly by altering or even disturbing the formation of the initial starting point of 54S assembly, thus leading to reduced levels of mitoribosomal subunits and therefore reduced mitochondrial translation. This example shows that information gained through studies in yeast mitochondria can be transferred to mammalian systems and especially on human cells. In particular, the analysis of conserved features regarding mitochondria-specific proteins and conserved regions like the peptidyl transferase center (PTC) can help in understanding processes causing severe diseases in human patients.

4. Outlook and concluding remarks

The assembly of the mitochondrial ribosome is a complex process involving the coordinated expression of nuclear genes encoding for mitoribosomal proteins and assembly factors together with transcription of mitoribosomal RNA encoded by the mitochondrial DNA. The elucidation of mitoribosomal structures was a difficult task due to their size but recent advances in cryo-electron tomography allowed to solve the structure of the mitoribosome in yeast and human with high resolution. The results shown in this thesis allowed, based on the structural information available, the identification of a building-block based assembly process of mitoribosomes in yeast comparable to the one reported for the bacterial large ribosomal subunit. The temporal resolution of these experiments although didn´t resolve the assembly of the full assembled mitoribosome. Thus, an extension of the applied timepoints would yield more information of later assembly steps and extend the knowledge of mitoribosome assembly.

Only a small number of assembly factors that are involved in this process are to date characterized. Still, it is tempting to speculate that many more factors are involved during mitoribosome assembly as seen for bacterial ribosomes. Thus, the identification of new assembly factors is one of the main goals in the mitoribosome field. A combination of quantitative mass spectrometry and cryo-EM reconstruction of mitoribosomal assembly intermediates could facilitate the identification of mitoribosome subcomplexes and associated assembly factors involved at different stages of mitoribosome biogenesis. Especially cryo-EM tomography of lamella milled from whole cells in collaboration with Stefan Pfeffer is a promising way to get insights into the on route assembly process in an intact surrounding without the danger of creating artifacts during isolation of mitochondria or purification of single ribosome particles like done in the past.

Interestingly, it seems to be more challenging to solve the structure of the small subunit than the structure of the large subunit, since in all cases the large subunit structure has been resolved first. Also, the assembly process of the large subunit is known in more detail than information for the small subunit is available. Thus, especially the assembly process of the small subunit is of interest and will be investigated in the future.

Former studies on the mitoribosomal assembly have been performed in different mutant strains. Thus, potential artifacts caused by fragmentation of subassemblies cannot be excluded. Although the experiments presented in this study have also been performed in a mutant strain, the conditions applied are assumed to be close to a wildtype situation. However, studies under “real” wildtype conditions are required to confirm the results of former studies on mitoribosome assembly and to clarify whether the identified subcomplexes are true intermediates involved in the assembly pathway of mitochondrial ribosomes in yeast.

5. Material & Methods

5.1 Molecular biology methods

Plasmid DNA isolation from *E. coli*

For isolation of plasmid DNA from E. coli 150 up to 200 ml selective LB-media was inoculated with bacteria. The cells were cultured overnight and the whole culture was used for plasmid isolation. Here, PureYieldTM Plasmid Midiprep System (Promega) was used as described by the manufacturer.

Determination of DNA concentration

To determine the concentration and purity of DNA the NanoDropTM 1000 Spectrophotometer (Thermo Fisher Scientific) was used. The machine was first calibrated and then 1 µl of DNA was used for the measurement. The absorbance was measured at 280, 260 or 230 nm. The ratios of 280/230 and 260/230 are a measure of contamination by proteins, RNA and organic compounds. A ratio around 2 for low amounts of contaminations was aimed for.

Polymerase chain reaction for DNA amplification

To amplify DNA for homologous recombination, polymerase chain reaction (PCR) was used. One reaction had volume of 50 µl containing 100 ng template DNA, 40 pmol of each primer, 0.2 mM dNTPs, 1 U polymerase and 1x reaction buffer. For the amplification of DNA used for homologous recombination the Phusion-HF polymerase and the according HF-buffer was used. The PCR program can be found in Table 1.

Denaturing temperatures was determined by the polymerase used (Phusion: 98°C). The elongation time was determined by the length of the amplified gene and the polymerase used (Phusion: 1 kbp/15 sec).

Table 1: Program used in the thermocycler to amplify DNA in PCR.

Temperature	Time	Cycles	Reaction
98°C	1 min		Initial denaturing of DNA
98°C	30 sec	35x	DNA denaturation
50-67°C	1 min	35x	Primer annealing
72°C	15-30 s/kb	35x	Elongation
72°C	10 min		Final elongation
4°C	∞		Cooling

Colony PCR was used for verification of successful homologous recombination. Therefore, one colony of yeast was solved in 30 µl of 0.2 % SDS and boiled for 10 min at 99°C. Afterwards, cell debris and intact cells were pelleted using a small table-top centrifuge for 30 sec. 1 µl of the supernatant was used as template DNA in above described reaction. All chemicals and enzymes used were purchased either from Thermo Science or New England Biolabs (NEB).

Table 2: Name and sequence of the different primers used in this study are listed.

Number	**Name**	**Sequence (5´-3´)**
SH14	5´ Rpo41-HIS3	GCAGATCTCCTGTTCATATACCATTTGTATTCTGCTTCTTTAC ATCTCTTGGCCTCCTCTAGT
SH15	3´Rpo41-GAL	TAACAGGGATGTTTTCACGAGCGATTTATAGGCCGGTCTCA

		GCATCGAATTCCTTGAATTTTCAAA
SH32	5´ Rpo41-ver his/kan	CAAAAGCAGA TCTCCT
SH33	3´Rpo41-ver his/kan	GTTACAAGGGGGTCT
SH118	Rpo41 fwd	CTTTCG CTGTCAACCC TGTTAATGCA AG
SH119	Rpo41 rev	CACCACATTCATAGTGTCTATATCAGATGC
SH120	21S rRNA fwd	GTTTGC AGATAGCTGG TTTTCTATGA AATATATG
SH121	21S rRNA rev	GGAACTTTATATCTTAATCTGGGCTGTTTCC
SH124	15S rRNA fwd	GTTAATCATAATGGTTTAAAGGATCCGTAGAATG
SH125	15S rRNA rev	GGTATCGAATCCGTTTCGCTACTCTAG
SH126	CoxII fwd	GTGATGAAGTT ATTTCACCAGCTATAACTATTAAAG
SH127	CoxII rev	CGAATCTAATATGTGTATCTACAGGTACAAC
	Cox2 ORF For	GGATGTTAGATTTATTAAGATTACAATTAAC
	Cox2 ORF Rev	GGTTATTGTTCATTTAATCATTCC

Agarose gel electrophoresis

Agarose gel electrophoresis was used for isolation of DNA fragments. DNA is negatively charged and in an electric field therefore migrates to the anode. Agarose is a polysaccharide and the polymerization leads to a network of fibers creating a matrix in which DNA fragments are separated by size. Small fragments migrate faster through the gel than large fragments.

To cast the agarose gel, 1% (w/v) agarose was dissolved in 1x TAE buffer (40 mM Tris, 1.14% acetic acid, 10 mM EDTA pH 8.0) by heating in a microwave. The gel was casted into the slide and 0.5 µg/ml ethidium bromide was added to visualize DNA under ultraviolet (UV) light. Samples were supplemented with 6x loading dye (60 mM Tris/HCl pH 7.5, 30 mM sodium acetate, 12 mM EDTA, 60% (v/v) glycerol, 0.36% (w/v) orange G) and loaded onto the gel. The electrophoresis was performed in 1x TAE buffer and at 10 V/cm. The gels were analyzed using UV light. In a preparative electrophoresis, the corresponding DNA fragments were cut out of the gel using a scalpel and purified with the NucleoSpin® Gel Clean-up kit (Macherey-Nagel) according to the instructions of the manufacturer.

Transformation of chemo competent Escherichia coli cells

Chemo competent *Escherichia coli* (*E. coli*) were transformed for the amplification of plasmid DNA. Therefore, the cells were thawed slowly on ice and 1 µl plasmid DNA was added. The mixture was incubated 30 min on ice followed by a 90 s heat shock at 42°C. Afterwards, 1 ml LB-media was added and the suspension was incubated further 45 min at 37°C. Cells were pelleted for 30 s at 17,000 xg and the supernatant was discarded. The cells were resuspended in the residual media and plated onto selective media or inoculated in liquid media for plasmid DNA isolation.

Transformation of S. cerevisiae cells

For homologous recombination to genomically integrate a DNA cassette, 1.5 ml yeast culture in exponential phase were harvested (30 s at 17, 000 x g at RT) and the cell pellet was washed with 1 ml sterile ddH2O. The cells were resuspended in 1 ml of 0.1 M lithium acetate and incubated for 10 min at 30°C. After centrifugation (30 s at 17, 000 x g at RT), the cell pellet was resuspended

in 34 µl ddH2O, 5 µl salmon sperm DNA (denatured at 96°C for 10 min and cooled down), 45 µl DNA, 36 µl 1 M lithium acetate (final concentration 0.1 M) and 240 µl 50% (w/v) polyethylene glycol (PEG) 3350. The mixture was vortexed for 1 min and incubated 30 min at 30°C followed by a heat shock for 25 min at 42°C. Afterwards, the cells were pelleted (1 min at 17, 000 x g at RT) and resuspended in 100 µl sterile water. The suspension was plated on selective media.

RNA extraction and cDNA synthesis

For isolation of whole cell RNA, 4 OD_{600} of an exponential growing culture were collected by centrifugation (17000 × g, 3 min, 2 °C) and washed with water. For further processing the RNeasy Mini Kit (Qiagen) with on-column removal of DNA was used as described by the manufacturer.

cDNA was prepared from 500ng total RNA using the qScript cDNA Synthesis Kit (Quanta bio) as described by the manufacturer. RNA and cDNA quality and concentration were assessed using a NanoDrop Fluorometer.

Quantitative real-time PCR

qPCR reactions were performed using a CFX96 Touch Real-Time PCR Detection System (Bio-Rad) in technical triplicates. DNA was PCR-amplified under the following conditions: 3 min at 95 °C followed by 44 cycles of 10 s at 95 °C, 30 s at 62 °C and 30 s at 60 °C. For all PCR assays, iQ SYBR Green Supermix (Bio-Rad) was used in the reaction. For normalization, TFC1 was selected as housekeeping gene based on the stability of published observations. Primers used for qPCR are listed in Table 2. Standard curves for primer efficiency were generated via the serial dilution of pooled cDNA. Only primer pairs with efficiency values between 90% and 110% were used.

The 2−ΔΔCt method was used for data analyses, normalizing the gene expression values to the geometric mean of the transcript levels of the housekeeping genes and to the wild-type empty vector control as the reference condition. Statistical significance was assessed using paired one-tailed Student's t-test.

5.2 Cell biology methods

Media for E. coli cultivation

Bacteria could be cultivated in liquid culture or on agar plates. LB medium (1% bacto-tryptone, 0.5% yeast extract, 1% sodium chloride, pH was adjusted to 7.5 with NaOH) was used for liquid culture and could be supplemented with 100 µg/ml ampicillin for plasmid selection. For agar plates, LB medium was solved together with 2% bacto-agar (w/v) and autoclaved. After cooling of the agar solution, ampicillin or chloramphenicol could be added prior pouring the plates.

Media for S. cerevisiae cultivation

Yeast could be cultured in full YP-media (1% yeast extract, 2% peptone, pH was adjusted to 5.5 with HCl) supplemented with 2% sugar as carbon source (D, glucose; Gal, galactose; G, glycerol). For YP-plates, 2% agar, 1% yeast extract, 2% peptone, pH was adjusted to 5.5 with HCl were autoclaved and afterwards supplemented with 2% of sugar and if needed 100 µg/ml G418 or clonNAT. The mixture was poured into petri dishes.

To select for plasmids, yeast cells were cultured in selective media containing of S medium (1.7 g /l yeast nitrogen base, 5 g/l ammonium sulfate, dropout mix without auxotrophic marker, 2% sugar). In Table 6 the composition of the 20x dropout mix can be found. SLac media contained 1.7 g /l yeast nitrogen base, 5 g/l ammonium sulfate, dropout mix without auxotrophic marker,

2.2% lactic acid (90%(v/v)) and could be supplemented with 0.5% of galactose to induce protein expression from a GAL-promotor.

For plates, 2% (w/v) agar was solved in half the volume of water and autoclaved. The solution was supplemented with S-medium and poured into petri dishes.

Cultures were inoculated from plates and cultivated shaking at 160 rpm and 30°C. Strains could be taken from glycerol stocks and plated onto agar plates. If not other mentioned, the plates were incubated at 30°C.

Table 3: Composition of the dropout mix. For selection the corresponding amino acids were left out.

Amino acids/Nucleobase	20x (mg/l)
L-adenine hemisulfate salt	400
L-arginine	400
L-histidine HCl monohydrate	400
L-isoleucine	600
L-leucine	2000
L-lysine HCl	600
L-methionine	400
L-phenylalanine	1000
L-threonine	400
L-tryptophan	400
L-tyrosine	400
L-uracil	400
L-valine	3000

Growth assays

Yeast strains were grown either in full or selective media and cells were harvested in their exponential phase and washed with sterile water. For growth tests on respiratory media precultures contained galactose as a carbon source.

For drop dilution assays an OD_{600} 0.5 was harvested, washed and a serial 1:10 dilution was done. From each dilution 3 µl were dropped on the respective media. The growth was documented after different days.

Preparation of mitochondria

For the isolation of mitochondria cells were grown in full media (1% yeast extract, 2% peptone, pH 5.5) containing 2% galactose as a carbon source and at 30°C. Cells were harvested (4,000 rpm, JA10 Beckmann rotor, 5 min, RT) in the exponential phase. After a washing step, cells were treated 10 min with 2 ml per g wet weight MP1 buffer (10 mM Tris pH unadjusted and 100 mM DTT) at 30°C. After washing with 1.2 M sorbitol, yeast cells were resuspended in 6.7 ml per g wet weight MP2 buffer (20 mM KPi buffer pH 7.4, 1.2 M sorbitol, 3 mg per g wet weight zymolyase from Seikagaku Biobusiness) and incubated for 1 h at 30°C. Spheroblasts were collected via centrifugation at 4°C and resuspended in ice cold homogenization buffer (13.4 ml/g wet weight) (10 mM Tris pH 7.4, 1 mM EDTA pH 8, 0.2% fatty acids free bovine serum albumin (BSA), 1 mM PMSF, 0.6 M sorbitol). Spheroblasts were disrupted by 10 strokes with a cooled glass potter. Cell debris was removed via centrifugation at 3300 rpm in a JA10 Beckmann rotor. The supernatant was centrifuged for 12 min at 10,000 rpm to collect mitochondria. Mitochondria were resuspended in 10 ml of ice cold SH-buffer (0.6 M sorbitol, 20 mM Hepes pH

7.4) and centrifuged again at 4,000 rpm in a JA25.50 Beckmann rotor to remove residual cell debris. To harvest the mitochondria the supernatant was again centrifuged for 12 min at 12,000 rpm. The amount of mitochondria was determined by Bradford assay.

Radioactive *in vivo* labelling of translation products

2 OD_{600} cells were collected, washed and resuspended in medium lacking methionine. To investigate mitochondrial translation, cycloheximide (150 µg ml–1) was added to stop cytosolic translation. ^{35}S-methionine (2 µl of a 22 µCi solution) was added to the cell suspension. Aliquots of 1.0 OD_{600} of cells were withdrawn after 15 and 30 min incubation at 30 °C, and incorporation of radioactive methionine was quenched by the addition of 8 mM cold methionine. Reactions were stopped on ice with 200 µM puromycin, and cells were lysed with 0.3 M NaOH, 1% β-mercaptoethanol and 3 mM PMSF. Proteins were precipitated with 12% trichloroacetic acid and analyzed by SDS–PAGE and autoradiography.

Radioactive *in organello* labelling of translation products

Isolated mitochondria (100 µg) were incubated in translation buffer (20 mM Hepes/KOH pH 7.4, 15 mM KPi, 0.6 M Sorbitol, 150 mM KCl, 12.66 mM $MgSO_4$, 12.13µg/ml Amino acid mix, 66.66µM Cys, 12.13 µg/ml Tyrosine, 7.5 mM Phosphoenolpyruvate, 6 mM ATP, 0.75 mM GTP, 5 mM α-Ketoglutarate, 10 µg/ml Pyruvat-Kinase) together with 1µl ^{35}S-methionine (of a 22 µCi solution) and incubated at 30°C for 10 min shaking at 600 rpm. Incorporation of radioactive methionine was quenched by the addition of 8 mM cold methionine and the reaction was stopped by the addition of 1 ml ice cold SH buffer (0.6 M Sorbitol, 20 mM Hepes). Mitochondria were pelleted by centrifugation (20000 x g, 10 min, 4 °C), resuspended in loading buffer and analyzed by SDS-PAGE and autoradiography.

DAPI staining of yeast cells and fluorescens microscopy

Cells were grown to exponential phase (~OD_{600} 0.5) in synthetic full medium followed by an incubation with 2.5 µg/ml DAPI (4',6-Diamidin-2-phenylindol) for 30 more min. 1 OD_{600} cells were subsequently harvested by centrifugation, washed with 1 ml PBS-buffer (137 mM NaCl, 2.7 mM KCl, 2 mM KH_2PO_4, 10 mM Na_2HPO_4) and finally resuspended in 500 µl PBS-buffer. 3-5 µl of the cell suspension were observed using a fully automated Zeiss inverted microscope (AxioObserver Z1) equipped with a MS-2000 stage (Applied Scientific Instrumentation, USA), the CSU-X1 spinning disk confocal head (Yokogawa, Herrsching), LaserStack Launch with selectable laser lines (Intelligent Imaging Innovations, USA) and an X-CITE Fluorescent Illumination System. Images were captured using a CoolSnap HQ camera (Roper Scientific, Canada) under the control of the Slidebook software (Intelligent Imaging Innovations, USA). The fluorescence signal was imaged with a 63x oil objective by using a 473 nm or 561 nm laser.

5.3 Protein biochemistry methods

SDS-polyacrylamide gel electrophoresis (SDS-PAGE)

In this study, self-made large casting systems and small bought casting system from BioRad were used. For the self-made gel system, glass plates with a size of 160 x 180 mm and spacers with 1 mm thickness were sealed using a base gel. The BioRad system seals the plates by sponge rubber pads. For both systems, first a running gel was casted, and isopropanol was added to straighten the gel. After the polymerization of the gel, the isopropanol was removed, and the stacking gel was added on top. The composition of the different gels is shown in Table 7.

Prior loading, samples were resuspended in reducing (50 mM) sample (Laemmli) buffer (50 mM Tris-HCl pH 6.8, 10% glycerine, 2% SDS, 0.01% bromophenol blue). To determine the protein size the unstained marker from peQLab and PageRuler™ Prestained Protein Ladder from ThermoFisher Scientific were used. The electrophoresis was conducted at 21-35 mA for 40 min up to 4 h and in SDS running buffer (25 mM Tris-HCl pH 8.3, 190 mM glycine, 0.1% SDS).

Table 4: Composition of the running, stacking and base gel.

Gel	Composition
Running Gel	16% acrylamide
	0.11% bisacrylamide
	375 mM Tris-HCl pH 8.8
	0.1% SDS
	0.1% ammonium persulfate (APS)
	0.03% N,N,N',N'-Tetramethylethylenediamine (TEMED)
Stacking Gel	5% acrylamide
	0.03% bisacrylamide
	60 mM Tris-HCl pH 6.8
	0.1% SDS
	0.05% APS
	0.1% TEMED
Base Gel	20% acrylamide
	0.13% bisacrylamide
	375 mM Tris-HCl pH 8.8
	0.1% SDS
	0.05% APS
	0.1% TEMED

Western blot to transfer proteins on a nitrocellulose membrane

Proteins separated in SDS-PAGE could be transferred onto a cellulose membrane, here, the semidry method was used. Therefore, two Whatman paper (17 cm x 12 cm) were shortly incubated in blotting buffer (20 mM Tris, 150 mM glycine, 0.08% SDS, 20% methanol) and placed in the blotting chamber. The nitrocellulose membrane (15 cm x 10 cm) and the SDS-gel were also incubated in the blotting buffer. The cellulose membrane was placed on top of the Whatman paper followed by the gel avoiding bubbles. Lastly, an additional Whatman paper was placed on top and the chamber was closed and weighted to press everything together. The anode is placed on the bottom and the cathode (lid) on top. The proteins were transferred for 90 min at 1.3 mA/cm2. To visualize the transferred proteins, the membrane was stained with Ponceau S solution (0.2% (w/v) Ponceau S, 3% (w/v) acetic acid) for 2 – 5 min.

Autoradiography

Radioactive proteins can be detected by autoradiography. Therefore, on top of the dried cellulose membrane was a radio-sensitive film placed (Fuji Medical X-Ray Film Super RX or Kodak BioMax MR Film). After the desired exposure time the film could be developed using the developing machine Optimax TR (MS Laborgeräte). Alternatively, the membrane was exposed to an imaging plate (Fujifilm) for phospho-imaging with the Typhoon FLA 7000 from GE Healthcare.

Trichloroacetic acid precipitation of proteins

Trichloroacetic acid (TCA) was used for protein precipitation. Samples were supplemented with 72% (w/v) TCA to a final concentration of 12% TCA. The samples were incubated at -80°C for 2

h or at -20°C overnight. Afterwards they were thawed slowly at RT (room temperature) and the precipitated proteins pelleted for 30 min at 30000 x g and 4°C. The protein pellet was washed with 1 ml of ice-cold Acetone 100%. After a second centrifugation (30 min at 30000 x g and 4°C) the pellet was dried at 30°C and resuspended in reducing sample buffer.

Immune decoration of cellulose membranes

Proteins could be detected by antibodies. Therefore, the cellulose membrane, still stained with Ponceau S, was cut in pieces to decorate against several antibodies at once. The membrane was incubated reeling for 30 min in 5% milk in 1x TBS buffer (10 mM Tris/HCl pH 7.5, 150 mM NaCl) to block unspecific binding of the antibody. Afterwards, the membranes were incubated with the primary antibody (1:1000 in 5% milk in TBS) overnight reeling at 4°C. The membrane was washed three times for 5 min with TBS buffer. Afterwards, the membranes were incubated for at least 60 min reeling at RT with the secondary antibody (1:5000 or 1:10,000 in 5% milk in TBS) on which the horse reddish peroxidase is coupled and washed again thrice for 5 min. ECL1 and ECL2 solutions (ECL 1: 100 mM Tris/HCl pH 8.5, 0.044% (w/v) luminol, 0.0066% p-coumaric acid; ECL 2: 100 mM Tris/HCl pH 8.5, 0.03% H2O2) were mixed 1:1 and poured onto the membrane to start the reaction, in which chemo luminescence is produced by the peroxidase. This luminescence was detected on Super RX Medical X-Ray Films (Fuji) using the Optimax Type TR-developer (MS Laborgeräte).

Antibodies were raised in rabbits using recombinant purified proteins. The secondary antibody was ordered from BioRad (Goat Anti-Rabbit IgG (H+L))-HRP Conjugate, #172-1019.

Sucrose gradient sedimentation

Isolated mitochondria (3 mg) were incubated with translation buffer (20 mM Hepes/KOH pH 7.4, 15 mM KPi, 0.6 M Sorbitol, 150 mM KCl, 12.66 mM $MgSO_4$, 12.13µg/ml Amino acid mix, 66.66µM Cys, 12.13 µg/ml Tyrosine, 7.5 mM Phosphoenolpyruvate, 6 mM ATP, 0.75 mM GTP, 5 mM α-Ketoglutarate, 10 µg/ml Pyruvat-Kinase) for 10 min at 30°C. Translation was stopped by addition of 10 µg/ml chloramphenicol. Mitochondria were pelleted, resuspended in 250 µl solubilization buffer (1% Triton X-100, 50 mM NH4Cl, 5 mM MgSO4, 1× complete protease inhibitor (Roche, Basel, Switzerland), and 20 mM 4-(2-hydroxyethyl)-1-piperazineethanesulfonic acid (HEPES), pH 7.4) and incubated on ice for 10 min. After a clarifying spin for 10 min at 25,000 × g, 4°C, the lysate was loaded onto a linear sucrose gradient (12 ml; 10–34% sucrose, 0.1% Triton X-100, 50 mM NH_4Cl, 5 mM $MgSO_4$, 1× complete protease inhibitor (Roche), 20 mM HEPES, pH 7.4) and centrifuged in an SW41 rotor (Beckman, Brea, CA) at 33,000 rpm for 5.5 h at 4°C. The gradient was fractionated, the containing proteins were precipitated with trichloroacetic acid and analyzed by SDS-PAGE and immune detection.

Blue Native Gel Electrophoresis

Protein concentrations were determined using the microBCA protein kit (Thermo Scientific). Mitochondria were solubilized with 6 g digitonin (Sigma) per gram of protein in 50 mM NaCl, 5 mM 6-aminohexanoic acid, 2 mM EDTA, and 50 mM imidazole/HCl (pH 7.0). Blue native electrophoresis was performed as described in Wittig et al. (2006).

In-Gel tryptic digestion

The in-gel digestions were performed essentially as previously described (Heide et al., 2012). In brief, the 1D blue native gel was incubated in fixing solution (50% methanol, 10% acetic acid, 100 mM ammonium acetate) for 30 min and stained with Coomassie blue. After two washing steps with ultrapure water for 30 min, the gel lanes were cut into 60 even slices of about 2 mm. Every gel slice was additionally diced into smaller pieces and then transferred to a 96-well filter

microplate containing 150 ml of 50% methanol, 50 mM ammonium hydrogen carbonate (pH unadjusted). The gel pieces were washed in destaining solution three times for 30 min at room temperature under gentle agitation to remove the Coomassie dye. Excess solution was removed by centrifugation (600 3 g, 3 min at room temperature). In the next step, gel pieces were incubated with 120 ml of 5 mM DTT for 60 min. After removal of excess solution (600 3 g, 3 min, room temperature), 120 ml of 15 mM chloroacetamide was added to each well and removed after 45 min. Gel pieces were then allowed to dry at room temperature for 45 min. The dried gel pieces were swollen in 20 ml of 5 ng/ml trypsin in 50 mM ammonium hydrogen carbonate and 1 mM CaCl2 (pH unadjusted) for 30 min at 4°C. Then, 150 ml of 50 mM ammonium hydrogen carbonate was added to cover the gel pieces, followed by an overnight incubation at 37°C to digest the proteins. The peptide-containing supernatants were collected by centrifugation (600 3 g, 3 min, room temperature) into a 96-well plate. The gel pieces in the filter plate were washed once with 30% acetonitrile, 3% formic acid for 20 min to elute the remaining peptides. The combined eluates were then dried in a Concentrator Plus (Eppendorf). Prior to mass spectrometry, peptides were resuspended in 20 ml of 5% acetonitrile/0.5% formic acid.

Mass spectrometry

Peptides were separated by liquid chromatography and analyzed by online tandem mass spectrometry (LC-MS/MS) in a Q-Exactive mass spectrometer equipped with an Easy nLC1000 nano-flow ultra-high-pressure liquid chromatography system (Thermo Fisher Scientific) at the front end. Peptides were separated using a 100 mm ID 3 15 cm length PicoTip emitter column (New Objective) filled with ReproSil-Pur C18-AQ reverse-phase beads of 3 mm particle size and 120 A ° pore size (Dr. Maisch GmbH) using linear gradients of 5%–35% acetonitrile/0.1% formic acid at a flow rate of 300 nl/min. The mass spectrometer operated in positive ion mode switching automatically between MS and data-dependent MS/MS of the top 20 most abundant precursor ions. Full-scan MS mode (400–1,400 m/z) was set at a resolution of 70,000 m/Dm with an automatic gain control target of 1 3 106 ions and a maximum injection time of 20 ms. Selected ions for MS/MS were analyzed using the following parameters: resolution 17,500 m/Dm, automatic gain control target 1 3 105; maximum injection time 50 ms; precursor isolation window 4.0 Th. Only precursor ions of charge z = 2 and z = 3 were selected for collision- induced dissociation. Normalized collision energy was set to 30% at a dynamic exclusion window of 60 s. A lock mass ion (m/z = 445.12) was used for internal calibration (Olsen et al., 2005).

Label-Free LC/MS-based protein quantification and hierarchical clustering

Intensity based absolute quantification (iBAQ) values derived from the MaxQuant analysis were corrected for loading variation between different samples using the average peak values of 13 nuclear-encoded proteins, which were not affected by CAP treatment. For each protein, gel migration profiles were created and normalized to the maximum abundance across all samples analyzed. Then the migration patterns of the identified proteins were hierarchically clustered by an average linkage algorithm with uncentered Pearson correlation distance measures using Cluster 3.0 software (de Hoon et al., 2004). Heatmaps of the resulting complexome profiles consisting of a list of proteins grouped according to the similarity of their migration profiles in blue native gel electrophoresis were generated by representing the normalized abundance in each gel slice by a three-color gradient (black/yellow/red). Microsoft Excel and NOVA v0.5 software (Giese et al., 2015) were used for visualization and analysis.

Mitoribosome structures

Structural information was taken from Desai et al. [24] and structures were generated using UCFS Chimera.

References

1. Dyall, S. D., Brown, M. T. & Johnson, P. J. Ancient Invasions: From Endosymbionts to Organelles. *Science* **304**, 253–257 (2004).

2. Lill, R. *et al.* Mechanisms of iron-sulfur protein maturation in mitochondria, cytosol and nucleus of eukaryotes. *Biochim. Biophys. Acta - Mol. Cell Res.* **1763**, 652–667 (2006).

3. Kawamata, H. & Manfredi, G. Mitochondrial dysfunction and intracellular calcium dysregulation in ALS. *Mech. Ageing Dev.* **131**, 517–526 (2010).

4. Donaldson, M. *et al.* p47(phox)-deficient immune microenvironment signals dysregulate naive T cell apoptosis. *Cell Death Differ.* **16**, 125–138 (2009).

5. Lang, B. F., Gray, M. W. & Burger, G. Mitochondrial Genome Evolution and the Origin of Eukaryotes. *Annu. Rev. Genet.* **33**, 351–397 (1999).

6. Gray, M. W., Burger, G. & Lang, B. F. Mitochondrial evolution. *Science* **283**, 1476–1481 (1999).

7. Martin, W. & Russell, M. J. On the origins of cells: a hypothesis for the evolutionary transitions from abiotic geochemistry to chemoautotrophic prokaryotes, and from prokaryotes to nucleated cells. *Philos. Trans. R. Soc. Lond. B. Biol. Sci.* **358**, 59–83; discussion 83-5 (2003).

8. Zick, M., Rabl, R. & Reichert, A. S. Cristae formation-linking ultrastructure and function of mitochondria. *Biochim. Biophys. Acta - Mol. Cell Res.* **1793**, 5–19 (2009).

9. Pfanner, N. *et al.* Uniform nomenclature for the mitochondrial contact site and cristae organizing system. *Journal of Cell Biology* **204**, 1083–1086 (2014).

10. Twig, G. *et al.* Fission and selective fusion govern mitochondrial segregation and elimination by autophagy. *EMBO J.* **27**, 433–446 (2008).

11. Bogenhagen, D. F., Martin, D. W. & Koller, A. Initial steps in RNA processing and ribosome assembly occur at mitochondrial DNA nucleoids. *Cell Metab.* **19**, 618–629 (2014).

12. Kurland, C. G. & Andersson, S. G. E. Origin and Evolution of the Mitochondrial Proteome. *Microbiol. Mol. Biol. Rev.* **64**, 786–820 (2000).

13. Hudspeth, M. E. S., Ainley, W. M., Shumard, D. S., Butow, R. A. & Grossman, L. I. Location and structure of the var1 gene on yeast mitochondrial DNA: Nucleotide sequence of the 40.0 allele. *Cell* **30**, 617–626 (1982).

14. Sanchirico, M. *et al.* Relocation of the unusual VAR1 gene from the mitochondrion to the nucleus. *Biochemistry and cell biology = Biochimie et biologie cellulaire* **73**, 987–995 (1995).

15. Ott, M., Amunts, A. & Brown, A. Organization and Regulation of Mitochondrial Protein Synthesis. *Annu. Rev. Biochem.* **85**, 77–101 (2016).

16. Rackham, O. *et al.* Hierarchical RNA Processing Is Required for Mitochondrial Ribosome Assembly. *Cell Rep.* **16**, 1874–1890 (2016).

17. PALADE, G. E. A small particulate component of the cytoplasm. *J. Biophys. Biochem. Cytol.* **1**, 59–68 (1955).

18. Pfeffer, S., Woellhaf, M. W., Herrmann, J. M. & Förster, F. Organization of the mitochondrial translation machinery studied in situ by cryoelectron tomography. *Nat. Commun.* **6**, (2015).

19. Englmeier, R., Pfeffer, S. & Förster, F. Structure of the Human Mitochondrial Ribosome Studied in Situ by Cryoelectron Tomography. *Structure* **25**, 1574-1581.e2 (2017).

20. Schuwirth, B. S. *et al.* Structures of the bacterial ribosome at 3.5 Å resolution. *Science (80-.).* **310**, 827–834 (2005).

21. Amunts, A. *et al.* Structure of the yeast mitochondrial. *Science (80-.).* **343**, 1485–1489 (2014).

22. Gao, Y. G. *et al.* The structure of the ribosome with elongation factor g trapped in the posttranslocational state. *Science (80-.).* **326**, 694–699 (2009).

23. Greber, B. J. *et al.* The complete structure of the large subunit of the mammalian mitochondrial ribosome. *Nature* **515**, 283–286 (2014).

24. Desai, N., Brown, A., Amunts, A. & Ramakrishnan, V. The structure of the yeast mitochondrial ribosome. *Science (80-.).* **355**, 528–531 (2017).

25. Brown, A. *et al.* Structure of the large ribosomal subunit from human mitochondria. *Science (80-.).* **346**, 718–722 (2014).

26. Kiparisov, S. *et al.* Structural and functional analysis of 5S rRNA in Saccharomyces cerevisiae. *Mol. Genet. Genomics* **274**, 235–247 (2005).

27. Ben-Shem, A., Jenner, L., Yusupova, G. & Yusupov, M. Crystal structure of the eukaryotic ribosome. *Science (80-.).* **330**, 1203–1209 (2010).

28. Bauerschmitt, H. *et al.* Ribosome-binding proteins Mdm38 and Mba1 display overlapping functions for regulation of mitochondrial translation. *Mol. Biol. Cell* **21**, 1937–1944 (2010).

29. Ott, M. *et al.* Mba1, a membrane-associated ribosome receptor in mitochondria. *EMBO J.* **25**, 1603–1610 (2006).

30. Preuss, M., Ott, M., Funes, S., Luirink, J. & Herrmann, J. M. Evolution of mitochondrial Oxa proteins from bacterial YidC: Inherited and acquired functions of a conserved protein insertion machinery. *J. Biol. Chem.* **280**, 13004–13011 (2005).

31. Keil, M. *et al.* Oxa1-ribosome complexes coordinate the assembly of cytochrome c oxidase in mitochondria. *J. Biol. Chem.* **287**, 34484–34493 (2012).

32. Hansen, J. L. *et al.* The structures of four macrolide antibiotics bound to the large ribosomal subunit. *Mol. Cell* **10**, 117–128 (2002).

33. Gruschke, S. *et al.* Proteins at the polypeptide tunnel exit of the yeast mitochondrial ribosome. *J. Biol. Chem.* **285**, 19022–19028 (2010).

34. Merten, S., Synenki, R. M., Locker, J., Christianson, T. & Rabinowitz, M. Processing of precursors of 21S ribosomal RNA from yeast mitochondria. *Proc. Natl. Acad. Sci. U. S. A.* **77**, 1417–1421 (1980).

35. Tabak, H. F., Van der Horst, G., Osinga, K. A. & Arnberg, A. C. Splicing of large ribosomal precursor RNA and processing of intron RNA in yeast mitochondria. *Cell* **39**, 623–629 (1984).

36. Dziembowski, A. *et al.* The yeast mitochondrial degradosome: Its composition, interplay

between RNA helicase and RNase activities and the role in mitochondrial RNA metabolism. *J. Biol. Chem.* **278**, 1603–1611 (2003).

37. Wiesenberger, G. & Fox, T. D. Pet127p, a membrane-associated protein involved in stability and processing of Saccharomyces cerevisiae mitochondrial RNAs. *Mol. Cell. Biol.* **17**, 2816–2824 (1997).

38. Fekete, Z., Ellis, T. P., Schonauer, M. S. & Dieckmann, C. L. Pet127 governs a 5′ →3′-exonuclease important in maturation of apocytochrome b mRNA in Saccharomyces cerevisiae. *J. Biol. Chem.* **283**, 3767–3772 (2008).

39. Schatz, G. & Dobberstein, B. Common principles of protein translocation across membranes. *Science (80-.).* **271**, 1519–1526 (1996).

40. Schulz, C., Schendzielorz, A. & Rehling, P. Unlocking the presequence import pathway. *Trends in Cell Biology* **25**, 265–275 (2015).

41. von Heijne, G. Signal sequences. *J. Mol. Biol.* **184**, 99–105 (1985).

42. Pfanner, N., Müller, H. K., Harmey, M. A. & Neupert, W. Mitochondrial protein import: involvement of the mature part of a cleavable precursor protein in the binding to receptor sites. *EMBO J.* **6**, 3449–3454 (1987).

43. Emanuelsson, O., Brunak, S., von Heijne, G. & Nielsen, H. Locating proteins in the cell using TargetP, SignalP and related tools. *Nat. Protoc.* **2**, 953–971 (2007).

44. Young, J. C., Hoogenraad, N. J. & Hartl, F. U. Molecular Chaperones Hsp90 and Hsp70 Deliver Preproteins to the Mitochondrial Import Receptor Tom70. *Cell* **112**, 41–50 (2016).

45. Kellems, R. E., Allison, V. F. & Butow, R. A. Cytoplasmic type 80s ribosomes associated with yeast mitochondria: IV. Attachment of ribosomes to the outer: Membrane of isolated mitochondria. *J. Cell Biol.* **65**, 1–14 (1975).

46. Marc, P. *et al.* Genome-wide analysis of mRNAs targeted to yeast mitochondria. *EMBO Rep.* **3**, 159–164 (2002).

47. Hill, K. *et al.* Tom40 forms the hydrophilic channel of the mitochondrial import pore for preproteins. *Nature* **395**, 516–521 (1998).

48. Neupert, W. & Herrmann, J. M. Translocation of proteins into mitochondria. *Annu. Rev. Biochem.* **76**, 723–749 (2007).

49. Waegemann, K., Popov-Čeleketić, D., Neupert, W., Azem, A. & Mokranjac, D. Cooperation of TOM and TIM23 complexes during translocation of proteins into mitochondria. *J. Mol. Biol.* **427**, 1075–1084 (2015).

50. Chacinska, A., Koehler, C. M., Milenkovic, D., Lithgow, T. & Pfanner, N. Importing Mitochondrial Proteins: Machineries and Mechanisms. *Cell* **138**, 628–644 (2009).

51. Sirrenberg, C. *et al.* Functional cooperation and stoichiometry of protein translocases of the outer and inner membranes of mitochondria. *J. Biol. Chem.* **272**, 29963–29966 (1997).

52. van der Laan, M. *et al.* Motor-free mitochondrial presequence translocase drives membrane integration of preproteins. *Nat. Cell Biol.* **9**, 1152–1159 (2007).

53. Schulz, C. *et al.* Tim50's presequence receptor domain is essential for signal driven transport across the TIM23 complex. *J. Cell Biol.* **195**, 643–656 (2011).

54. Shariff, K., Ghosal, S. & Matouschek, A. The force exerted by the membrane potential during protein import into the mitochondrial matrix. *Biophys. J.* **86**, 3647–3652 (2004).

55. Wickner, W. & Schekman, R. Protein translocation across biological membranes. *Science* **310**, 1452–1456 (2005).

56. Kang, P. J. *et al.* Requirement for hsp70 in the mitochondrial matrix for translocation and folding of precursor proteins. *Nature* **348**, 137–143 (1990).

57. Ostermann, J. *et al.* Precursor proteins in transit through mitochondrial contact sites interact with hsp70 in the matrix. *FEBS Lett.* **277**, 281–284 (1990).

58. Westermann, B., Prip-Buus, C., Neupert, W. & Schwarz, E. The role of the GrpE homologue, Mge1p, in mediating protein import and protein folding in mitochondria. *EMBO J.* **14**, 3452–3460 (1995).

59. Liu, Q., D'Silva, P., Walter, W., Marszalek, J. & Craig, E. A. Regulated cycling of mitochondrial Hsp70 at the protein import channel. *Science (80-.).* **300**, 139–141 (2003).

60. De Los Rios, P., Ben-Zvi, A., Slutsky, O., Azem, A. & Goloubinoff, P. Hsp70 chaperones accelerate protein translocation and the unfolding of stable protein aggregates by entropic pulling. *Proc. Natl. Acad. Sci. U. S. A.* **103**, 6166–6171 (2006).

61. Vögtle, F. N. *et al.* Global Analysis of the Mitochondrial N-Proteome Identifies a Processing Peptidase Critical for Protein Stability. *Cell* **139**, 428–439 (2009).

62. Vögtle, F. N. *et al.* Mitochondrial protein turnover: Role of the precursor intermediate peptidase Oct1 in protein stabilization. *Mol. Biol. Cell* **22**, 2135–2143 (2011).

63. Herrmann, J. M., Stuart, R. A., Craig, E. A. & Neupert, W. Mitochondrial heat shock protein 70, a molecular chaperone for proteins encoded by mitochondrial DNA. *J. Cell Biol.* **127**, 893–902 (1994).

64. Böttinger, L. *et al.* Mitochondrial heat shock protein (Hsp) 70 and Hsp10 cooperate in the formation of Hsp60 complexes. *J. Biol. Chem.* **290**, 11611–11622 (2015).

65. Nolden, M. *et al.* The m-AAA protease defective in hereditary spastic paraplegia controls ribosome assembly in mitochondria. *Cell* **123**, 277–289 (2005).

66. Bonn, F., Tatsuta, T., Petrungaro, C., Riemer, J. & Langer, T. Presequence-dependent folding ensures MrpL32 processing by the *m* -AAA protease in mitochondria. *EMBO J.* **30**, 2545–2556 (2011).

67. Longen, S., Woellhaf, M. W., Petrungaro, C., Riemer, J. & Herrmann, J. M. The Disulfide Relay of the Intermembrane Space Oxidizes the Ribosomal Subunit Mrp10 on Its Transit into the Mitochondrial Matrix. *Dev. Cell* **28**, 30–42 (2014).

68. Antonicka, H. & Shoubridge, E. A. Mitochondrial RNA Granules Are Centers for Posttranscriptional RNA Processing and Ribosome Biogenesis. *Cell Rep.* **10**, 920–932 (2015).

69. Paul, M. F., Alushin, G. M., Barros, M. H., Rak, M. & Tzagoloff, A. The putative GTPase encoded by MTG3 functions in a novel pathway for regulating assembly of the small subunit of yeast mitochondrial ribosomes. *J. Biol. Chem.* **287**, 24346–24355 (2012).

70. Tu, Y. T. & Barrientos, A. The Human Mitochondrial DEAD-Box Protein DDX28 Resides in RNA Granules and Functions in Mitoribosome Assembly. *Cell Rep.* **10**, 854–864 (2015).

71. De Silva, D., Fontanesi, F. & Barrientos, A. The DEAD box protein Mrh4 functions in the assembly of the mitochondrial large ribosomal subunit. *Cell Metab.* **18**, 712–725 (2013).

72. Barrientos, A. *et al.* MTG1 codes for a conserved protein required for mitochondrial translation. *Mol. Biol. Cell* **14**, 2292–2302 (2003).

73. Taylor, S. W. *et al.* Characterization of the human heart mitochondrial proteome. *Nat. Biotechnol.* **21**, 281–286 (2003).

74. Greenleaf, A. L., Kelly, J. L. & Lehman, I. R. Yeast RP041 gene product is required for transcription and maintenance of the mitochondrial genome. *Proc. Natl. Acad. Sci. U. S. A.* **83**, 3391–3394 (1986).

75. Zeng, R., Smith, E. & Barrientos, A. Yeast Mitoribosome Large Subunit Assembly Proceeds by Hierarchical Incorporation of Protein Clusters and Modules on the Inner Membrane. *Cell Metab.* **27**, 645-656.e7 (2018).

76. Morales, M. J., Dang, Y. L., Lou, Y. C., Sulo, P. & Martin, N. C. A 105-kDa protein is required for yeast mitochondrial RNase P activity. *Proc. Natl. Acad. Sci. U. S. A.* **89**, 9875–9879 (1992).

77. Arredondo, J. J. *et al.* Mitochondrial tRNA valine as a recurrent target for mutations involved in mitochondrial cardiomyopathies. *Mitochondrion* **12**, 357–362 (2012).

78. Rötig, A. Human diseases with impaired mitochondrial protein synthesis. *Biochimica et Biophysica Acta - Bioenergetics* **1807**, 1198–1205 (2011).

79. Perez-Martinez, X. *et al.* Protein Synthesis and Assembly in Mitochondrial Disorders. *Curr. Top. Med. Chem.* **8**, 1335–1350 (2008).

80. Turk, E. M., Das, V., Seibert, R. D. & Andrulis, E. D. The Mitochondrial RNA Landscape of Saccharomyces cerevisiae. *PLoS One* **8**, 78105 (2013).

81. Sykes, M. T., Shajani, Z., Sperling, E., Beck, A. H. & Williamson, J. R. Quantitative proteomic analysis of ribosome assembly and turnover in vivo. *J. Mol. Biol.* **403**, 331–45 (2010).

82. Chen, S. S., Sperling, E., Silverman, J. M., Davis, J. H. & Williamson, J. R. Measuring the dynamics of E. coli ribosome biogenesis using pulse-labeling and quantitative mass spectrometry. *Mol. Biosyst.* **8**, 3325–3334 (2012).

83. Klootwijk, J., Klein, I. & Grivell, L. A. Minimal post-transcriptional modification of yeast mitochondrial ribosomal RNA. *J. Mol. Biol.* **97**, 337–350 (1975).

84. Sirum-Connolly, K. & Mason, T. L. Functional requirement of a site-specific ribose methylation in ribosomal RNA. *Science (80-.).* **262**, 1886–1889 (1993).

85. Sirum-Connolly, K., Peltier, J. M., Crain, P. F., McCloskey, J. A. & Mason, T. L. Implications of a functional large ribosomal RNA with only three modified nucleotides. *Biochimie* **77**, 30–39 (1995).

86. Metodiev, M. D. *et al.* Methylation of 12S rRNA Is Necessary for In Vivo Stability of the Small Subunit of the Mammalian Mitochondrial Ribosome. *Cell Metab.* **9**, 386–397 (2009).

87. Greber, B. J. Mechanistic insight into eukaryotic 60S ribosomal subunit biogenesis by cryo-electron microscopy. *RNA* **22**, 1643–1662 (2016).

88. Holt, I. J. *et al.* Mammalian mitochondrial nucleoids: Organizing an independently

minded genome. *Mitochondrion* **7**, 311–321 (2007).

89. Bogenhagen, D. F., Rousseau, D. & Burke, S. The layered structure of human mitochondrial DNA nucleoids. *J. Biol. Chem.* **283**, 3665–3675 (2008).

90. Gilkerson, R. *et al.* The mitochondrial nucleoid: Integrating mitochondrial DNA into cellular homeostasis. *Cold Spring Harb. Perspect. Biol.* **5**, (2013).

91. Kukat, C. *et al.* Super-resolution microscopy reveals that mammalian mitochondrial nucleoids have a uniform size and frequently contain a single copy of mtDNA. *Proc. Natl. Acad. Sci. U. S. A.* **108**, 13534–13539 (2011).

92. Iborra, F. J., Kimura, H. & Cook, P. R. The functional organization of mitochondrial genomes in human cells. *BMC Biol.* **2**, (2004).

93. Lee, K. W., Okot-Kotber, C., La Comb, J. F. & Bogenhagen, D. F. Mitochondrial ribosomal RNA (rRNA) methyltransferase family members are positioned to modify nascent rRNA in foci near the mitochondrial DNA nucleoid. *J. Biol. Chem.* **288**, 31386–31399 (2013).

94. Antonicka, H., Sasarman, F., Nishimura, T., Paupe, V. & Shoubridge, E. A. The mitochondrial RNA-binding protein GRSF1 localizes to RNA granules and is required for posttranscriptional mitochondrial gene expression. *Cell Metab.* **17**, 386–398 (2013).

95. Jourdain, A. A. *et al.* GRSF1 regulates RNA processing in mitochondrial RNA granules. *Cell Metab.* **17**, 399–410 (2013).

96. Shiber, A. *et al.* Cotranslational assembly of protein complexes in eukaryotes revealed by ribosome profiling. *Nature* **561**, 268–272 (2018).

97. Barrientos, A. Mitochondriolus: Assembling mitoribosomes. *Oncotarget* **6**, 16800–16801 (2015).

98. Jourdain, A. A., Boehm, E., Maundrell, K. & Martinou, J. C. Mitochondrial RNA granules: Compartmentalizing mitochondrial gene expression. *J. Cell Biol.* **212**, 611–614 (2016).

99. Spillmann, S., Dohme, F. & Nierhaus, K. H. Assembly in Vitro of the 50 S subunit from Escherichia coli ribosomes: Proteins essential for the first heat-dependent conformational change. *J. Mol. Biol.* **115**, 513–523 (1977).

100. Nierhaus, K. H. The assembly of prokaryotic ribosomes. *Biochimie* **73**, 739–755 (1991).

101. Shajani, Z., Sykes, M. T. & Williamson, J. R. Assembly of bacterial ribosomes. *Annu. Rev. Biochem.* **80**, 501–526 (2011).

102. Rugarli, E. I. & Langer, T. Mitochondrial quality control: A matter of life and death for neurons. *EMBO J.* **31**, 1336–1349 (2012).

103. Kaur, J. & Stuart, R. A. Truncation of the Mrp20 protein reveals new ribosome-assembly subcomplex in mitochondria. *EMBO Rep.* **12**, 950–955 (2011).

104. Box, J. M., Kaur, J. & Stuart, R. A. Mrpl35, A Mitospecific Component of Mitoribosomes, Plays A Key Role in Cytochrome C Oxidase Assembly. *Mol. Biol. Cell* **28**, 3471–3561 (2017).

105. Jomaa, A. *et al.* Functional domains of the 50S subunit mature late in the assembly process. doi:10.1093/nar/gkt1295

106. Guerrero-Castillo, S. *et al.* The Assembly Pathway of Mitochondrial Respiratory Chain Complex I. *Cell Metab.* **25**, 128–139 (2017).

107. Jarzab, A. *et al.* Meltome atlas—thermal proteome stability across the tree of life. *Nat. Methods* **17**, 495–503 (2020).

108. Boos, F. *et al.* Mitochondrial protein-induced stress triggers a global adaptive transcriptional programme. *Nat. Cell Biol.* **21**, 442–451 (2019).

109. Davis, J. H. *et al.* Modular Assembly of the Bacterial Large Ribosomal Subunit. *Cell* **167**, 1610-1622.e15 (2016).

110. Morgenstern, M. *et al.* Definition of a High-Confidence Mitochondrial Proteome at Quantitative Scale. *Cell Rep.* **19**, 2836–2852 (2017).

111. Emanuelsson, O. & Nielsen, H. Predicting subcellular localization of proteins based on their N-terminal amino acid sequence. *J. Mol. …* **300**, 1005–16 (2000).

112. Boos, F., Mühlhaus, T. & Herrmann, J. Detection of Internal Matrix Targeting Signal-like Sequences (iMTS-Ls) in Mitochondrial Precursor Proteins Using the TargetP Prediction Tool. *BIO-PROTOCOL* **8**, (2018).

113. Backes, S. *et al.* Tom70 enhances mitochondrial preprotein import efficiency by binding to internal targeting sequences. *J. Cell Biol.* **217**, 1369–1382 (2018).

114. Mårtensson, C. U. *et al.* Mitochondrial protein translocation-associated degradation. *Nature* **569**, 679–683 (2019).

115. Weidberg, H. & Amon, A. MitoCPR—A surveillance pathway that protects mitochondria in response to protein import stress. *Science (80-.).* **360**, (2018).

116. Tsuboi, T. *et al.* Dom34: Hbs1 Plays a General Role in Quality-Control Systems by Dissociation of a Stalled Ribosome at the 3’ End of Aberrant mRNA. *Mol. Cell* **46**, 518–529 (2012).

117. Masters, B. S., Stohl, L. L. & Clayton, D. A. Yeast mitochondrial RNA polymerase is homologous to those encoded by bacteriophages T3 and T7. *Cell* **51**, 89–99 (1987).

118. Schinkel, A. H., Groot Koerkamp, M. J. & Tabak, H. F. Mitochondrial RNA polymerase of Saccharomyces cerevisiae: composition and mechanism of promoter recognition. *EMBO J.* **7**, 3255–3262 (1988).

119. Galmiche, L. *et al.* Exome sequencing identifies MRPL3 mutation in mitochondrial cardiomyopathy. *Hum. Mutat.* **32**, 1225–1231 (2011).

120. Carroll, C. J. *et al.* Whole-exome sequencing identifies a mutation in the mitochondrial ribosome protein MRPL44 to underlie mitochondrial infantile cardiomyopathy. *J. Med. Genet.* **50**, 151–159 (2013).

121. Distelmaier, F. *et al.* MRPL44 mutations cause a slowly progressive multisystem disease with childhood-onset hypertrophic cardiomyopathy. *Neurogenetics* **16**, 319–323 (2015).

Abbreviations

Å	Ångström = 0.1 nm
°C	Grade Celsius
^{35}S	Radioactive sulfur isotope
µCi	Microcurie
µg	Microgram
µl	Microliter
µM	Micromolar
Amp	Ampicillin
APS	Ammonium persulfate
A-site	Aminoacyl site of the ribosome
BN-PAGE	Blue native- Polyacrylamide Gel Electrophoresis
cm	Centimeter
DHFR	Dihydrofolate reductase
DMSO	Dimethyl sulfoxide
DNA	Deoxyribonucleic acid
dNTP	Deoxyribonucleoside triphosphate
DTT	Dithiothreitol
Δ ψ	Membrane potential
ECL	Enhanced chemiluminescence
E. coli	Escherichia coli
EDTA	Ethylene diamine tetraacetate
ER	Endoplasmic reticulum
g	Gravity of earth
GTP	Guanosine triphosphate
h	Hours
HEPES	N-2 hydroxyl piperazine-N`-2-ethane sulphonic acid
IM	Inner membrane
IMS	Intermembrane space
kDa	Kilodalton
LB	Luria Bertani media

Abbreviations

M	Molarity
mA	Milliampere
mg	Milligram
Mia40	Mitochondrial intermembrane space import and assembly
Min	Minute
ml	Milliliter
mM	Millimolar
mRNA	Messenger RNA
MTS	Matrix targeting signal
Nm	Nanometer
NADH	Nicotine amide adenine dinucleotide
NADPH	Nicotine amide adenine dinucleotide phosphate
OD_{600}	Optical density at 600 nm
OXPHOS	Oxidative phosphorylation system
P-site	Ribosomal peptidyl site
RNA	Ribonucleic acid
rRNA	Ribosomal RNA
SDS	Sodium dodecyl sulfate
tRNA	Transfer RNA

Curriculum Vitae

Steffen Hess

E-Mail hesss@rhrk.uni-kl.de

Education

2005 – 2008	**Abitur**, Secondary school diploma qualifying for university admission Heinrich-Heine-Gymnasium Kaiserslautern
2011 – 2014	**Bachelor of Science** (Biowissenschaften) TU Kaiserslautern
2014 – 2016	**Master of Science** (Molecular Cell- and Neurobiology) TU Kaiserslautern
2016- present	**PhD**, Cellbiology TU Kaiserslautern, Prof. Dr. Johannes Herrmann

Publications

Backes S*, **Hess S***, Boos F, Woellhaf MW, Gödel S, Jung M, Mühlhaus T, Herrmann JM. (2018). Tom70 enhances mitochondrial preprotein import efficiency by binding to internal targeting sequences.

Journal of Cell Biology 217(4), 1369-1382. (*authors contributed equally)

Zimmermann, J., Oestreicher, J., **Hess, S**., Herrmann, J. M., Deponte, M., & Morgan, B. (2020). One cysteine is enough: A monothiol Grx can functionally replace all cytosolic Trx and dithiol Grx.

Redox biology, 36, 101598.

Danksagung

Zuerst geht ein großer Dank an Prof. Dr. **Johannes Herrmann**, der mir die Möglichkeit gegeben hat in dieser großartigen Arbeitsgruppe zu arbeiten und zu promovieren. Hannes, durch deine Unterstützung konnte ich mich als Wissenschaftler aber auch ganz besonders als Mensch weiterentwickeln und viele tolle Erfahrungen in den vergangenen Jahren sammeln.

Vielen Dank an Junioprof. Dr. **Felix Willmund** für die freundliche Übernahme des Zweitgutachtens.

Danke auch an Prof. Dr. **Mathias Hahn** für den Vorsitz meiner Promotions-Kommission.

Ein großer Dank geht auch an Prof. Dr. **Ulrich Brand** und seine Arbeitsgruppe in Nijmegen (Niederlande) die einen wesentlichen Beitrag zu meiner Arbeit geleistet haben.

Prof. Dr. **Bruce Morgan** danke ich für stetes kritisches Hinterfragen und einen legendären Spruch (Import shmimport…)

Vielen Dank für die schöne Zeit mit euch und Gruß nach Saarbrücken an die ehemalige Bruce Gruppe **Julian, Jannik, Marie, Gurleen und Prince.**

Vielen Dank an die beste Sekretärin der Welt, **Simone**, die immer ein offenes Ohr und eine Lösung für (fast) alle Probleme hat. Danke **Andrea** für all die kulinarischen Unterhaltungen über Rouladen und Gerichte aus deiner Kindheit. Danke **Connie** für deine stets fröhliche Begrüßung am Morgen. Danke **Vera** für deine Hilfsbereitschaft im Labor und darüber hinaus.

Danke **Sabine** für deine tägliche Unterstützung bei allen Angelegenheiten im Labor, die Unterhaltungen über Hund, Pferd, Hühner und das grüne Hobby.

Ein ganz besonderer Dank geht natürlich an euch alle die nicht nur Kollegen, sondern Freunde und **Laborfamilie** sind. Danke **Felix** für die männliche Unterstützung in diesem Hühnerhaufen, dass du meine Hilferufe erhört hast, wenn R mich wieder zum Verzweifeln gebracht hat und dafür, dass du Freund, Mentor und Labor-(Ehe)partner für mich warst und bist. Danke **Janina** für eine tolle Zeit, musikalische Unterstützung und Gespräche über Gott und die Welt. Danke **Katha** für die Beste Labortochter, die man sich vorstellen kann und tägliches knuddeln. Danke **Tamara** für immer gute Laune und das Talent immer für einen Lacher zu sorgen. Danke **Sandra** für deine Art die Dinge besser zu machen. Danke **Anna** für die gemeinsame Leidenszeit an den PCR-Maschinen. Danke **Christian** für die gemeinsamen Unterhaltungen über Fußball und andere männliche Angelegenheiten. Danke **Lea,** dass ich dich seit deiner Bachelorarbeit als Betreuer begleiten durfte und für deine herzliche Art. Danke **Eva** für deine leckeren Dips zu jeder Gelegenheit. Danke **Lena** und **Carina**, dafür, dass ihr die saarländische Fraktion in unserem Labor stets gut vertreten habt. Danke an **Katja** für die beste Fahrgemeinschaft aller Zeiten. Thank you **Sree** for funny moments. Auch ein Dank an die „Ehemaligen“ **Vale**, **Micha** und **Ajay** für hilfreiche Tips und Tricks im Laborleben.

Ich kann hier gar nicht alles in Worte fassen was über jeden von euch zu sagen wäre, daher fühlt euch einfach alle gedrückt!

Meinen Eltern danke ich für die Unterstützung und dafür, dass sie mir das alles ermöglicht haben.

Zuletzt und der größte Dank geht an meine Frau **Vanessa**, für die Geduld während der letzten Wochen und Monate, dafür dass wir alle Situationen gemeinsam meistern und du immer an meiner Seite bist.

Danke!